Universitat Autònoma de Barcelona

EFFECT OF SEX ON EXPERIMENTAL DIABETIC NEPHROPATHY AND THE RENINANGIOTENSIN SYSTEM. ROLE OF ACE2

Sergi Clotet Freixas

EFFECT OF SEX ON EXPERIMENTAL DIABETIC NEPHROPATHY AND THE RENIN-ANGIOTENSIN SYSTEM. ROLE OF ACE2

Thesis submitted by

Sergi Clotet Freixas

For the degree of Doctor of Biochemistry, Molecular Biology and Biomedicine

Directors

Dr. Julio Pascual Santos

Dr. Mª José Soler Romeo

Dr. Marta Riera Oliva

Tutor

Dr. Assumpció Bosch

PhD Student

Sergi Clotet Freixas

Department of Biochemistry and Molecular Biology
Universitat Autònoma de Barcelona

Barcelona, July 2016

OUTLINE

ACKNOWLEDGEMENTS

ACKNOWLEDGEMENTS

Aquesta tesi ha estat possible gràcies al suport de tots vosaltres, tant a nivell personal com científic.

Agraeixo als meus directors de tesi haver confiat en mi com a doctorand per aquest projecte tant ambiciós. Moltes gràcies Marta, Pepa, i Julio, per haver estat al peu del canó des del primer dia, fent possible l'evolució del projecte fins a un punt que al principi era inimaginable, i fent possible la meva formació com a científic. Cadascun amb les vostres qualitats, m'heu ensenyat que la disciplina, el rigor, la constància i la perseverança acaben donant els seus fruits.

To my Canadian supervisors Ana and Jim, for giving me the opportunity to join your exceptional team during my stay in Toronto. At a scientific level, your wisdom, expertise and sense of logics helped me to improve my skills on study rationale and experimental design. At a more personal level, thanks for making me feel like home since the very beginning. In one word, my experience in your lab was just…TERRYFIC!!!

Als meus companys de lab. Heleia, ja saps que va ser un plaer envair la teva poiata, deixar-te els pòrex al fons a la nevera, acabar-te les tires de glicèmia cada dimecres...gràcies per la teva paciència, empatia, saber escoltar, valentia, transparència i lleialtat. A la Lídia, no sé si és el rollo Biotec UAB, o la nostra addicció a Master Chef, però sempre hem connectat a la perfecció tot i tenir caràcters tant diferents. Gràcies per l'alegria i vitalitat que ens has aportat sempre. Fora d'aquí no ens podem aguantar gaires hores seguides, però si ens "organitçem" bé, saps que tu i el Salus sempre tindreu la porta oberta allà on estigui. A la Dra. Marquez...gracias por tus superconsejos y también por tus momentazos cachondos! Qué risas nos echábamos, que tiempos aquellos! Als tècnics més peculiars, divertits i pintorescos que un doctorand pot demanar. Al Guillem, per aportar una mica de Hakuna Matata i sentit de l'humor al laboratori, ambdues coses imprescindibles pel funcionament de l'equip. A la Judit, per la teva naturalitat i simpatia. Haver competit prèviament en esports d'alt rendiment ens va unir des del principi, i al final hem acabat forjant una amistat! A la Marta, crec que el nostre bon rotllo no pot haver crescut de forma més exponencial. Gràcies per tots els moments frikis, per les cookies, per les teories rebullianes, per les anades de l'olla, per lligar-me la bata a la cadira, per les enganxines motivacionals, per ser tant genuïna! Budour, it was a pleasure working with you! Thanks for your help and hospitality. I will miss the justeat dinners, the scanned films, the ice creams and our "secret missions" lol Gràcies als estudiants que heu anat passant pel laboratori: Raquel, Paola, Vanesa i Oriol. Sempre m'heu volgut fer sombra, mira que us hi heu escarrassat dia a dia fent mèrits i mèrits...però em sap greu dir-vos que no val la pena...no teniu res a fer...el més despistat sóc jo i punt!!!! xD Gràcies per venir cada dia amb un somriure a la boca, espero que tingueu molta sort!

To my canadian labmates: Richard, Anne, Christy, Vanessa, Fei, Julie, Nick, Joyce. You guys are golden! For all the moments together, all the improvised hangouts, the walks across the whole downtown at -32^{o}C, the snippers and the balconies, and all the stupid and endless conversations…Thanks to you guys, my first winter in Toronto and the coldest February ever were a lot easier to me. And thanks for celebrating with me my first bday far away from home!

Als meus millors amics, l'Albert I l'Arnau. Per donar-me sostre quan més ho vaig necesitar. I per estar allà sempre, per les faves, pels riures, per seguir comptant amb

mi després de les meves èpoques de desaparició…encara que no us ho sembli, teniu molt a veure amb aquesta tesi. Vaig dir que hi serieu, i punt. Sou collunuts!

A la grupeta. Com podia deixar-me-la? Per demostrar cada vegada més que, per molt que passin els anys, estarem sempre allà els uns pels altres. Gràcies Laia, Alba i Roser per venir-me a veure a Canadà! I a la resta també! Pels yakisoba, les barbacoes i els sopars a la fresca, les tonteries…per tot el que hem viscut els últims 12 anys i el que ens queda per viure!

Als primos. Per ser tant rematadament primos. Per fer-me veure que un primo pot arribar a ser doctor. Fins i tot dos…o tres…Per ensenyar-me que el Marçal no sempre té la raó, però normalment sí. Pels galets anuals que ens han donat força per arribar a finals de tesi…per seguir jugant a la loteria sabent que no ens tocarà mai perquè som uns primos. Pels linars. Pel poder de les rastes. Per l'Aytor i pel Yonatan. Pels gordis. I pels gironins encara que siguin uns creguts.

A tots els meus companys de pis, amb qui he compartit moments de tots colors durant els últims 5 anys. Cesc, Terri, Justyna, Vladek, Eugènia, Victor, Nil, i Anna...Sabadell amb vosaltres va ser una llar molt millor! Also to my amazing crazy roomies in Canada: Princess Meligy, Mahmoud Allyoucaneat and Karim Kimono.I als meus tres últims companys de viatge: Juna, Alba i Tango. Hem tingut poc temps per conviure, però crec que ha cundit molt. Moltes gràcies per la vostra simpatia, naturalitat i espontaneïtat, i per fer-me sentir un més des del primer dia. ja trobo a faltar el sushi i les sèries del dilluns...i fins i tot la cesta de verdures!!! És broma la cesta no xD

To Momo and Lyle. I wouldn't have been able to accomplish my objectives in Canada without your friendship and support. You are an example of how being positive, charm, friendly and determined can take you far in life. That's why everybody love you guys. I have learned a lot from both of you, and was a pleasure to explore this country with such a good company. Also to my buddies Alan, Alex and Eseosa. Thanks for sharing with me a piece of this unforgettable experience!!!

A tota la meva família. Tiets, avis i cosins, pel seu interès per la tesi i els progressos realitzats. Per preguntar i fer-me adonar que, a vegades, ni jo mateix sabia què estava investigant ni per què.

A la que va ser la meva segona família durant el 80% de la tesi: els companys d'equip del Sant Nicolau. És inevitable que la vida ens hagi acabat separant, però no hi ha dia que no em recordi d'aquells any preciosos i les sensacions inoblidables que vam compartir a la pista. La lluita per superar-me una mica més cada dia no seria possible sense aplicar els valors de d'esperit d'equip, constància, competitivitat, i joc net que vaig aprendre a explotar fixant-me amb tots vosaltres. Santi i Roser, us dono mil gràcies per haver-me obert les portes de casa vostra des del segon zero.

Al meu germà Carles. Quan vaig començar la tesi eres un nen encantador, i ara ets un adolescent insuportable! Tot i així, et dono les gràcies per l'alegria que m'ha portat sempre en aquesta vida tenir-te com a germà. No saps la ràbia que em fa tots els moments teus que m'he perdut per culpa de la P_ _ _ tesi. Saps que l'admiració que em tens és totalment mútua. Sé que vals molt i t'espera un gran futur! ;)

I per acabar, als meus pares. Pel suport incondicional, per oferir-me aixopluc sense preguntar, per aguantar els meus moments absents, els de mal humor… per confiar en mi i fer-me creure en les meves capacitats. I per donar tot el que podeu i més per fer-me la vida una mica millor. I no només en aquesta última etapa, sinó sempre. Sóc molt feliç de tenir-vos com a pares, i per això **us dedico aquesta tesi. Us estimo!**

PARTICIPATION IN CONGRESSES

PARTICIPATION IN CONGRESSES

INTERNATIONAL CONGRESSES

Oral Communications

- **Clotet S**, Soler MJ, Rebull M, Pascual J, Riera M. LOSS OF ACE2 ACCENTUATED RENAL HYPERTROPHY AND ANGII-INDUCED HYPERTENSION IN DIABETIC MICE. 52th ERA-EDTA Congres. London 2015. *(Abstract awarded with the ERA-EDTA Travel Award)*.

Posters

- **Clotet S**, Soler MJ, Rebull M, Pascual J, Riera M. EFFECT OF *ACE2* DELETION AND ROLE OF GONADECTOMY IN MALE MICE WITH DIABETIC NEPHROPATHY. ASN Kidney Week. Atlanta 2013.

- **Clotet S**, Soler MJ, Rebull M, Pascual J, Riera M. EFFECT OF GENDER AND DIABETES IN CIRCULATING ACE AND ACE2 ACTIVITY IN STREPTOZOTOCIN(STZ)-INDUCED MICE. ASN Kidney Week. Philadelphia 2014.

- **Clotet S**, Soler MJ, Rebull M, Pascual J, Riera M. EFFECT OF *ACE2* DELETION AND ROLE OF GONADECTOMY IN MALE MICE WITH DIABETIC NEPHROPATHY. ASN Kidney Week. Philadelphia 2014.

- **Clotet S**, Soler MJ, Rebull M, Pascual J, Riera M. EFFECT OF GENDER AND DIABETES IN CIRCULATING AND RENAL ACE AND ACE2 IN STREPTOZOTOCIN-INDUCED MICE. 51th ERA-EDTA Congress. Amsterdam 2014.

- **Clotet S**, Soler MJ, Rebull M, Pascual J, Riera M. LOSS OF ACE2 ACCENTUATED RENAL HYPERTROPHY AND ANGII-INDUCED HYPERTENSION IN DIABETIC MICE. ASN Kidney Week. San Diego 2015.

- **Clotet S**, Soler MJ, Riera M, Pascual J, Fang F, Zhou J, Batruch I, Vasiliou SK, Dimitromanolakis A, Barrios C, Diamandis EP, Scholey JW, Konvalinka A. SILAC-BASED PROTEOMICS OF PRIMARY HUMAN KIDNEY CELLS REVEALS A NOVEL LINK BETWEEN MALE SEX HORMONES AND IMPAIRED ENERGY METABOLISM IN DIABETIC KIDNEY DISEASE. 53th ERA-EDTA Congress. Vienna 2016.

- **Clotet S**, Soler MJ, Riera M, Pascual J, Fang F, Zhou J, Batruch I, Vasiliou SK, Dimitromanolakis A, Barrios C, Diamandis EP, Scholey JW, Konvalinka A. SILAC-BASED PROTEOMICS OF PRIMARY HUMAN KIDNEY CELLS REVEALS A NOVEL LINK BETWEEN MALE SEX HORMONES AND IMPAIRED ENERGY METABOLISM IN DIABETIC KIDNEY DISEASE. ISN Forefronts Symposium on Microbiomics and Metabolomics. San Diego 2016.

Online reviews

- **Clotet S**, Riera M, Pascual J, Soler MJ. GENDER DIFFERENCES IN ANGIOTENSIN CONVERTING ENZYME 2 (ACE2). CIN 2013.

NATIONAL CONGRESSES

Oral Communications

- **Clotet S**, Soler MJ, Collell G, Pascual J, Riera M. Oral Comunication. LA DELECIÓN DEL *ECA2* EN RATONES MACHO PREDISPONE A LA APARICIÓN DE HIPERTENSIÓN ARTERIAL TRAS LA INDUCCIÓN DE DIABETES CON ESTREPTOZOTOCINA (STZ). XLII Congreso de la Sociedad Española de Nefrología. Maspalomas 2012.

- **Clotet S**, Soler MJ, Rebull M, Pascual J, Riera M. LA GONADECTOMIA PREVÉ L'INCREMENT DE LA PRESSIÓ ARTERIAL I LA LESIÓ GLOMERULAR EN RATOLINS MASCLE DIABÈTICS I KNOCKOUT PEL GEN D'*ECA2*. XXX Reunió Anual de la Societat Catalana de Nefrologia. Terrassa 2014.

- **Clotet S**, Soler MJ, Rebull M, Pascual J, Riera M. EFECTE DEL GÈNERE I LA DIABETIS EN ECA I ECA2 CIRCULANTS I RENALS. XXX Reunió Anual de la Societat Catalana de Nefrologia. Terrassa 2014.

- **Clotet S**, Soler MJ, Rebull M, Pascual J, Riera M. EFECTO DEL GÉNERO Y LA DIABETES EN LA ACTIVIDAD DEL ECA Y ECA2 CIRCULANTE EN RATONES INDUCIDOS CON ESTREPTOZOTOCINA. XLIV Congreso de la Sociedad Española de Nefrología. Barcelona 2014.

- **Clotet S**, Soler MJ, Rebull M, Pascual J, Riera M. EFECTO DE LA DELECIÓN DEL *ECA2* Y LA GONADECTOMÍA EN RATONES MACHO CON NEFROPATÍA DIABÉTICA. XLIV Congreso de la Sociedad Española de Nefrología. Barcelona 2014.

- **Clotet S**, Soler MJ, Rebull M, Pascual J, Riera M. LA DELECIÓN DEL *ECA2* ACENTÚA LA HIPERTENSIÓN ARTERIAL INDUCIDA MEDIANTE ANGIOTENSINA II EN RATONES DIABÉTICOS. EFECTO EN LA HIPERTROFIA RENAL Y ALBUMINURIA. XXI Reunión nacional de la Sociedad Española de Hipertensión. Valencia 2016. *(Awarded as the best oral comunication)*.

Posters

- **Clotet S**, Soler MJ, Rebull M, Pascual J, Riera M. LA GONADECTOMIA PREVEU L'AUGMENT EN LA PRESSIÓ ARTERIAL I L'ACTIVITAT SÈRICA DE L'ECA EN RATOLINS MASCLES DIABÈTICS *KNOCKOUT* PER L'ENZIM CONVERSOR D'ANGIOTENSINA 2. XXIX Reunió Anual de la Societat Catalana de Nefrologia. Barcelona 2013.
- **Clotet S**, Soler MJ, Rebull M, Pascual J, Riera M. EFECTO DEL GÉNERO Y LA DIABETES EN LA ACTIVIDAD DEL ECA Y ECA2 CIRCULANTE EN RATONES INDUCIDOS CON ESTREPTOZOTOCINA (STZ). XLIII Congreso de la Sociedad Española de Nefrología. Bilbao 2013.

PUBLICATIONS

PUBLICATIONS

1. Riera M, Marquez E, **Clotet S**, Gimeno J, Roca-Ho H, Lloreta J, Juanpere N, Batlle D, Pascual J, Soler MJ. EFFECT OF INSULIN ON ACE2 ACTIVITY AND KIDNEY FUNCTION IN THE NON-OBESE DIABETIC MOUSE. *PLoS One*. 2014;9(1):1-11.

2. Riera M, Anguiano L, **Clotet S**, Roca-Ho H, Rebull M, Pascual J, Soler MJ. PARICALCITOL MODULATES ACE2 SHEDDING AND RENAL ADAM17 IN NOD MICE BEYOND PROTEINURIA. *Am J Physiol - Ren Physiol*. 2016;310(6):F534-F546.

3. **Clotet S**, Soler MJ, Rebull M, Gimeno J, Gurley SB, Pascual J, Riera M. GONADECTOMY PREVENTS THE INCREASE IN BLOOD PRESSURE AND GLOMERULAR INJURY IN ANGIOTENSIN-CONVERTING ENZYME 2 KNOCKOUT DIABETIC MALE MICE. EFFECTS ON RENIN-ANGIOTENSIN SYSTEM. *J Hypertens*. 2016; 34(1). (See Annex I).

4. **Clotet S**, Riera M, Pascual J, Soler MJ. RAS AND SEX DIFFERENCES IN DIABETIC NEPHROPATHY. Review. *Am J Physiol - Ren Physiol*. 2016. (See Annex II).

5. **Clotet S**, Soler MJ, Riera M, Pascual J, Fang F, Zhou J, Batruch I, Vasiliou SK, Dimitromanolakis A, Barrios C, Diamandis EP, Scholey JW, Konvalinka A. SILAC-BASED PROTEOMICS OF PRIMARY HUMAN KIDNEY CELLS REVEALS A NOVEL LINK BETWEEN MALE SEX HORMONES AND IMPAIRED ENERGY METABOLISM IN DIABETIC KIDNEY DISEASE. *(Submitted).*

FUNDING

FUNDING

This thesis was supported by funding from the following grants:

1. Sociedad Española de Nefrología. Fundación SENEFRO 2010. PI: Dr. Marta Riera.

2. AYUDAS PREDOCTORALES DE FORMACIÓN EN INVESTIGACIÓN EN SALUD (PFIS). Convocatoria 2011, exp nº FI11/00480. Fondo de Investigación Sanitaria-Instituto Carlos III-FEDER (ISCIIIFEDER). PI: Dr. Julio Pascual Santos.

3. Fondo de Investigación Sanitaria-Instituto Carlos III-FEDER (ISCIII-FEDER PI11/01549). PI: Dr. Maria José Soler.

4. Fondo de Investigación Sanitaria-Instituto Carlos III-FEDER (ISCIII-FEDER PI14/00557). PI: Dr. Maria José Soler.

5. Red de Investigación Renal. Fondo de Investigación Sanitaria-Instituto Carlos III. Subprograma RETICS (RD12/0021/0024_ISCIII-RETICS REDinREN). PI: Dr. Julio Pascual.

6. Kidney Foundation of Canada (KFOC) Award. PI: Dr. Ana Konvalinka.

7. Heart & Stroke foundation, Canadian Institutes of Health Research (CIHR) and KFOC Award. PI: Dr. James W. Scholey.

8. Ajut per a la finalització de la tesi doctoral de la Fundació IMIM, 2016.

ABBREVIATIONS

ABBREVIATIONS

ACE: angiotensin-converting enzyme

ACE2: angiotensin-converting enzyme 2

ACE2KO: ACE2 knockout

ACR: albumin-to-creatinine ratio

AGEs: advanced glycation end products

AGT: angiotensinogen

AKT: protein kinase B

ANG (1-7): angiotensin (1-7)

ANGI: angiotensin I

ANGII: angiotensin II

APA: aminopeptidase A

APN: aminopeptidase N

AR: androgen receptor

ARB: angiotensin receptor 1 blockers

ARE: androgen response element

AT1R: angiotensin II type 1 receptor

AT2R: angiotensin II type 2 receptor

BA: Bowman space area

bpm: beats per minute

BW: body weight

C-terminal: Carboxi-terminal

CKD: chronic kidney disease

CONT: control

CTGF: connective tissue growth factor

CTSG: cathepsyn G

CV: cardiovascular

Da: dalton

DB: diabetic

DBP: diastolic blood pressure

ddH2O: double distilled water

DHT: dihydrotestosterone

DN: diabetic nephropathy

DNA: deoxyribonucleic acid

ECM: extracellular matrix

EDTA: ethylenediamine-tetraacetic acid

EMT: epithelial-mesenchymal transition

ERα / ERβ: estrogen receptor alpha / estrogen receptor beta

ERE: estrogen response element

ESRD: end-stage renal disease

EST: 17β-estradiol

FAO: fatty acid beta-oxidation

GAPDH: glyceraldehyde 3-phosphate dehydrogenase

GBM: glomerular basement membrane

GDX: gonadectomy

GFR: glomerular filtration rate

GNPNAT1: glucosamine-6-phosphate-N-acetyltransferase 1

GPER: G protein coupled estrogen receptor 1

GPI: glucose-6-phosphate isomerase

GSL: glycosphingolipid

HADHA: mitochondrial trifunctional protein subunit alpha

HBP: hexosamine biosynthetic pathway

HEXB: hexosaminidase B

HHL: hippuryl-histidyl-leucine

HK-2: immortalized human kidney cells

HPRT: hypoxanthine-guanine phosphoribosyltransferase

HW: heart weight

IP: intraperitoneal

KW: kidney weight

LC-MS/MS: liquid chromatography-tandem mass spectrometry

Ln: natural logarithm

M: molar

MASR: mas receptor

MCP1: monocyte chemoattractant protein 1

mg: mil·ligrams

MGV: mean grey value

mL: milliliter

mM: millimolar

mmHg: Millimeter of mercury

MI: mesangial index

MME: mesangial matrix expansion

MW: molecular weight

NEP: neprilysin

nm: nanometers

nM: nanomolar

NOD: non-obese diabetic

N-terminal: amino-terminal

o/n: overnight

PBS: phosphate buffer solution

PCR: polymerase chain reaction

PKC: protein kinase C

PTEC: proximal tubular epithelial cells

RAS: renin-angiotensin system

REN: renin

RFU: relative fluorescence units

RNA: ribonucleic acid

ROS: reactive oxygen species

RT: room temperature

SBP: systolic blood pressure

SCX: strong cationic exchange

SD: standard deviation

SE: standard error

SILAC: stable isotope labeling with amino acids in cell culture

SMA: smooth muscle actin

STZ: streptozotocin

T1DM: type 1 diabetes mellitus

T2DM: type 2 diabetes mellitus

TCA: tricarboxylic acid

TGF-β: transforming growth factor-beta

UAE: urinary albumin excretion

WT: wild-type

WT-1: wilms tumor 1

µg: micrograms

µL: microliters

µM: micromolar

SUMMARY

SUMMARY

Male sex increases the incidence, prevalence, and progression of chronic kidney disease. However, little is known about the effect of sex hormones in diabetic nephropathy (DN). The renin-angiotensin system (RAS) is an important regulator of cardiovascular and renal function. Within this system, angiotensin-converting enzyme 2 (ACE2) plays a protective role by degrading angiotensin II (ANGII) and preventing its deleterious downstream events. RAS is altered in diabetes, and plays a critical role in the development DN. Sex differences in the renal response to RAS blockade have been demonstrated. Thus, the sexual dimorphism in DN may be related to sex-specific regulations of circulating and renal RAS. Our objective was to study the effect of sex on glomerular and tubular injury markers in a model of type 1 diabetes mellitus, the streptozotocin(STZ)-induced mice, and its relationship with sex-specific changes of RAS. We also aimed to evaluate the influence of androgen reduction by gonadectomy (GDX), *Ace2* deletion, and ANGII infusion on this effect. In our model, STZ administration led to hyperglycemia, body weight loss, renal and glomerular hypertrophy, hyperfiltration, polyuria, albuminuria, mesangial expansion, podocyte loss and cortical fibrosis. The severity of these renal alterations differed between sexes. Diabetic males presented a more important worsening in all the glomerular hallmarks of DN studied, including albuminuria, hyperfiltration, glomerular hypertrophy, and mesangial matrix expansion. Male sex hormones played a direct role in this accentuated glomerular injury, as GDX prevented all these alterations. Studies in *Ace2* knockout mice revealed that the role of ACE2 in DN was sex-specific. In females, loss of ACE2 aggravated DN progression by worsening albuminuria, renal hypertrophy and cortical fibrosis. In males, loss of ACE2 increased blood pressure and accentuated glomerular injury and renal fibrosis, and GDX prevented these alterations by modulating the expression of renal and circulating RAS and decreasing cortical Akt phosphorylation. In the context of experimental hypertension, loss of ACE2 accentuated ANGII-induced cardiac hypertrophy, hypertension, albuminuria, and glomerular hypertrophy in diabetic females, as well as exacerbated ANGII-mediated glomerular hypertrophy, mesangial expansion and podocyte loss in diabetic males. Sexual dimorphism in experimental DN was accompanied by a sex-specific regulation of the compensatory mechanisms of RAS. In the *in vitro* part of this project, we performed SILAC-based proteomics in proximal tubular epithelial cells incubated with sex hormones, and discovered a novel link between dihydrotestosterone and impaired glucose and lipid metabolism in these cells. Further validation studies confirmed that male sex altered energy metabolism in the diabetic kidney, in association with increased renal hypertrophy and oxidative stress levels. In this work we demonstrate a strong effect of sex in DN progression, as well as a sex-specific renoprotective role of ACE2. With our findings, we aim to improve the understanding of the sexual dimorphism in diabetic kidney disease, and its relation with the dysregulation of RAS.

1. INTRODUCTION

1. INTRODUCTION

1.A DIABETIC NEPHROPATHY

1.A.I Definition

Diabetic nephropathy is a microvascular complication of type 1 and type 2 diabetes mellitus, characterized by an increased protein excretion in urine and chronic histopathological lesions in the kidney[1]. This complication, which appears after many years of diabetes beginning[2,3], is the leading cause of chronic kidney disease (CKD) in patients starting renal replacement therapy, and is associated with increased cardiovascular (CV) mortality[4].

1.A.II Epidemiology

Diabetes is the leading cause of end-stage renal disease (ESRD) in the Western world[5]. Among all diabetic complications, DN has become the principal cause of CV mortality. Indeed, approximately one-third of all diabetics die of ESRD due to progressive renal damage and hypertension[6]. In the USA, the prevalence of DN ranges between 20% and 40% among diabetic patients[7,8]. In Catalunya, the last register of renal patients (http://trasplantaments.gencat.cat) indicates that in 2014 DN was the second cause of ESRD (with an incidence of 22%), following the renal diseases of unknown etiology (31.6%)[9].

1.A.III Etiology

The presence of maintained elevated glucose levels in diabetes causes long-term damage in different organs. Despite the exact mechanisms have not been described, glucose dependent processes play a crucial role on the establishment and progression of DN[3,10].

Disease progression has been attributed to many risk factors, including poor glycemic control, ethnicity, uncontrolled hypertension, tobacco use, age of diabetes onset, and genetic predisposition[1,11–14]. Ethnicity also exerts a significant influence on the progression of DN[15]. Specific populations, such as African-Americans, Asians, and native Americans, seem to be affected more than Caucasians[16].

1.A.IV Clinical evaluation

Albuminuria and progressive loss of kidney function are the clinical hallmarks of DN. In the early stages of DN there is an increase in the urinary albumin excretion (UAE), defined as an albumin-to-creatinine ratio (ACR) in urine between 30 and 299 mg/g. The increase in the levels of albumin in urine is considered the first clinical sign of DN and is termed microalbuminuria[17]. In fact, the screening and early diagnosis of DN is based on the detection of microalbuminuria[18]. From this point, there is a progressive increase in albuminuria. When values of ACR exceed 300mg/g, clinicians consider it as macroalbuminuria, a stage of overt DN[1]. The progressive increase in proteinuria leads to a variable decline in renal function. Once the subject has developed macroalbuminuria, there is a decrease in the glomerular filtration rate (GFR)[19]. Although measurement of albuminuria is essential to diagnose DN, there are some patients who present decreased GFR when ACR values are normal[20]. Based on this, the classification of the National Kidney Foundation can also be used to stage CKD in these patients[21,22].

The management of DN is based on the general recommendations in the treatment of patients with diabetes, including optimal glycemic and blood pressure control, adequate lipid management and abolishing smoking, in addition to the lowering of albuminuria. In this sense, recent studies have demonstrated a regression in microalbuminuria in up to 50-60% of patients, probably associated to advances in blood pressure and glycemic control strategies[23,24]. At present, still nearly 20–40% of diabetic patients develop microalbuminuria within 10–15 years of the diagnosis of diabetes, and about 80–90% of those with microalbuminuria progress to more advanced stages. Thus, after 15–20 years, macroalbuminuria occurs approximately in 20–40% of patients, and around half of them will present renal insufficiency within 5 more years[18].

1.A.V Pathophysiology of DN

Several factors such as hyperglycemia, hyperlipidemia, hypertension, and proteinuria contribute to the progression of renal damage in DN. High blood glucose induces renal damage by affecting all cell types in the kidney, including endothelial cells, tubulointerstitial cells, podocytes and mesangial cells[25]. However, all these factors are supported by a specific genetic background because not all the patients

with diabetes develop DN, irrespective of glycemic control[26]. In this sense, several loci in human chromosome 10p and 10q have been linked to DN[27].

At early stages, DN is characterized by hemodynamic modifications and increases in proximal tubular reabsorption that are manifested through increased renal weight and structural changes such as glomerular hypertrophy, thickness of tubular and glomerular basement membranes and abnormal enlargement and accumulation of extracellular matrix (ECM) in mesangial cells[28,29]. ECM accumulation is due not only to excessive synthesis of matrix proteins, but also to their decreased degradation by matrix metalloproteases (MMPs)[30]. While glomerular basement membrane (GBM) thickening is the earliest lesion observed in patients with DN by electron microscopy[5,31,32], mesangial expansion is the most commonly observed histopathological lesion by light microscopy[3].

At functional level, patients with early DN initially show hyperfiltration, represented by high values of GFR, and occasional occurrence of microalbuminuria[33,34], which are considered the main hallmarks of kidney disease progression[27]. Persistence of microalbuminuria can lead to many other glomerular abnormalities at podocyte level, including foot process effacement, hypertrophy, detachment, loss, and death[35–38]. In turn, the damaged podocyte may contribute to nephropathy via alterations in its expression of paracrine factors that affect other glomerular cells[39].

As the disease progresses, microalbuminuria comes mild and subsequently moderate proteinuria, accompanied by accentuated ECM deposition in the mesangium and glomerular basement membrane, ultimately leading to the formation of Kimmelsteil-Wilson nodules and glomerulosclerosis[27,30]. After the establishment of overt nephropathy, the decline in GFR is accompanied by advanced glomerular lesions namely arteriolar thickening and hyalinization of the vascular compartment of the kidney, as well as by tubular atrophy and tubulointerstitial fibrosis[1,27].

Stimulation of epithelial-mesenchymal transition (EMT) also takes place in the diabetic kidney when damaged epithelial cells dedifferentiate to myofibroblasts and start to express α-smooth muscle actin (α-SMA)[40,41]. Following myofibroblasts accumulation and activation, tubulointerstitial fibrosis include other features such as atypical collagen deposition, migration of inflammatory cells, and loss of capillary architecture[42]. Exacerbated levels of tubulointerstitial fibrosis often herald the onset of progression towards ESRD. The final step of the natural history of the disease is characterized by severe macroalbuminuria and chronic renal insufficiency that declines to ESRD[27,33,34].

In DN, there is an interplay between hemodynamic changes (blood pressure affecting the renal microcirculation), and tissue changes due to glucose-dependent

metabolic alterations. At a molecular level, hyperglycemia mediates the pathological perturbation of intracellular metabolism in the kidney[3]. Specifically, alterations of at least five major pathways contribute to the glucose-mediated vascular and renal damage in DN. These alterations are (1) accumulation of advanced glycation end-products (AGEs)[43,44]; (2) increased polyol pathway flux[45,46]; (3) increased hexosamine pathway flux[47]; (4) activation of protein kinase C (PKC)[48,49]; and (5) stimulation of angiotensin II (ANGII) synthesis[49–51].

The chronic effects of hyperglycemia on inducing tissue injury may occur via the generation of AGEs. AGEs accumulate in the kidney, particularly in people with diabetes and/or declining renal function[44]. Their importance in the pathogenesis of diabetic complications has been demonstrated in animal models, where two structurally unrelated AGEs inhibitors partially prevented various functional and structural manifestations of diabetic microvascular disease[52,53]. Another glucose-dependent pathway, known as the polyol pathway, has been implicated in the pathogenesis of DN[46]. This pathway is activated as a response to high levels of intracellular glucose with the objective to metabolize, through aldose reductase activity, glucose to sorbitol. The excessive entry of glucose into the hexosamine pathway has also been linked to mechanisms of DN, particularly the increase in the expression of the fibrogenic cytokine transforming growth beta 1 (TGF-β1)[47]. Intracellular accumulation of glucose also increases *de novo* formation of diacylglycerol, which activates several isoforms of PKC[54]. Finally, glucose-induced ANGII generation is attributed to an activation of the renin-angiotensin system, via overexpression of angiotensinogen[51]. In turn, ANGII induces endothelial lesion and increases in blood pressure, and is linked to processes of cellular proliferation and hypertrophy[49,50]. ANGII has also been related to the activation of NADPH oxidase, leading to the generation of oxidative stress[50]. As a consequence, presence of ANGII increases tubular reabsorption of proteins and stimulates tissue damage, including proteolysis, inflammation and fibrosis[49].

Overall, the signaling pathways described above induce the regulation of vascular permeability, vasoconstriction, ECM synthesis and turnover, cell growth, angiogenesis and cytokine activation[55]. These changes are mediated by the activation of several transcription factors, including NF-kB, AP-1, STAT and EGR1, which have been proposed to promote the synthesis and the secretion of growth factors and cytokines[56–58]. Specifically, overexpression of TGF-β1 increases ECM protein deposition by inducing expression of collagen types I, IV, V, and VI, fibronectin, and laminin[27]. Fibrotic processes can occur in the tubulointerstitial compartment but also in the glomerulus, as ANGII can stimulate resident renal cells to produce TGF-β1 and consequently increase ECM accumulation in the mesangium[59]. Furthermore, high

glucose–induced expression and activation of TGF-β contributes to podocyte apoptosis, which in turn leads to disruption of the filtration barrier and impaired kidney function[60]. Other growth factors such as PDGF-β and CTGF are also involved in structural alterations at the glomerular level[61,62].

Cumulative evidence has reinforced the role of inflammation in the pathogenesis of DN[63]. Expression of cell adhesion molecules, growth factors, chemokines and pro-inflammatory cytokines are increased in renal tissues of diabetic patients. In addition, serum and urinary levels of cytokines and cell adhesion molecules correlated with albuminuria[64]. In this sense, it has been demonstrated that the immune cells implicated in diabetes pathogenesis, basically monocytes, lymphocytes and macrophages, infiltrate the renal interstitium and therefore play a role in DN[2,65].

Since reactive oxygen species (ROS) interplay with RAS and inflammation pathways, it is considered that oxidative stress status also play a key role in the pathogenesis of DN[66]. Several authors have suggested that the pathologic event linking between all glucose-mediated molecular alterations is oxidative stress, defined as a defect in the mitochondrial electron transport chain resulting in overproduction of ROS molecules, and subsequent stimulation of the pathways mentioned above[43]. ROS overproduction triggers different signaling pathways in the diabetic kidney, such as MAPK, PI3K/AKT and JAK-STAT [67].

In the context of diabetes, renal cells undergo a series of pathophysiological changes that ultimately lead to podocyte loss, reduced glomerular filtration, loss of glomerular and interstitial capillaries, tubulointerstitial fibrosis and tubular atrophy, resulting in permanent renal dysfunction[27,68].The clinical features and molecular mechanisms involved in the progression of DN are summarized in Figure 1.

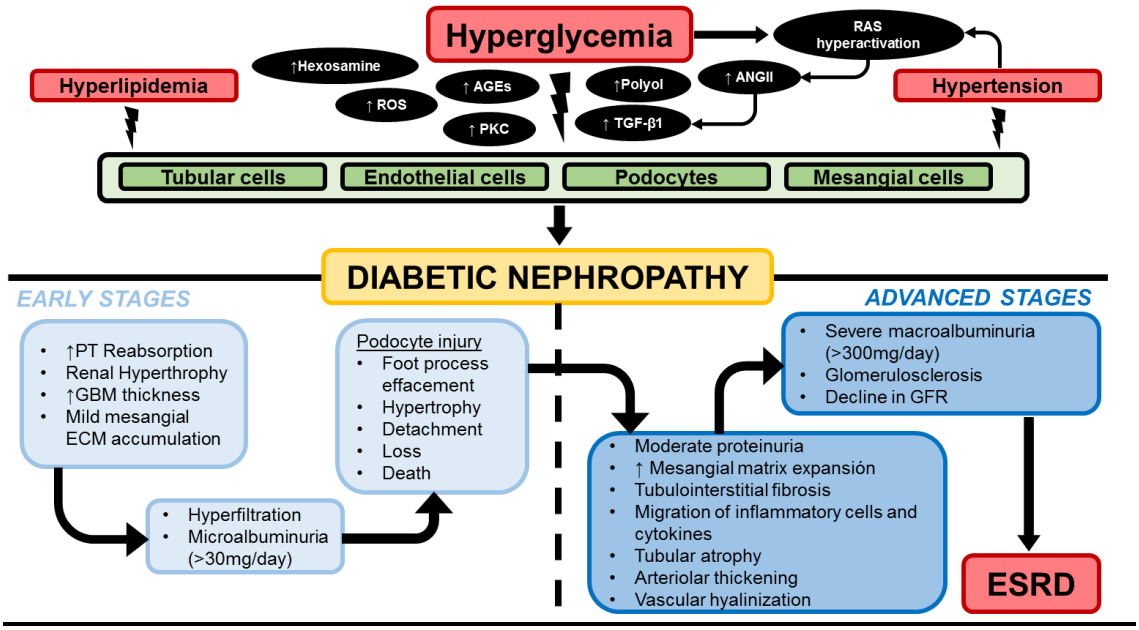

Figure 1. Pathophysiology of diabetic nephropathy. The principal factors for development of diabetic renal disease are depicted in red. The main molecules, pathways and biologic processes involved in these detrimental effects are shown in black ovals. Renal cell types susceptible to damage under diabetic conditions are depicted in green. Early renal complications are depicted in light blue. Advanced renal complications are depicted in dark blue. Progression to ESRD is represented in red. ROS, reactive oxygen species; AGEs, advanced glycosylation end-products; PKC, protein kinase C; TGF-β1, transforming growth factor 1; ANGII, angiotensin II; RAS, renin-angiotensin system; PT, proximal tubule; GBM, glomerular basement membrane; GFR, glomerular filtration rate; ESRD, end-stage renal disease.

1.A.VI Stages in the development of diabetic nephropathy

Mogensen *et al*. first characterized the natural evolution of DN into several distinct phases that can be used for both forms of diabetes (Table 1)[69]. Stage 1 includes glomerular hyperfiltration and hyperperfusion. Stage 2 is characterized by hyperfiltration and is associated with subtle morphological changes, including thickening of the GBM, glomerular hypertrophy, mesangial expansion, and modest expansion of the tubulointerstitium. This second phase is followed by changes in proteinuria that lead to an incipient DN in terms of ACR levels in the range of microalbuminuria (stage 3). Microalbuminuria has been associated with other microvascular complications, glomerular ultrastructural injury, and endothelial dysfunction or insulin resistance. After the phase of microalbuminuria, stage 4 is characterized by a continuous increase in ACR (macroalbuminuria) with declining GFR and increased blood pressure. Gradual deterioration of renal function ultimately leads to renal failure (phase 5).[69,70].

Table 1. Stages in the development of DN. Adapted from Mogensen CE et al., *Diabetes*, 1983. GFR, glomerular filtration rate; ACR: albumin-creatinine ratio; GBM, glomerular basement membrane; DN, diabetic nephropathy; ESRD: end-stage renal disease.

STAGE	DESIGNATION	CHARACTERISTIC	GFR (mL/min)	ACR (mg/g)	BLOOD PRESSURE
STAGE 1	Hyperfunction and hypertrophy	Glomerular hyperfiltration	>150	>30	Normal
STAGE 2	Silent	Thickened GBM and expanded	~ 150	>30	Normal
STAGE 3	Incipient DN	Microalbuminuria	~ 130	30-299	Increased
STAGE 4	Overt DN	Macroalbuminuria	<100	>300	Hypertension
STAGE 5	Uremic	ESRD	0-10	>300	Hypertension

1.A.VII Histopathology

The morphologic lesions in DN are predominant in the glomerular compartment[10]. Using human biopsies of patients affected by DN, Tervaert *et al*. established a standard classification of the main glomerular structural changes observed during the progression of DN, describing four classes of glomerular lesions (Table 2)[31].

Table 2. Glomerular classification of DN. Adapted from Tervaert TW et al., *J Am Soc Nephrol*, 2010. LM, light microscopy; EM, electron microscope; GBM, glomerular basement membrane.

CLASS	DESCRIPTION
CLASS I	Mild or nonspecific changes by LM, and GBM thickening by EM
CLASS IIa	Mild mesangial expansion
CLASS IIb	Severe mesangial expansion
CLASS III	Nodular sclerosis (Kimmelstiel-Wilson lesion)
CLASS IV	Advanced diabetic glomerulosclerosis

According to this classification, early histological changes include GBM thickening (Class I), glomerular hypertrophy and mild mesangial expansion (Class II). GBM thickening has been detected as early as 1.5 to 2.5 years after the onset of diabetes[10]. A first increase in the matrix component of the mesangium, which is usually moderate, focal, and segmental, can be detected as early as 5 to 7 years after the onset of diabetes (Class IIa). In a more advanced stage of disease progression, there is a more severe and diffuse mesangial matrix expansion (Class IIb). Both GBM thickening and mesangial expansion are a consequence of extracellular matrix accumulation, with increased deposition of the normal extracellular matrix local components of types IV and VI collagen, laminin and fibronectin[71,72]. In a later stage, a nodular sclerosis is observed based on the apparition of Kimmelstiel-Wilson glomerular nodules (Class III). Glomerular nodules are areas of marked mesangial expansion, with oval tuft shape, fibrillary appearance and absence of nuclei that contribute to glomerular function loss in addition to a congestion of the surrounding capillaries, especially when this lesion

progresses to advanced diabetic glomerulosclerosis (Class IV)[10]. Representative images of typical glomerular lesions in DN are shown in Figure 2.

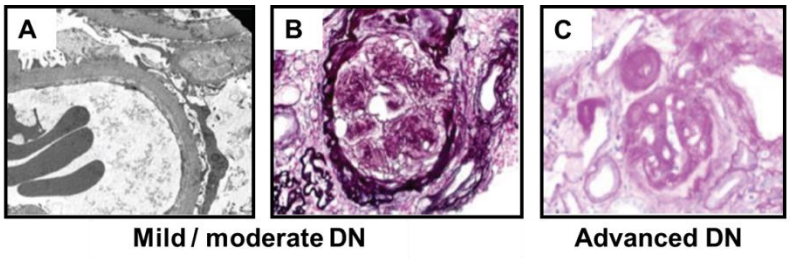

Figure 2. Glomerular histological lesions of diabetic nephropathy. Glomerular basement membrane thickening by electron microscope (A), nodular mesangial expansion (B), and nodular glomerulosclerosis (C) are associated to DN progression in humans.(Adapted from Soler *et al.*, *Experimental Diabetes Research*, 2012).

Beyond the glomerular lesions, renal vasculature lesions have also been described in terms of progressive thickening of the wall capillaries by hyaline deposition (hyalinosis). In the diabetic tubule, the most described lesions are interstitial fibrosis and tubular atrophy[31]. Moreover, other alterations such as tubular dilatation[73,74], proximal tubule vacuolization[75–77], and accumulation of large tubular glycogen deposits[78,79] have been attributed to tubular damage in both, human and experimental DN. Tubule glycogen accumulation has been associated to over-expression of muscle glycogen synthase in the human diabetic kidney[80]. Representative images of typical tubular and tubulointerstitial lesions in DN are shown in Figure 3.

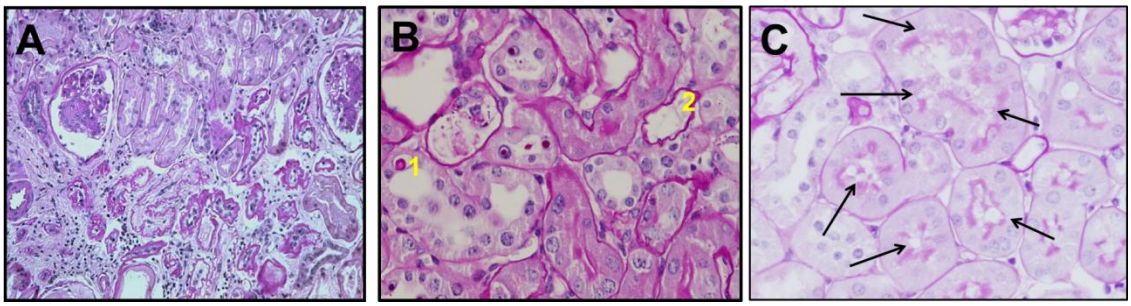

Figure 3. Tubular histological lesions of diabetic nephropathy. Panel A depicts a representative image of generalized tubular atrophy and interstitial fibrosis in a patient with T1DM (Adapted from Fioretto *et al*., *Semin Nephrol*, 2007). Panel B shows glycogen accumulation (1) and tubular atrophy (2) in the streptozotocin-induced model of T1DM. In panel C, black arrows indicate tubule vacuolization in this model.

1.A.VIII Animal models of diabetic nephropathy

Several studies have been focused in developing animal models to assess the evolution of DN and the molecular mechanisms implicated in the progression of this disease, as well as the positive and negative effects of new therapeutic strategies. Unfortunately, there are few animal models that mimic human DN and, when they do, they do not progress to advanced stages and subsequent renal failure. Whereas these

models exhibit albuminuria, development of glomerular hyperfiltration and some of the characteristic histopathological changes related to diabetes have not been consistently observed[81,82].

1.A.VIII.1 Validation criteria

In front of the lack of robust and reliable models of DN, the Diabetic Complications Consortium (www.diacomp.org) Nephropathy Committee developed a series of criteria to evaluate how mouse models resemble the human form of DN disease. These criteria define which measurements must be taken in order to assess the DN phenotype, and are summarized in Table 3.

Table 3. Functional and structural validation criteria in murine models of DN. GFR, glomerular filtration rate; GBM, glomerular basement membrane.

RENAL FUNCTION	
GFR	>50% reduction over the lifetime of the animal
ALBUMINURIA	Greater than 10-fold increase compared with controls for that strain at the same age and gender
RENAL HISTOPATHOLOGY	
GLOMERULAR PATHOLOGY	Advanced mesangial matrix expansion ± nodular sclerosis and mesangiolysis. GBM thickening by >50% over baseline
VASCULAR PATHOLOGY	Any degree of arteriolar hyalinosis
TUBULOINTERSTITIAL PATHOLOGY	Tubulointerstitial fibrosis

Despite the efforts of the consortium, currently there is not any ideal model fulfilling all the validation criteria. Therefore, when working with mouse models of DN, these criteria should be considered as goals rather than requirements, and validation of any animal model should include reasonable efforts to exclude other types of kidney disease or damage unrelated to that from diabetes[83]. Creating new experimental models that resemble human DN has been a challenge for biomedical researchers in the last decades. However, different models of type 1 and type diabetes mellitus (T1DM and T2DM) presenting histological lesions of DN have been achieved[84]. These animal models can be classified as spontaneous, pharmacologically induced, or genetically modified models, and the most widely used are described in the following lines.

1.A.VIII.2 Murine models of type 1 diabetes

1.A.VIII.2.1 Non-obese diabetic mice model

The non-obese diabetic (NOD) is a mouse model that spontaneously develop and mimics human T1DM[85]. The NOD strain practices endogamy and presents a polygenic autoimmunity that affects MHC genes and causes a progressive destruction of the pancreatic β cells by insulitis, initiated at 3-4 weeks of age[86]. An additional important

feature of this model is the variable age of diabetes onset. The incidence of diabetes in the NOD model shows a markedly sexual dimorphism, with females presenting a higher incidence rate (~80% at 30 weeks of age) than males (~20%)[87]. Albuminuria, glomerular hypertrophy, mesangial matrix expansion and podocyte loss (Figure 4), as well as structural alterations in proximal tubule, have been described in this model[88,89]. One of the main disadvantages of this strain is the need of insulin therapy for surviving long periods of time[85].

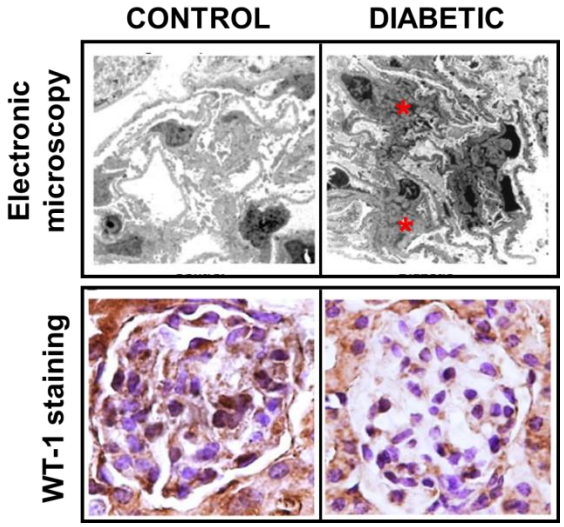

Figure 4. Glomerular lesions in the NOD model. Ultrastructural alterations analysis under the electronic microscope revealed the presence of focal mesangial expansion (red asterisks) in the glomeruli from female NOD mice after 40 days of diabetes. This matrix accumulation in the mesangium was accompanied by podocyte loss, based on a significant decrease on postitive cells fot the podocyte marker Wilms Tumor 1 (WT-1). (Adapted from Riera *et al.*, *PLOS ONE*, 2014).

1.A.VIII.2.2 Streptozotocin-induced murine model

The streptozotocin(STZ) model is a pharmacologically induced model of T1DM. STZ was originally identified as an antibiotic[90] composed of a glucosamine-nitrosourea, produced by the gram positive soil bacterium *Streptomyces achromogenes*, which exhibits a broad spectrum of antibacterial properties[91]. It was soon recognized to cause diabetes in animals secondary to pancreatic β-cell toxicity[92,93]. This drug has a glucose moiety in its molecular structure, which facilitates its transportation into β-cells by GLUT2[94].

The cytotoxic action of this drug is mediated by DNA alkylation and ROS[95]. Briefly, STZ enters the β-cell via GLUT2 and causes alkylation of DNA. DNA damage induces activation of poly ADP-ribosylation, a process that is more important for the diabetogenicity of STZ than DNA damage itself. Poly ADP-ribosylation leads to depletion of cellular NAD+ and ATP. In turn, enhanced ATP dephosphorylation after STZ treatment supplies a substrate for xanthine oxidase resulting in the formation of

superoxide radicals. Consequently, hydrogen peroxide and hydroxyl radicals are also generated. Furthermore, STZ liberates toxic amounts of nitric oxide that inhibits aconitase activity and participates in DNA damage. As a result of the STZ action, β-cells are subjected to destruction by necrosis[96].

The STZ-diabetic model typically develops albuminuria[97–99] and shows histological renal lesions such as glomerular hypertrophy, mesangial matrix expansion (in a variable degree depending on the mouse strain[82,83]), arteriolar hyalinosis or nodular glomerulosclerosis[81]. Of mention that glomerulosclerosis has been observed only in some strains with demonstrated higher susceptibility to DN disease, such as the FVB[100].

The main disadvantage of the STZ model is that STZ is also toxic to a variety of other tissues expressing GLUT2, like the kidney (nephrotoxicity)[81]. Sometimes, substantial collateral tissue toxicity may occur and complicate the interpretation of the results[101–103].

There are two standardized protocols for STZ diabetes induction: a) a high dose protocol, consisting in a single dose of STZ (150-200mg/Kg) injected intraperitoneally and b) a multiple low dose protocol consisting in 40-60mg/Kg injections for 5 consecutive days[82]. The first protocol is related to a higher degree of nonspecific toxicity. In turn, animals induced through the second protocol show less secondary toxicity, but also present a lower rate of diabetes onset and a milder DN, especially in terms of attenuated albuminuria, as compared to the animals receiving the high dose[81].

Despite its unspecific toxicity, STZ acts preferably in the pancreatic β-cells of the Langerhans islets due to its high GLUT2 expression[96]. In addition, the aforementioned potential for nonspecific renal toxicity has not been proven rigorously, and the high-dose STZ model of diabetes is widely accepted and commonly used. The STZ protocol for diabetes induction has been applied in various murine strains and genetic backgrounds[82,83,100]. Although requiring some adjustments depending on the strain employed, at present the STZ-induced is considered an established model of pancreatic toxicity, deeply studied and reproducible, that resembles several features of kidney disease described in human DN[85].

1.A.VIII.2.3 Akita (Ins2$^{WT/C96Y}$) mice model

The Akita (*Ins2*$^{WT/C96Y}$) mouse is a genetically modified model of T1DM[104–106]. This model presents a single autosomal dominant mutation in the Insulin 2 (*Ins2*) gene causing the misfolding of insulin protein[107]. This mutation exists on the C57BL/6 and C3H/He strains[108]. In these animals, accumulation of non-functional insulin promotes

proteotoxicity in pancreatic β-cells toxicity and, in consequence, the ability of the pancreatic islets to secrete insulin is substantially reduced, leading to the onset of T1DM[106].

Mice heterozygous for the Akita spontaneous mutation (*Ins2*$^{WT/C96Y}$) are viable and fertile. Mice homozygous for the Ins2-Akita allele (*Ins2*$^{C96Y/C96Y}$) exhibit failure to thrive and die within 1 to 2 months. Symptoms in heterozygous mutant mice include hyperglycemia, hypoinsulinemia, polydipsia, and polyuria beginning at approximately 3 to 4 weeks of age.

Histopathological lesions of DN, namely mesangial matrix expansion and GBM thickening, have been described in the Akita mouse model, with no evidence for mesangiolysis or nodular mesangial sclerosis[81]. In terms of glomerular function, albuminuria is not a prominent feature[109]. However, as reported in more recent studies, the previous histological lesions were accompanied by albuminuria, glomerular enlargement, renal hypertrophy, tubulointerstitial fibrosis, and oxidative stress[110,111].

One advantage on using these mice in experimental studies of DN is that, in contrast to the STZ model, Akita mice do not show non-specific toxicity. A sexual dimorphism is observed in this model, as milder hyperglycemia and lower incidence rates are detected in Akita females as compared to males. In consequence, a sufficient degree of albuminuria is rarely achieved in Akita females, which make it challenging their use in studies of DN[85,109].

1.A.VIII.2.4 The OVE26 murine model

The OVE26 is another genetically modified model of T1DM in the FVB background[81]. This model develops pancreatic damage due to overexpression of calmodulin transgene regulated by insulin promoter[112]. OVE26 mice present albuminuria, increased blood pressure and a decrease in GFR values, features that are similarly found in human DN. Nevertheless, animals show high mortality rate and need insulin therapy for long survival periods[83]. At kidney level, diabetes in OVE26 leads to augmented glomerular size, nodular and diffuse expansion of the mesangial matrix, GBM expansion, nodular glomerulosclerosis and tubulointerstitial fibrosis accompanied by mononuclear infiltration[113].

1.A.VIII.3 Murine models of type 2 diabetes

1.A.VIII.3.1 The $LepR^{db}/LepR^{db}$ (db/db) mice model

The *db/db* are genetically modified and spontaneously obese insulin-resistant mice. This model was originally obtained in the C57BLKS background and is characterized by an autosomal recessive mutation in the leptin receptor gene, responsible for the regulation of satiety[114]. The diabetic (*db*) gene encodes for a G-to-T point mutation of the leptin receptor, leading to abnormal splicing and defective signaling of the adipocyte-derived hormone leptin[115,116].

The *db/db* mutation on the C57BLKS background has been investigated intensively and exhibits many features similar to human T2DM. Specifically, the model presents obesity, hyperglycemia and hyperinsulinemia at 8 weeks of age[81]. Histopathological studies in 16-week *db/db* mice revealed the presence of glomerular hypertrophy[117], mesangial matrix expansion and GBM thickening[118], with no mesangiolysis or nodular mesangial sclerosis[119]. Arteriolar hyalinosis has also been described in this model; but there is virtually no evidence of advanced tubulointerstitial fibrosis[81]. *Db/db* mice are widely used for studies of DN and obesity[84].

1.A.VIII.3.2 The high-fat diet model

The high-fat diet (HFD) provides a commonly used approach to induce the apparition of obesity and insulin resistance in C57BL/6 mice[120–122], and is particularly useful for the study of accelerated atherosclerosis[123–126]. The effect of the diet may vary depending on the strain of mouse studied[127], with A/J mice being relatively resistant to this effect[120]. HFD-fed mice are considered a good model of DN and arteriosclerosis in T2DM[128]. Mice given a HFD present mesangial expansion and terminal glomerulosclerosis accompanied by lipid accumulation, macrophage infiltration and increased oxidative stress[129], with no evident changes in blood pressure and GFR[130,131]. Variability of glomerular functional alterations in this model may add some complexity to the study of DN, as reported effects of HFD on albuminuria are controversial[81,132].

The most relevant characteristics of each of the animal models described above are summarized in Table 4.

Table 4. Main murine models of type 1 and type 2 diabetes and their features. NOD, non-obese diabetic; STZ, streptozotocin; HFD, high-fat diet; T1DM, type 1 diabetes mellitus; T2DM, type 2 diabetes mellitus; BP, blood pressure; GFR, glomerular filtration rate; GBM, glomerular basement membrane.

MODEL	DIABETES TYPE	DIABETES ONSET/INDUCTION	MECHANISM	PHENOTYPE ALTERATIONS	KIDNEY HISTOPATHOLOGY
NOD	T1DM	Spontaneous	Autoimmune disease contributing to β-cells failure	Hyperglycemia Polydispsia Polyuria Renal hypertrophy	Glomerular hypertrophy Mesangial expansion Structural alterations of proximal tubules Podocyte loss
STZ		Pharmacologically induced	Acute necrosis of β-cells	Hyperglycemia Albuminuria Polydispsia Polyuria Renal hypertrophy	Glomerular hypertrophy Mesangial expansion Arteriolar hyalinosis Nodular glomerulosclerosis Structural alterations of proximal tubules Podocyte loss
Akita		Genetic modification	Spontaneous mutation in the *Ins2* gene, that leads to the missfolding of insuling (toxic to the β-cells)	Hyperglycemia Albuminuria Polydispsia Polyuria Renal hypertrophy	Glomerular hypertrophy Mesangial expansion GBM thickening
OVE26		Genetic modification	Overexpression of calmodulin transgene regulated by insulin	Albuminuria Increased BP Decreased GFR	Glomerular hypertrophy Mesangial expansion GBM thickening Nodular glomerulosclerosis Tubulointerstitial fibrosis Mononuclear infiltration
Db/db	T2DM	Genetic modification and spontaneous	Mutation of the leptin receptor gene induces spontanous development of obseity and T2DM	Albuminuria	Glomerular hypertrophy Mesangial expansion GBM thickening Arteriolar hyalinosis
HFD		Diet induction	Apparition of obesity and insulin resistance	Albuminuria ?	Mesangial expansion Glomerulosclerosis Lipid accumulation Macrophage infiltration

1.B RENIN-ANGIOTENSIN SYSTEM

1.B.I Definition

The renin-angiotensin system (RAS) is a coordinated hormonal cascade that regulates blood pressure and fluid balance. The physiological significance of this system resides in the homeostasis of peripheral vascular resistance as well as the regulation of volume and electrolyte composition in body fluids. RAS is an important regulator of the CV and renal function[133]. Thus, dysregulations of this system are associated to the development of CV pathologies, including kidney injury[134]. At kidney level, RAS exerts powerful influence to regulate many aspects of renal hemodynamic and transport function including the cortical and medullary circulations, glomerular hemodynamics, and the glomerular filtration coefficient in normal physiological and pathological conditions[135,136].

RAS is comprised of different angiotensin peptides with diverse biological actions mediated by distinct receptor subtypes. The emerging view of different axes within this highly complex system has led many authors to differ between classic and non-classic RAS[134]. Classic RAS is initiated by the synthesis of renin (REN) in the juxtaglomerular

apparatus, which cleaves angiotensinogen (AGT) to an inactive decapeptide, angiotensin I (ANGI). This is converted by angiotensin converting enzyme (ACE) to ANGII, a biologically active peptide that interacts mainly with AT1R at the cell surface to induce functions as diverse as vascular contractility, cellular transport, hypertrophy, growth factors synthesis, ROS generation and changes in gene expression[137,138]. The non-classic RAS is based on the ACE2-ANG(1–7)-Mas receptor axis, and generally opposes the actions of the ANGII-AT1R axis by increasing nitric oxide and prostaglandins levels, and mediating vasodilation, vascular protection, diuresis, and antioxidant effects, among other actions[134] (Figure 5).

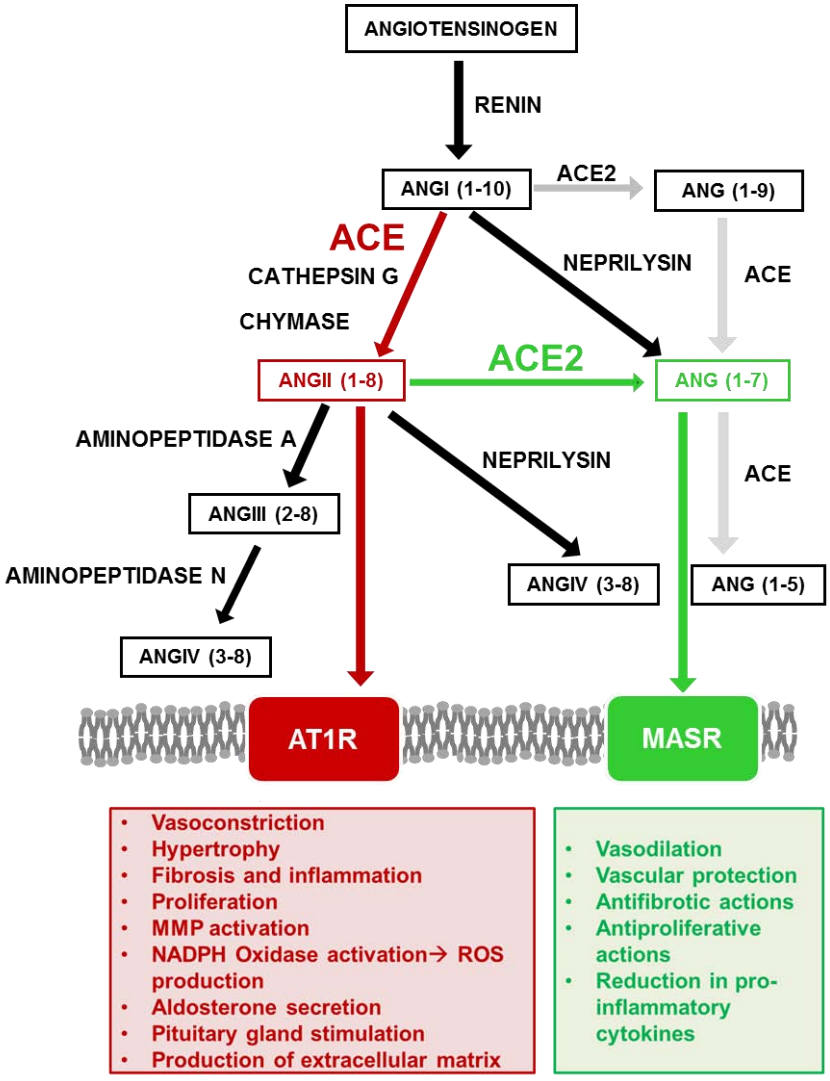

Figure 5. Schematic representation of RAS and downstream effects of ANGII and ANG(1-7) upon binding to their receptors on the cell membrane. The classic ACE-ANGII-AT1R axis and its deleterious actions (red color), and the non-classic ACE2-ANG(1-7)-MAS receptor axis and its protective effects (green) are represented. Grey arrows indicate low affinity ACE- and ACE2- activities. ANG, angiotensin; ACE, angiotensin converting enzyme; ACE2, angiotensin converting enzyme 2; AT1R and AT2R, angiotensin type 1 and type 2 receptors.

All RAS components are expressed in the kidney, suggesting the potential for local production, action and metabolism of ANGII[139]. In addition, changes in circulating and renal RAS have been associated to the progression of nephropathy[140–142]. The main components of renal RAS are described in the following pages.

1.B.II RAS activators: Angiotensinogen and renin

AGT is a 485aa plasma glycoprotein constitutively and mainly synthetized by the liver[143–145]. It is expressed in the kidney, adipose tissue, brain, heart, kidney, adrenal glands and testes[146–149]. In situ hybridization experiments localized renal *Agt* mRNA to the proximal convoluted tubule and the intrarenal vasculature, providing evidence for a local renin angiotensin system within the kidney[150].

It is generally accepted that the rate-limiting step of the renin–angiotensin system is the enzymatic cleavage of AGT to an inactive decapeptide, angiotensin I (ANGI) by renin[149]. Renin is an aspartyl protease that is synthetized by the juxtaglomerular cells on the afferent arterioles of the kidney and released to the plasma in response to various stimuli such as cAMP signaling[151–153]. Several studies in mice tissues provided evidence for *Ren* mRNA not only in the kidney, but also in adrenal glands, submandibular glands and testes[154–156]. However, it is widely accepted that systemic RAS activation is mainly controlled by the production and rapid release of renin from the kidneys into the distal tubular fluid, the interstitium and the vascular compartment, providing a pathway for local generation of ANGI[151,157–159].

Transgenic models overexpressing *Agt* and *Ren* exhibit increased blood pressure and manifest hypertensive lesions[160,161]. In addition, administration of AGT antisense mRNA to hypertensive rats induces a profound reduction in blood pressure[162]. In this sense, the AGT locus has been linked with hypertension in humans[163,164].

Urinary AGT has been proposed as a new marker for hypertension and tubular damage in diabetes. In T1DM, augmented urinary AGT precedes higher blood pressure[165], in association with intrarenal RAS activation[166]. In T2DM, urinary AGT also showed correlation with ACR and urinary α1-microglobulin[167]. It has been demonstrated that urinary AGT originates from the AGT formed and secreted in the proximal tubules[168]. Intrarenal AGT mRNA and protein levels are increased in patients and rats with diabetes as compared to their controls[169,170]. These data suggest that the enhanced AGT expression in the kidney plays an important role in the pathogenesis of DN.

1.B.III ACE

ACE is a zinc metalloprotease that acts as a carboxyl-directed dipeptidase and converts ANGI to ANGII. There are several forms of ACE, and all of them are heavily glycosylated[171,172]. Somatic ACE (MW=130-180 KDa) is mainly located in endothelial, epithelial, and neuronal cells[173,174]. This form consists on a membrane-bound protein with two large domains (N and C domains). The two domains share a high homology in their structure, and each domain contains an extracellular Zn-dependent active site[174,175]. ACE was first described within the lung[176]. Although somatic ACE is synthetized and highly expressed in this organ, evidence for ACE expression and activity has been reported in many other tissues such as the kidney, pancreas, heart, liver, adrenal gland, and testes[177,178]. ACE exerts its functions in the body tissues mainly in the membrane form, but this enzyme may be present also in its soluble form in plasma, lymph, cerebrospinal, and other biological fluids. The soluble form is generated from the membrane form by posttranslational hydrolysis of a hydrophobic peptide anchor[179].

It is generally accepted that the intrarenal formation of ANGII is largely mediated by ACE[156,180]. Thus, ACE is considered to play an important role regulating kidney function and blood pressure[181,182]. Renal ACE protein has been localized in the apical brush borders of the proximal tubules in both mice and human kidneys. Endothelial cells have also shown to express ACE within the glomeruli[183,184] and the renal vasculature[185].

Studies in human renal biopsies have revealed up-regulation of the *Ace* gene in both, the glomerular and the tubular compartments, in T2DM[186]. Despite several animal studies also detected increased ACE expression in the diabetic glomeruli, a decrease in tubular ACE has been demonstrated in diabetes[187]. In humans, the *Ace* gene is located on chromosome 17q23.3, and exhibits an insertion/deletion (I/D) polymorphism in the intron 16[188,189], which has been linked to hypertension[190–192] and CKD[193] specifically in male subjects. In the context of diabetes, however, the presence of the *Ace* I/D polymorphism seems to be irrelevant[194]. In this sense, several authors have evaluated the effect of sex on ACE expression, and its relation to DN, from a hormonal rather than from a genetic perspective[150,195].

1.B.IV ACE2

In 2000, the discovery of ACE2 led to new perspectives in the study of the RAS[138]. ACE2 is thought to counteract the effects of ACE action by catabolizing ANGII and generating ANG(1-7) through its monocarboxypeptidase activity. ACE2 also degrades ANGI to ANG(1-9), an inactive peptide (Figure 6).

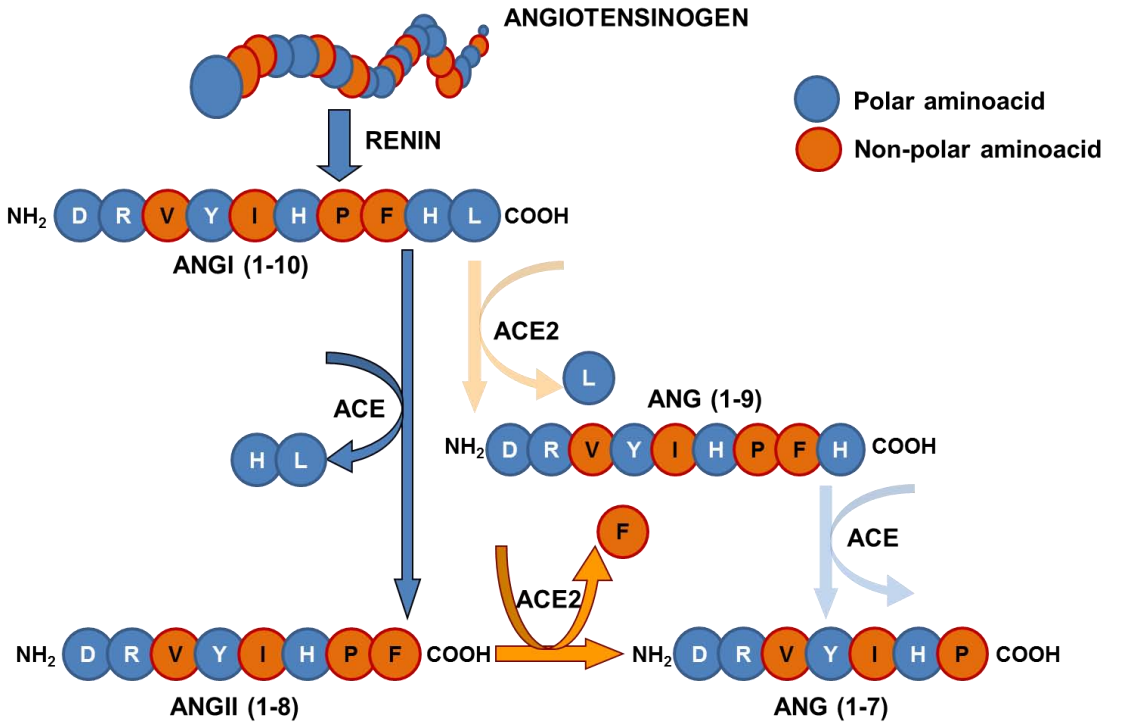

Figure 6. Opposite actions of ACE and ACE2 in the metabolism of angiotensin peptides. While ACE generates ANGII from ANGI through cleavage of the C-terminal dipeptide His-Leu, ACE2 catalyzes the conversion of ANGII into ANG(1-7) by removing the C-terminal aminoacid phenylalanine. In addition, ACE2 can cleave the C-terminal residue of the decapeptide ANGI, thus generating the nonapeptide ANG(1-9), which may be subsequently converted to ANG(1-7) by ACE.

ACE2 is a type I transmembrane glycoprotein of 120kDa and 805aa with a short C-terminal cytoplasmic tail, an hydrophobic transmembrane region and a highly N-glycosylated N-terminal ectodomain (where the active site of the enzyme is located)[196,197]. This enzyme contains a single catalytic domain (amino acids 147 to 555) that is 42% identical to each of the two catalytic domains in endothelial ACE. The domains of ACE and ACE2 and the structure of their somatic forms are compared in Figure 7.

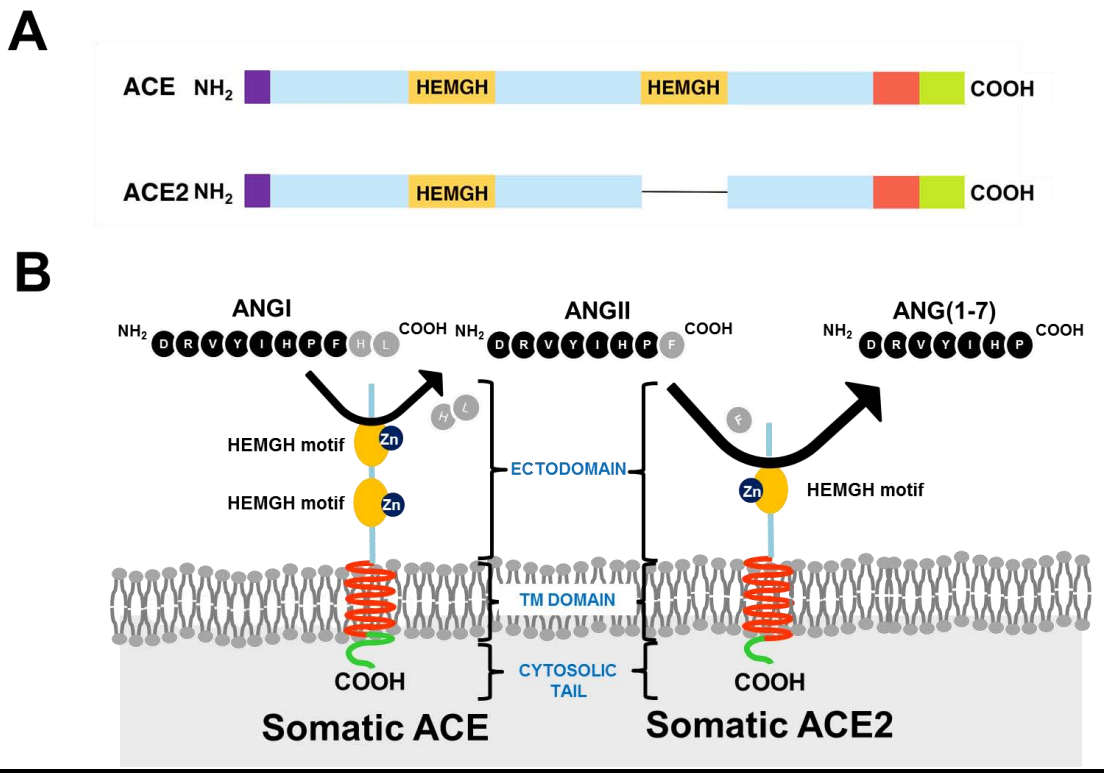

Figure 7. Comparison between ACE and ACE2 domains and structure. As shown in panel A, ACE and ACE2 share some similarities in their domain distribution, as both enzymes have a signal peptide sequence in the N-terminus (purple), an extracellular domain (blue), a transmembrane region (red) and an intracellular domain (green). The main difference between the peptide backbones of ACE and ACE2 is located in their ectodomain, and is based on the presence of two HEMGH motifs in ACE, and only one HEMGH motif in the ACE2 active site. The structure formed by these domains in the somatic, membrane-bound forms of ACE and ACE2 is also represented (B).

ACE2 is detected at high levels in kidney and heart, but is also found in other tissues such as lung, central nervous system and placenta[198–202]. *Ace2* was cloned originally from a cDNA library obtained from the left ventricle of a human heart[138]. This gene is located on the sexual X chromosome, specifically in a defined QTL associated with hypertension in animal models[196].

Within the kidney, ACE2 is predominantly localized in the tubules[183,203,204], mainly on the apical surface of S3 proximal tubules[205], where it may be subjected to a proteolytic process[206]. In this area, ACE2 has been co-localized with ACE and ANG(1-7)[183,207]. At the glomerular level, ACE2 is mainly localized in the epithelial (podocytes) and mesangial cells[183]. Soler *et al*. have demonstrated the expression of ACE2 also in the renal microvasculature (especially in the tunica media)[208]. ACE2 has a renoprotective role in the diabetic kidney[187,203,209,210]. In addition, several authors have shown that under pathological conditions ACE2 can be regulated in a sex-dependent manner[150,211,212].

1.B.V RAS effector mechanisms: ANGII, ANG(1-7), and their receptors

The octapeptide hormone ANGII is generally considered the main effector of RAS[213]. ANGII causes oxidative stress, inflammation, cell proliferation, and, as a consequence, interstitial matrix accumulation and target organ damage. In the kidney, ANGII has been shown to promote most of its effects in the renal vasculature, the glomeruli and the tubules, as they all express ANGII receptors in their cells[214]. In the blood vessels, ANGII basically induces vasoconstriction, but also endothelial dysfunction and oxidative stress, among other actions[215,216]. In the glomeruli, ANGII promotes generation of ROS, mesangial matrix accumulation, alterations in GFR, glomerulosclerosis, albuminuria and podocyte loss[217–219]. In the tubulointerstitial compartment, ANGII has shown to stimulate Na^+ reabsorption, apoptosis, renal fibrosis, and inflammation by stimulation of superoxide formation and chemokine release[220,221]. Progression of these alterations may lead to cell apoptosis and irreversible lesions in the renal tissue[222,223]. The specific actions of ANGII reported in each of the renal compartments are listed in Figure 8.

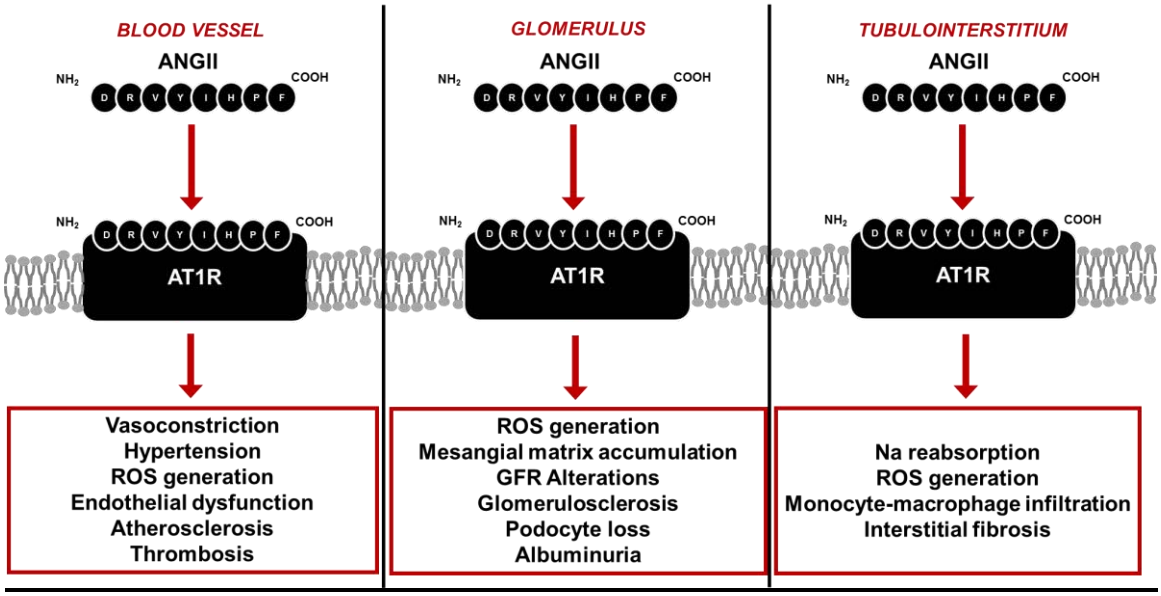

Figure 8. Principal effects of ANGII in the different compartments of the kidney. Upon binding to AT1R, ANGII activate a series of downstream deleterious effects in the renal blood vessel, the glomeruli, the tubules, and the interstitium.

ANGII exerts its effects through 2 main receptor subtypes. While stimulation of the angiotensin type 1 receptors (AT1R) causes vasoconstriction, sodium reabsorption, and cell proliferation, binding to angiotensin type 2 receptor (AT2R) triggers vasodilation, sodium excretion, and apoptosis[224,225].

Numerous studies confirm that the AT1R receptor mediates the majority of the actions of ANGII (Figure 8) and that blockade of this receptor ameliorates the deleterious effects of the peptide[226]. AT1R is widely distributed in all organs, including liver, adrenals, brain, lung, kidney, heart, and vasculature. Composed of 359 amino acids, the AT1R (40 kDa) belongs to the seven-membrane superfamily of G protein-coupled receptors. Nuclear ANGII receptors in the kidney are altered in ANGII-dependent hypertension[227]. Furthermore, Single Nucleotide Polymorphisms (SNPs) of the *At1r* gene have been attributed to an increased development of cardiovascular disease. Specifically, the A1166C polymorphism of *At1r* has been linked to hypertension[228] and ANGII sensitivity[229]. A1166C polymorphism has also been associated with the presence of diabetes mellitus in male but not female subjects with documented coronary artery disease[230]. However, there are some discrepancies about the relation between sex and the distribution of A1166C polymorphism in hypertensive populations[231,232].

Angiotensin (1-7) (ANG(1-7)) is a biologically active heptapeptide that regulates blood pressure by opposing the pressor and proliferative actions of ANGII[233,234]. Accordingly, ANG(1-7) is described as an important vasodilator, anti-fibrotic and natriuretic peptide[235]. Several investigators report that ANG(1-7)-induced vasodilatory responses may be mediated, at least in part, by increased production of prostaglandins. Nitric oxide release may also contribute to the antihypertensive actions of ANG(1-7)[236]. To date, the G-protein coupled Mas receptor is the unique identified receptor for ANG(1-7)[134].

1.B.VI Alternative pathways of RAS

The regulation of angiotensin peptides levels is also mediated by other peptidases apart from ACE and ACE2. ACE-independent mechanisms of ANGII generation involve the activity of chymase and cathepsin G (CTSG)[237,238]. Neprilysin (NEP), aminopeptidase A(APA), and aminopeptidase N(APN) are responsible for ACE2-independent ANG(1-7) production and ANGII degradation[239,240]. These enzymes are all part of the alternative RAS pathways (Figure 6), and are described below.

1.B.VI.1 ACE-independent mechanisms of ANGII generation: chymase and cathepsin G

Chymase and CTSG are chymotrypsin-like serine proteinases. Since the cleavage site between ANGI and ANGII is a phenylalanyl–histidyl peptide bond, this site is susceptible to enzymes of the chymotrypsin family[241]. Chymase and CTSG show high

structure homology (47%), and their activity toward substrates of low molecular weight (MW) is similar. However, they do not hydrolyze exactly the same peptide and protein substrates[237].

1.B.VI.1.1 Chymase

Chymase mainly exists in secretory granules of mast cells and in the extracellular interstitium[242,243]. In turn, mast cells are present in various tissues[244]. Mammalian chymases can be divided into α and β forms. It is remarkable that α–chymases but not β–chymases efficiently convert ANGI to ANGII by splitting the Phe8–His9 bond in the decapeptide[237]. To our knowledge, only one α-type chymase gene has been identified in the human body[221].

Widespread tissue distribution of human chymase has been shown, but the abundance of active enzyme varies across tissues[245]. Whereas high levels of chymase-like, ANGII-forming enzymatic activity have been detected in the skin, esophagus, stomach, and uterus; moderate levels have been found in the heart, lung, colon, tonsil, adenoid, and renal cortex; and low levels are detectable in the coronary artery, aorta, spleen, renal medulla, and liver[244–246]. As compared to other ANGII-generating enzymes, chymase is considered a very specific peptidase, as it does not hydrolyze other peptide hormones such as bradykinin and somatostatin[242]. Due to its localization, the role of this enzyme is more relevant under certain pathological conditions, especially in processes involving infiltration of mast cells[240]. In this sense, infiltration of mast cells and release of chymase into the tubular interstitium by degranulation play a pathogenic role in the development of diabetic nephropathy[247], as chymase-dependent ANGII formation contributes to the progression of tubulointerstitial fibrosis[248].

1.B.VI.1.2 Cathepsin G

CTSG was first found in the early 1980s in mammalian neutrophils, and was described as a serine proteinase that could convert circulating AGT to ANGII[249,250]. A few years later, it was stablished that this enzyme was also present in the spleen, and subcellular in the lisosomes[251]. CTSG has the capacity to degrade a wide variety of proteins including complement components, immunoglobulins, and fibronectin[252]. In addition, CTSG activity can influence the vascular tone and enhance the permeability of the endothelium [253]. Within RAS, CTSG preferentially cleaves ANGI at the Phe8–His9 site, although can also break the Tyr4–Ile5 bond[250]. In contrast to chymase, CTSG can also generate ANGII directly from AGT[251].

1.B.VI.2 ACE2-independent mechanisms of ANGII escape: neprilysin and aminopeptidases

1.B.VI.2.1 Neprilysin

NEP is a membrane-bound zinc-containing metalloproteinase with widespread tissue distribution including the brain, vascular endothelial cells, smooth muscle cells, cardiac myocytes and neutrophils. Interestingly, NEP has greatest abundance in the brush border of proximal renal tubular cells[254,255]. Together with APA, APN and dipeptidylpeptidase IV, this enzyme is one of the major kidney ectopeptidases[256], playing an important role in the catabolism of various vasoactive peptides including bradykinin, substance P, angiotensins and endothelin[257].

Within the RAS cascade, NEP transforms ANGI to ANG(1-7) with high catalytic activity, and also catalyzes ANGII conversion to ANGIV[258] (Figures 6 and 9). Thus, up-regulation of renal NEP activity in certain contexts can be considered an ANGII escape mechanism, as this enzyme not only degrades ANGII, but also prevents the production of the octapeptide[259].

1.B.VI.2.2 Aminopeptidase A and aminopeptidase N

Aminopeptidases are enzymes that catalyze the cleavage of aminoacids from the amino terminus of proteins or peptides. APA, also known as glutamyl aminopeptidase, is a zinc-dependent membrane-bound metalloprotease that catalyzes the cleavage of glutamic and aspartic amino acid residues from the N-terminus of polypeptides[260]. In turn, APN (or alanine aminopeptidase), cleaves alanine residues and also belongs to the zinc-binding superfamily of metalloproteases[240]. Within the kidney, APN has been localized in the brush border of the proximal tubular epithelial cells[239]. In this sense, urinary excreted APN is considered a marker of renal tubular damage in the context of diabetes and hypertension[261,262].

As part of the RAS alternative mechanisms, ANGII is cleaved at the N-terminus by APA to form ANGIII which, in turn, is depleted of the last N-terminal aminoacid by APN and subsequently metabolized to ANGIV (Figures 6 and 9). ANGIV is ultimately degraded into small fragments[263].

Similarly to ANGII, ANGIII (or ANG(2-8)) increases blood pressure[264] and augments aldosterone concentration[265]. Moreover, ANGIII may increase expression of growth factors and ECM proteins such as TGF-β1 and fibronectin[266], as well as attract polymorphonuclear leukocytes[240]. Of mention that ANGIII is less potent than ANGII in

terms of vasoconstrictor activity[267]. To date, there is no evidence for a specific ANGIII receptor. In the kidney, ANGIII normally binds to AT1R with greater affinity than to the AT2R receptor inducing natriuresis[268,269]. However, intrarenal also ANGIII promotes natriuresis via the AT2R in the proximal tubule by a nitric oxide /cGMP-dependent mechanism[270].

ANGIV (or ANG(3-8)) exerts very important functions in the central nervous system, where regulates memory and displays proliferative effects[271], but also acts in other tissues such as the kidney[238]. Since APA and APN are abundant in the proximal nephron, ANGII metabolism in this segment facilitates the formation of ANGIV in the glomerulus[263,272]. The receptor for ANGIV, AT4R, is an insulin-regulated aminopeptidase[273] that was initially detected in the guinea pig hippocampus[270]. AT4R is also found in the kidney, where ANGIV can elicit many responses. Upon binding to AT4R, ANGIV increases blood flow in the kidney and decreases Na^+ transport in proximal tubules[274]. Studies in AT4R knockout mice revealed that ANGIV mediates its renal vasoconstrictor effects also through binding and stimulation of AT1R[275].

In summary, RAS is a very complex hormonal pathway, where many enzymes participate in a fine tuning to regulate the levels of angiotensin peptides and their downstream effects. The specific peptide bonds hydrolyzed by the main enzymes of the classic, non-classic and alternative RAS in the aminoacid chain of AGT and the generated angiotensin peptides are illustrated in Figure 9.

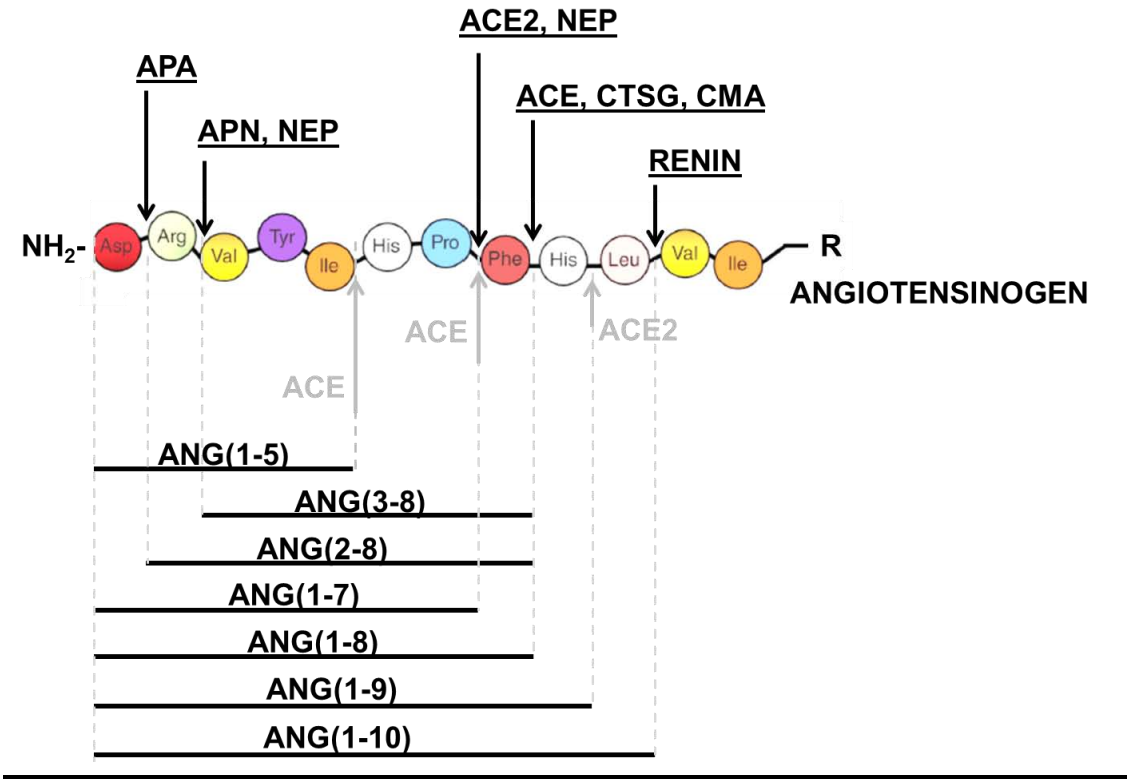

Figure 9. Cleavage sites in the metabolism of angiotensin peptides mediated by RAS carboxy- and aminopeptidases. For ACE and ACE2, high-affinity activities are colored in black, while low-affinity actions are depicted in grey.

1.B.VII RAS pharmacological modulation as a therapeutic strategy for DN treatment

The main goal for management of CKD resides on reducing the rate of progression to ESRD. In DN, the basis for the prevention and control of CKD progression is the treatment of its known risk factors, namely hypertension, hyperglycemia and dyslipidemia. The current main challenges in the treatment of patients with DN are based on preventing the progression from micro- to macroalbuminuria, as well as the occurrence of CV events[276]. To achieve this reduction of DN progression, pharmacologic modulation of the RAS at different levels has become a routinely used therapeutic strategy in the clinical practice[277].

1.B.VII.1 Classic treatments

Continuous activation of the ACE-ANGII-AT1R axis of RAS is associated to vasoconstriction of renal arterioles and triggering of pro-inflammatory and pro-fibrotic processes within the kidney, which ultimately lead to the progressive loss of renal

function[278]. Therefore, blockade of classic RAS has been largely proposed for the treatment in many kidney diseases.

Clinical studies have shown that inhibiting ACE-ANGII-AT1R axis through the action of ACE inhibitors (ACEi) or AT1R blockers (ARB) slow the progression of CKD, especially when the renal disease is associated with proteinuria[140,141,279,280]. These drugs have been considered the gold standard of treatment for more than 20 years, as their blood pressure-lowering effects have improved clinical outcomes in both diabetic and non-diabetic renal disease[141,281,282]. Thus, current clinical guidelines recommend RAS blockade in patients with DN[283].

Despite the demonstrated positive effects of RAS blockade with ACEi or ARB in DN progression, this strategy only achieves partial and non-durable suppression of the system[284]. In front of this issue, dual blockade with ACE inhibitors and ARBs was proposed as a new therapy for a better management of progressive CKD[285]. In fact, dual RAS blockade in patients with diabetes and other CV diseased resulted on a more pronounced reduction in albuminuria as compared to the monotherapies[286,287]. However, later studies demonstrated several deleterious effects of the dual RAS blockade in DN[288].

1.B.VII.2 Novel treatments

Classic treatments of RAS blockade might not be effective in some patients. Thus, there is a need for new therapeutic strategies to slow down the incidence of ESRD[289].

As a novel therapeutic approach, the dual blockade with ACE inhibitors or ARBs and aldosterone blockers is currently being studied in randomized clinical trials with DN patients[290].

Direct renin inhibitor aliskiren was also proposed as a treatment for the progression of CKD and DN. Aliskiren downregulates the first and rate-limiting step in the RAS cascade, the conversion of AGT to ANGI, thereby reducing synthesis of all subsequent components of the cascade[291]. Experimental studies showed a decrease in blood pressure, albuminuria, and serum levels of creatinine, TNF-α and C-reactive protein after Aliskiren treatment[292,293]. The antihypertensive and antialbuminuric effects of Aliskiren were also observed in the clinics[294–297]. However, these positive outcomes were not achieved when Aliskiren treatment was added to the standard RAS blockade in type 2 diabetic patients at a high risk of CV events, as this therapy resulted in an increased number of adverse effects, precipitating the cancellation of the trial[298,299].

Many authors have recently examined at experimental level the impact of compound 21 (C21), a selective AT2R agonist, on DN. Encouraging data have emerged from these studies, as C21 showed a renoprotective effect when given to animal models of diabetes[300–302]. Specifically, administration of this novel compound attenuated renal hypertrophy, albuminuria, mesangial expansion, glomerulosclerosis, oxidative stress, inflammation, and fibrosis in STZ-induced type 1 diabetic animals[300,301]. Moreover, C21 treatment enhanced the antiproteinuric effects of losartan in rats with T2DM[302].

Another very novel approach for RAS modulation is the inhibition of NEP, which has been tested in combination with the classic treatment with ARB. In clinical trials, the dual treatment with valsartan (an ARB) and sacubitril (a NEP inhibitor) was able to reduce the cardiovascular death for heart failure hospitalization. However, many trials evaluating the use of sacubitril in the renal failure of patients with diabetes are still in progress[303]. At the experimental level, as recently published by et al., beneficial effects on blood pressure and kidney function were observed after dual treatment with irbesartan (an ARB) and thiorphan (a NEP inhibitor) in diabetic and hypertensive STZ-induced transgenic mREN2 rats[304].

The classic and novel strategies of RAS pharmacological modulation mentioned above, as well as the most representative inhibitors and antagonists employed in the clinical and the experimental practice, are shown in Figure 10.

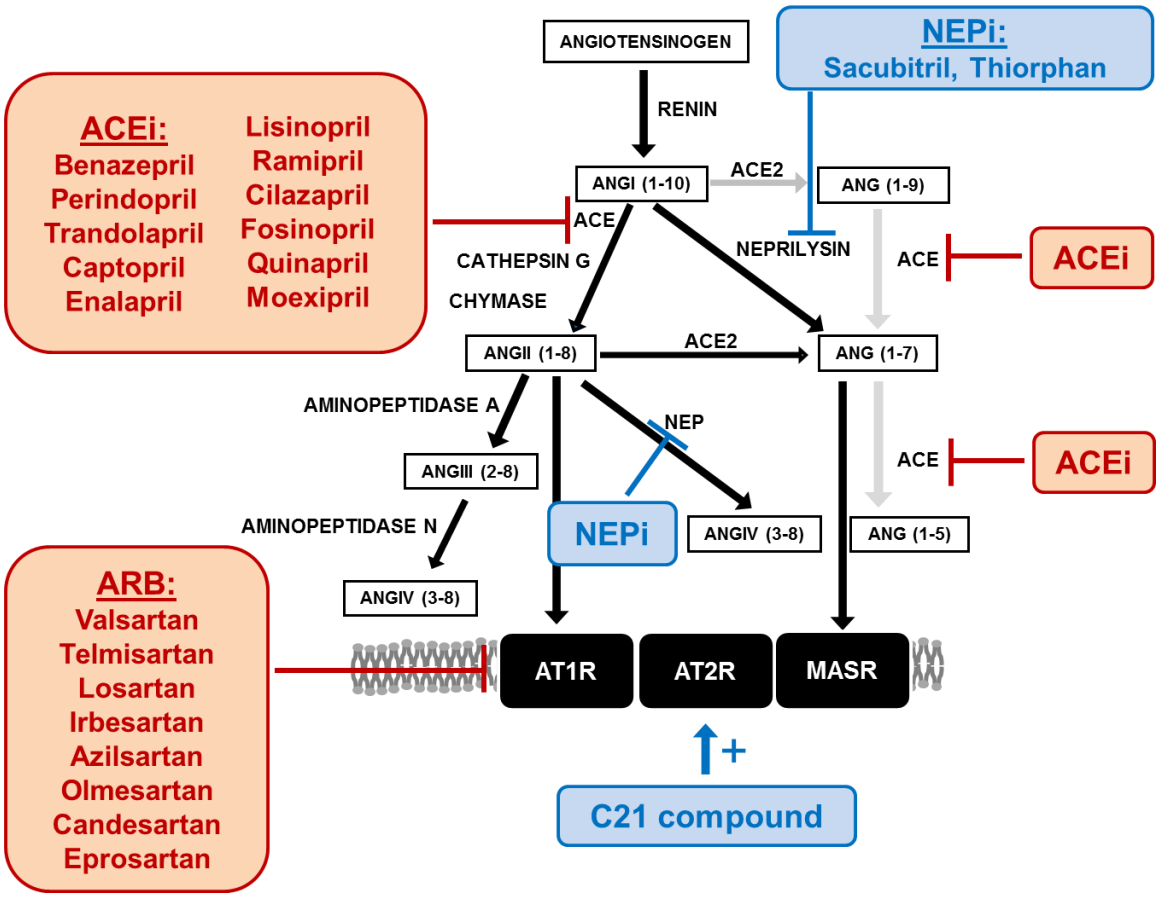

Figure 10. Pharmacological inhibition of RAS. Schematic representation of the role of ACE inhibitors (ACEi), angiotensin type 1 receptor blockers (ARB), C21 compound, and neprilysin inhibitors (NEPi) in the negative regulation of RAS. The most relevant classic treatments and drugs are depicted in red, and novel therapeutic strategies are colored in blue.

1.B.VIII ACE2 in diabetic nephropathy

1.B.VIII.1 Clinical studies

1.B.VIII.1.1 ACE2 expression in human T1DM

In human studies, serum ACE2 activity is increased in patients with T1DM, showing a positive correlation with systolic blood pressure (SBP) and diabetes duration in men. In addition, circulating ACE2 activity is increased in type 1 diabetic male and female patients with vascular complications and decreased estimated GFR, suggesting that counter-regulatory mechanisms involving changes in ACE2 levels are activated in DN[305]. Furthermore, urinary ACE2 activity and protein expression are increased in type 1 diabetic patients prior to the onset of clinical complications[306].

1.B.VIII.1.2 ACE2 expression in human T2DM

In type 2 diabetic patients with overt DN, Mizuiri *et al*. observed downregulated ACE2 and up-regulated ACE expression in the glomerular and the tubulointerstitial compartments, which led to significantly higher ACE/ACE2 ratios as compared to controls[307]. In this study, a positive correlation was found between this ACE/ACE2 ratio and the values of serum creatinine, fasting blood glucose, proteinuria and blood pressure. The same pattern of ACE2 expression was observed in the glomeruli and tubules of biopsy samples collected from patients with T2DM[308]. Conversely, Lely *et al*. detected up-regulated ACE2 expression associated to diabetes in both compartments; however, they only examined 8 diabetic patients[309].

1.B.VIII.2 Animal studies

Previous studies have shown that, in experimental DN, the pattern of renal ACE2 expression is influenced by the type of diabetes, the animal model employed and the area of the kidney evaluated[310].

1.B.VIII.2.1 ACE2 expression in experimental T1DM

In one of the first studies analyzing the modulation of ACE2 in the context of T1DM, male Sprague-Dawley rats receiving STZ and followed for 24 weeks showed a decrease of approximately 30% in renal ACE2 protein levels[204]. Whereas this decrease was reflected in the diabetic renal tubules by immunohistochemistry, a significant number of glomerular cells still showed strong positive staining for ACE2. Interestingly, when a subgroup of STZ-diabetic rats were treated with an ACE inhibitor (ramipril), the diabetes-associated decrease in renal ACE2 was prevented at the protein but not at the gene level, suggesting a posttranscriptional crosstalk between the two main regulatory arms of RAS[204]. In contrast to these observations, Wisocky *et al*. described an increase in renal ACE2 activity and protein expression after 7 weeks of diabetes in female STZ mice[187] (Figure 11). Increased renal ACE2 content was also observed in STZ males after 10 weeks of T1DM[311]. These contradictory results indicate that several factors such as the experimental model, sex and duration of T1DM may modulate the effect of diabetes on renal ACE2 expression.

Increases in ACE2 activity have also been observed recently in female diabetic NOD mice followed for 21 days (early stage) and 40 days (late stage)[89] (Figure 11). In this study, Riera *et al*. found that ACE2 activity was increased in the renal cortex, the

serum and the urine of NOD mice at both, the early and the late stages of the disease, in correlation with augmented UAE and GFR as markers of early DN. Interestingly, glycemic control by insulin administration prevented the diabetes-induced increase in circulating and urinary ACE2 activity[89], supporting the significant contribution of hyperglycemia on increasing the concentration of the soluble active form of ACE2. The effects of diabetes and insulin administration on urinary ACE2 activity were also observed in STZ male mice followed for 12 weeks[312]. Similar findings in terms of the diabetes-induced increase in renal and urinary ACE2 activity, as well as the normalization of urine ACE2 by insulin administration, have been reported in male mice from the Akita model of T1DM[313].

Interestingly, when STZ was administered to female and male hypertensive mRen2.Lewis rats, a clear increase in circulating ACE2 activity was already observed after 4 weeks of diabetes in both sexes[150]. However, this increase in ACE2 activity was not observed in the renal cortex, suggesting that the effect of diabetes on renal ACE2 can also be conditioned by the presence or absence of hypertension.

1.B.VIII.2.2 ACE2 expression in experimental T2DM

In the setting of T2DM, evident increases in renal ACE2 in terms of enzymatic activity[187,203], protein expression by Western Blot[187], and tubular expression by immunohistochemistry[209] have been consistently reported (Figure 11). Within the glomeruli, ACE2 was decreased in female *db/db* mice as compared to the *db/m* controls[209]. In contrast, ACE2 activity was increased in renal tubules[187,312].

Experimental data on DN in models of T1DM and T2DM suggest that there is a mirror effect between the patterns of renal ACE2 and ACE expression in diabetes, as up-regulation of ACE2 was always accompanied by lower ACE at the activity, protein and gene levels of expression[187,203,311]. As suggested by these investigators, increased ACE2 and decreased ACE activity may be a response mechanism in the diabetic kidney as an attempt to limit the renal accumulation of ANGII and favor the formation of ANG(1-7).

In concordance to the renal data, ACE2 activity in female *db/db* mice was increased in the serum and to a much greater extent in the urine compared with *db/m* controls. Again, the presence of a “pro-hypertensive environment” modified the effects of diabetes on ACE2, as high-salt diet (8%) increased, whereas low-salt diet (0.1%) decreased, urinary ACE2 activity in these mice *db/db* mice[312].

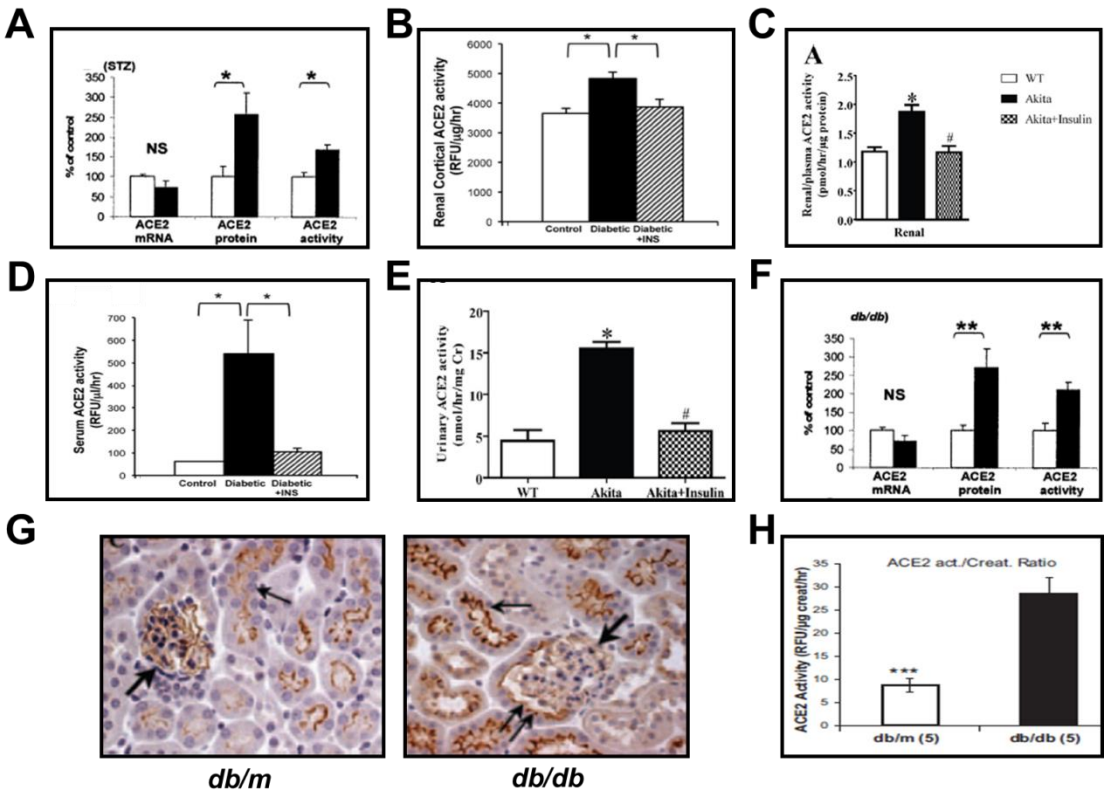

Figure 11. Up-regulation of cortical, serum and urinary ACE2 activity in experimental models of type 1 and type 2 diabetes. Increased cortical ACE2 was observed in the STZ-induced (A), NOD (B) and Akita (C) models of T1DM. The same pattern was observed in the serum and urine of NOD (D) and Akita (E) mice, respectively. In T2DM, *db/db* mice presented greater renal ACE2 than the *db/m* controls (F). These mice showed increased ACE2 positive staining in the tubule brush borders, but decreased glomerular expression (G), as well as higher urinary ACE2 activity (H). Panels A and F have been adapted from Wysocki *et al.*, *Diabetes*, 2007; panels B and D have been adapted from Riera *et al*., *PLOS ONE*, 2014; panels C and E have been adapted from Salem *et al.*, *Am J Renal Physiol*, 2012; panel G has been adapted from Ye *et al.*, *J Am Soc Nephrol*, 2006; panel H has been adapted from Whysocki *et al*., *Am J Physiol Renal Physiol,* 2013.

1.B.IX Genetic and pharmacologic modulation of ACE2

1.B.IX.1 Effects of *Ace2* deletion in the cardiovascular system

The first *Ace2* knockout (ACE2KO) animals were generated with the aim to define the role of ACE2 in the cardiovascular system and blood pressure regulation. Three lines of ACE2KO mice were generated by gene targeting by different research groups:

1. In 2002, **Crackower** *et al*. published the first study of a mouse model carrying a deletion of *Ace2* on its active site[137]. This group demonstrated that ACE2KO males in the C57BL/6 background showed a severe cardiac contractility defect at 6 months of age. This impairment in cardiac function was accompanied by morphological changes. Specifically, hearts of *Ace2* mutant mice displayed a slight wall thinning of

the left ventricle and increased chamber dimensions. These mice also presented a decrease in blood pressure[137]. However, hypertrophy and signs of cardiac fibrosis ascribed to the loss of ACE2 were not observed in this study. It is remarkable that the effects of *Ace2* deletion in CV parameters were accompanied by higher ANGII levels in the heart, kidney and plasma of these mice[137]. Interestingly, in another study, lower blood pressure values in ACE2-deficient mice under physiological conditions were already observed at the age of 3 months[314].

2. A few years later, **Yamamoto** *et al.* generated a new ACE2KO model based on the deletion of exon 3 (resulting in the absence of detectable ACE2 mRNA and protein) in the 129/SvEV and C57BL/6 mouse backgrounds[315]. This group observed a different cardiac phenotype than the reported by Crackower *et al*., without differences in contractile function and cardiac morphology between 12 and 14 weeks of age. In this study, the role of ACE2 in the CV system was further investigated by evaluating the effect of ACE2 deficiency in response to blood pressure overload in a model of cardiac failure. Blood pressure overload induced by transverse aortic constriction (TAC) led to increased cardiac hypertrophy and dilatation, as well as reduced cardiac contractility, in ACE2KO male mice as compared to the wild-type(WT)[315]. These alterations in the ACE2KO group were accompanied by the development of pulmonary congestion and increased incidence of cardiac death. On a biochemical level, cardiac angiotensin II concentration and activity of mitogen-activated protein kinases (MAPK) were markedly increased in ACE2KO mice in response to TAC. Blocking of the AT1R with candesartan attenuated the hypertrophic phenotype and suppressed the activation of MAPK in ACE2KO mice[315]. Together with the findings from Crackower *et al.*, these results suggested that the effects of *Ace2* deletion on cardiac function and morphology could be ascribed to a deficit on ANGII degradation, subsequent intracardiac accumulation of this peptide, and activation of its downstream mechanisms such as the MAPK signaling pathways.
3. In parallel, **Gurley** *et al*. generated a third ACE2KO mouse line on the ACE2 active site in 129/SvEV and C57BL/6 congenic strains, as well as in several cohorts of a 129/SvEV and C57BL/6 mixed background[316]. Results at 6 months of age showed that, in contrast to the observations from Crackower *et al.*, cardiac alterations and hypertrophy were observed in any of the three studied strains. When analyzing blood pressure, a significant increase was found in male ACE2KO animals of the mixed cohort and the C57BL/6 background. Interestingly, loss of ACE2 accentuated the increase in blood pressure induced by chronic ANGII administration, regardless of the genetic background (Figure 12A). These mice also presented a more

pronounced increase in plasma ANGII after acute infusions of the peptide (Figure 12B), reinforcing the hypothesis that major susceptibility to hypertension in ACE2KO mice was ascribed, at least in part, to a deficient ANGII degradation[316].

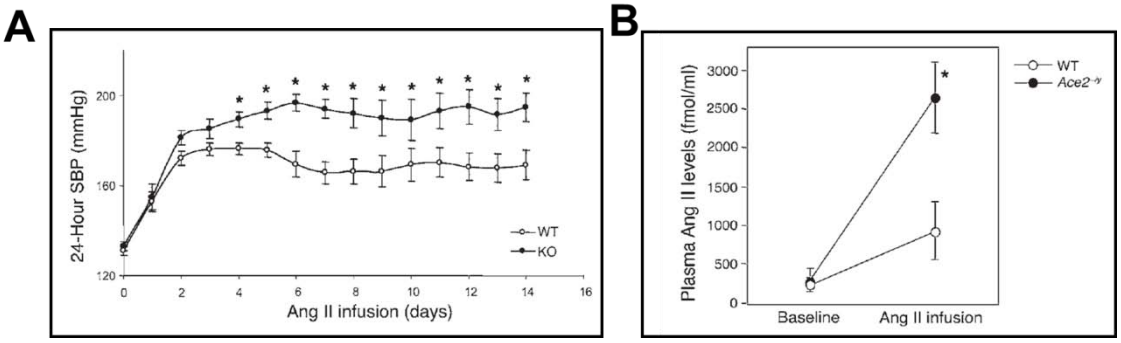

Figure 12. Loss of ACE2 accentuated the ANGII-induced increase in blood pressure and plasma ANGII levels. ACE2KO male mice presented a more pronounced increase in systolic blood pressure (SBP) after 14 days of ANGII infusion in comparison to the wild-type (WT) group (A). This higher susceptibility to ANGII-induced hypertension was accompanied by an accentuated elevation in plasma ANGII levels after acute infusion of the peptide. Adapted from Gurley *et al*., *The Journal of Clinical Investigation,* 2006.

By employing AT1R-deficient mice, the same group demonstrated that AT1 receptors are absolutely required for the development of ANGII-dependent hypertension and cardiac hypertrophy[317]. In this sense, recently it has been reported that heterozygote loss of ACE2 in females (as *Ace2* is an X-linked gene) is sufficient to increase the susceptibility ANGII-induced heart and vascular disease[318].

1.B.IX.2 Effects of *Ace2* deletion in the kidney

Oudit *et al*. were the first to assess the effect of the *Ace2* deletion in kidneys from male and female mice. According to their data, loss of ACE2 was associated with the development of age- and ANGII-dependent glomerular damage specifically in males[319]. At 3 months of age, ACE2KO male mice showed normal glomerular architecture and only mild ultrastructural alterations in terms of early fibrillary collagen deposition. At 12 months of age, loss of ACE2 led to the development of albuminuria, glomerulosclerosis, mesangial matrix expansion, and glomerular capillary hyalinosis and microaneurysms in males. These abnormalities in glomerular function and morphometry were accompanied by increased glomerular expression of the fibrotic markers collagen I and III, fibronectin, and smooth muscle actin. In addition, 1-year-old ACE2KO males displayed a marked increase in renal lipid peroxidation product formation and activation of MAPK and extracellular signal-regulated kinases 1 and 2 (ERK1/2) in the glomeruli. It is worth to mention that the structural and functional changes in the glomeruli of ACE2KO male mice, as well as the alteration of ANGII-

related mechanisms, were prevented by treatment with the AT1R blocker (ARB) irbesartan[319]. These observations were very relevant in the nephrology field, as they demonstrated a protective role of ACE2 within the kidney and opened new perspectives in the study of kidney diseases (Figure 13).

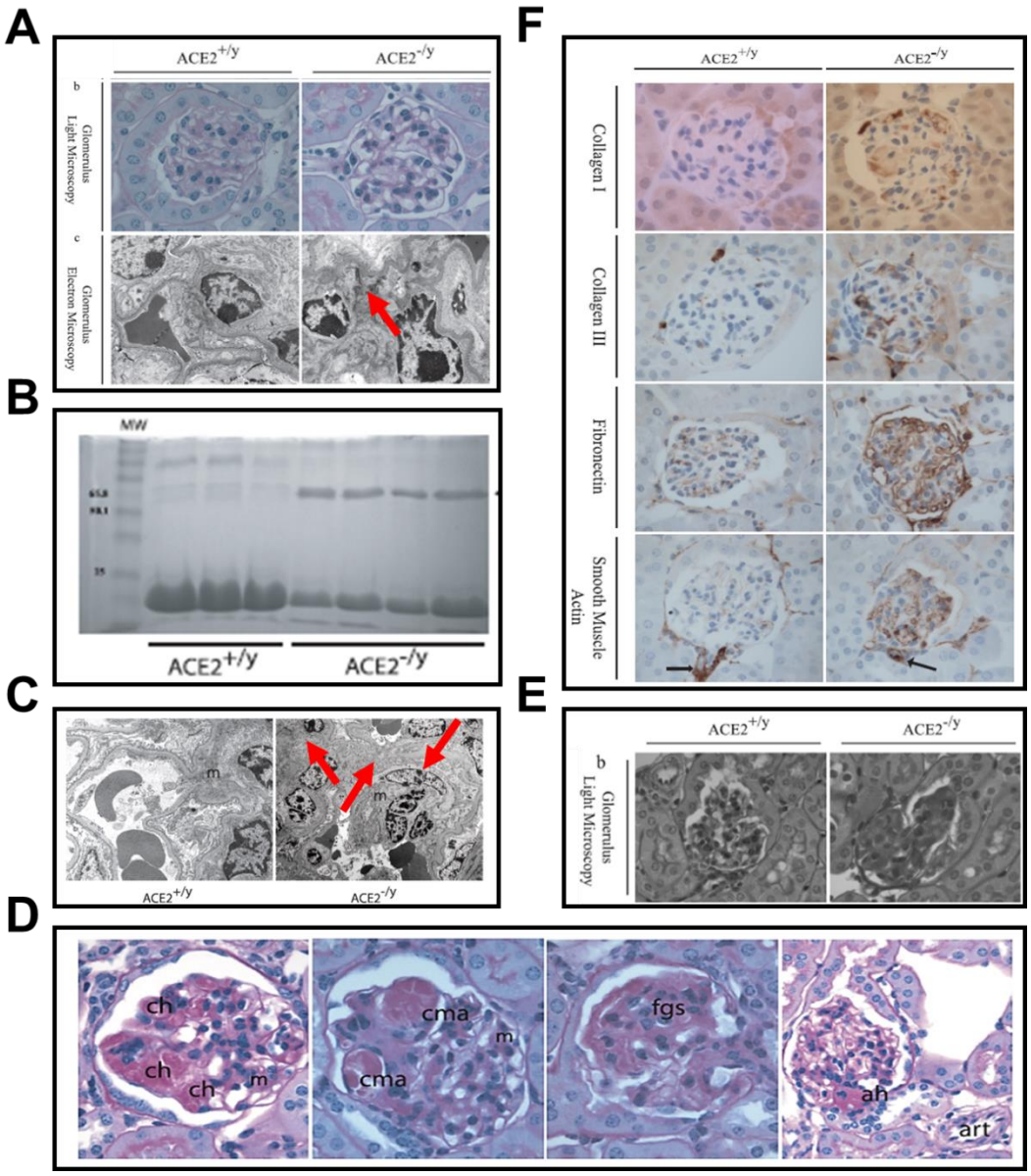

Figure 13. Functional and histological glomerular alterations associated to the loss of ACE2 in the murine kidney. At the age of 3 months, ACE2 mutant male mice ($ACE2^{-/y}$) showed normal glomerular architecture and glomerular function, and only displayed mild ultrastructural changes in terms of early fibrillary collagen deposition (red arrows) observed by electron microscopy (A). In contrast, loss of ACE2 in 1-year-old male mice led to the apparition of albuminuria (B), mesangial cell transition to smooth muscle cell phenotype (red arrows, C), capillary hyalinosis (ch), mesangial expansion (m), capillar microaneurysms (cma), arterial hyalinosis (ah, D), increased glomerular expression of several markers of fibrosis (E) and late development of glomerulosclerosis (F). Adapted from Oudit *et al.*, *American Journal of Pathology*, 2006.

Since ANGII is a strong activator of oxidative stress, Wysocki *et al*. reasoned that ACE2 could be involved in the regulation of renal oxidative stress by controlling the levels of ANGII. After assessing the levels of oxidative stress in the kidney cortex of ACE2KO and WT male mice under baseline conditions, they found that *Ace2* deletion was accompanied by increased expression of several oxidative stress markers, namely NOX4 mRNA, H_2O_2 release and urinary 8-isoprostane excretion, as well as overactivity of NADPH oxidase, which was normalized by the administration of the an ARB (losartan)[320]. In this study, kidneys from ACE2-deficient males presented a reduced capability of hydrolyzing exogenous spiked-in ANGII. The authors concluded that, similarly to previous findings in the heart[137,317], less efficient ANGII degradation in the absence of ACE2 contributed to increased renal oxidative stress levels through AT1R-dependent mechanisms[320].

1.B.IX.3 Genetic and pharmacologic inhibition of ACE2 in diabetic nephropathy

1.B.IX.3.1 Pharmacologic inhibition of ACE2 in DN

To date, pharmacologic ACE2 inhibition has been primarily performed through chronic infusion of MLN-4760, a specific ACE2 inhibitor. Supporting the protective role of ACE2 in the glomeruli observed under physiological conditions, it has been demonstrated that pharmacological inhibition of this carboxypeptidase worsens the increase in proteinuria and the development of glomerular and tubular damage in type 1[311,321] and type 2[183] diabetic mice.

After performing *in vivo* experiments of chronic infusion of MLN-4760 in female *db/db* mice, Ye *et al*. found that ACE2 inhibition promoted a more pronounced albuminuria, mesangial matrix expansion, and deposition of glomerular fibronectin[183]. Since the increase in albuminuria could be prevented by the administration of the ARB telmisartan, the authors concluded that the effects of ACE2 pharmacologic inhibition were mediated via ANGII[183].

Soler *et al.* studied the influence of ACE2 inhibition in STZ-injected females with T1DM. In a similar fashion than in the *db/db* model, ACE2 inhibition in STZ females led to a more advanced glomerular injury in terms of accentuated albuminuria mesangial matrix expansion[321]. In these mice, ACE2 inhibition exacerbated the diabetes-induced increase in glomerular and vascular ACE positive staining, as well as the decrease in tubular and cortical ACE expression (Figure 14). In concordance, Tikellis *et al*. reported

enhanced albuminuria and blood pressure in MLN-4760 treated males after 10 weeks of STZ-induced diabetes[311].

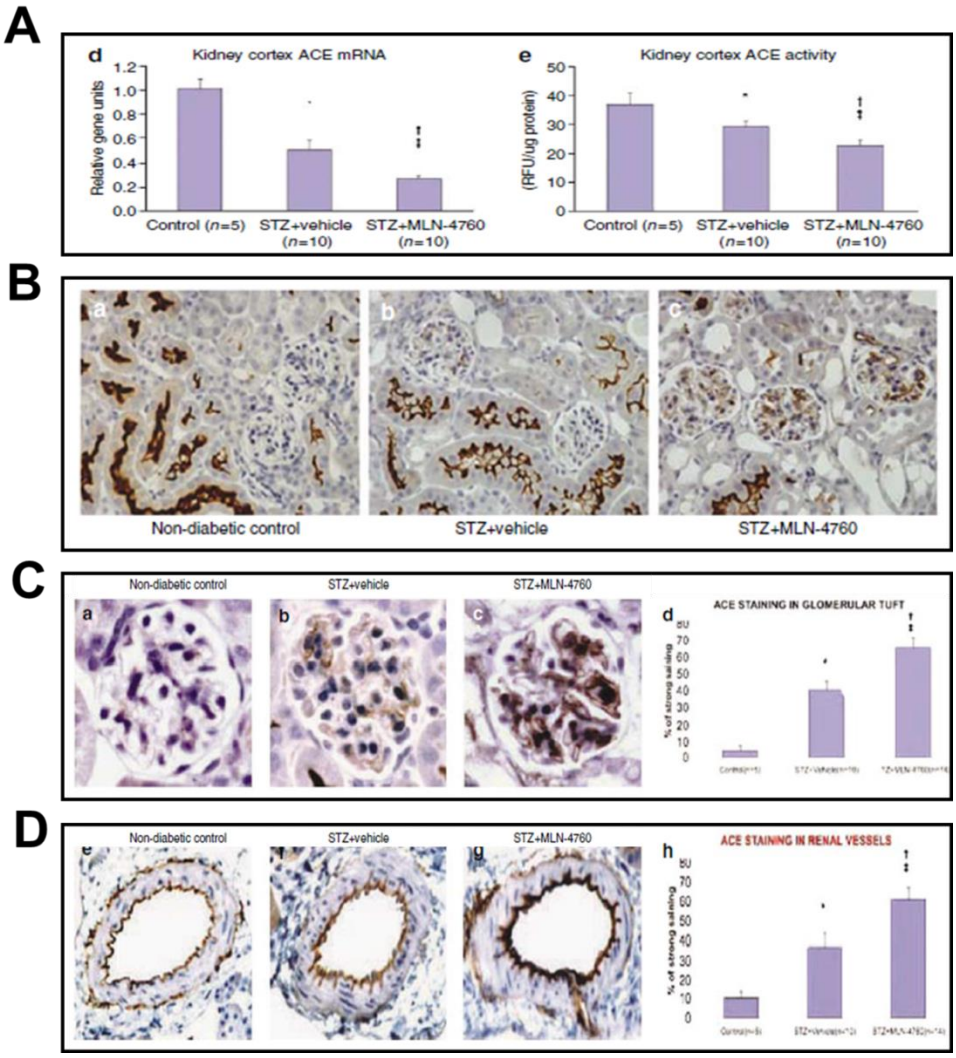

Figure 14. Pharmacological inhibition of ACE2 accentuated the effects of STZ-induced diabetes in renal ACE expression. Treatment with the ACE2 inhibitor MLN-4760 accentuated the decrease in cortical ACE mRNA and activity in STZ-induced type 1 diabetic mice (A). This decrease was primarily ascribed to lower ACE protein expression in the brush border of the cortical tubules from the diabetic and ACE2-deficient mice (B). In contrast, *Ace2* deletion was accompanied by a more pronounced increase in glomerular (C) and vascular (D) ACE immunostaining in the setting of experimental T1DM. Adapted from Soler *et al.*, *Kidney International*, 2007.

In the studies mentioned above, the glomerular structural and functional alterations in the context of diabetes and reduced ACE2 were associated to enhanced glomerular ACE-dependent ANGII production[183,321]. In fact, pharmacologic inhibition of ACE2 accentuated the decrease in cortical ACE expression and activity associated to diabetes[311,321]. Taken together, these results suggest that the classic axis of RAS may be pathologically regulated in the ACE2-deficient diabetic kidneys, and that this regulation may vary across the different renal compartments.

1.B.IX.3.2 Ace2 deletion in DN

Using a model of Akita mice crossed with previously generated ACE2KO on the C57BL/6 background[137], Wong *et al*. studied the effect of loss of *Ace2* gene in diabetic male mice at 3 months of age. The absence of ACE2 accentuated the renal hypertrophy, albuminuria, mesangial matrix expansion, GBM thickening, and glomerular fibronectin and α-SMA overexpression associated to diabetes, without altering blood pressure[314].

Tikellis and coauthors reported different results after inducing STZ-diabetes in ACE2KO males from the same strain. After 10 weeks of T1DM, the ACE2KO animals presented higher albuminuria and blood pressure than the WT. Surprisingly, glomerular hyperfiltration and renal hypertrophy and fibrosis were attenuated in diabetic mice carrying the mutated *Ace2* gene[311]. The divergences between the two mentioned studies may be explained by the variation of the severity and duration of the diabetes.

Shiota *et al*. also studied the effect of *Ace2* deletion in STZ-induced males[322]. This group, however, employed the ACE2KO mice generated by Yamamoto and colleagues[315]. Pathophysiological changes were evaluated at 4 and 18 weeks of diabetes, aiming to represent an early and a late stage of DN, respectively. Diabetic ACE2KO mice showed earlier onset and more severe progression of albuminuria, as well as a more elevated serum creatinine and urea nitrogen levels, glomerular injury and fibrosis, tubulointerstitial damage, and decreased expression of nephrin (suggesting accentuated podocyte loss) as compared to the WT group[322]. All these changes were more prominent after 18 weeks of diabetes than in the early stage, and significantly ameliorated by the ARB, olmesartan. Overall, the conclusions extracted from this study were consistent with the findings reported by Wong *et al*. in the Akita ACE2KO model[314]. The most relevant findings regarding the effects of *Ace2* deletion in T1DM are shown in Figure 15.

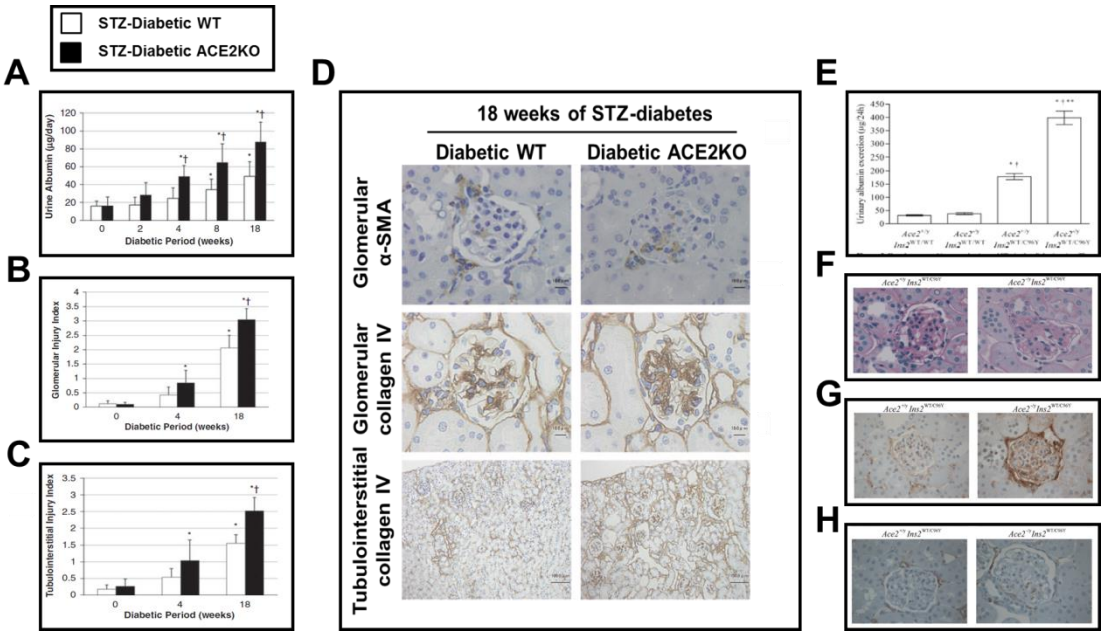

Figure 15. Loss of ACE2 in experimental T1DM. It has been reported that *Ace2* deletion accelerated and accentuated de development of albuminuria (A) and glomerular (B) and tubular injury (C) in STZ-diabetic male mice. These alterations were accompanied by increased expression of the fibrotic markers α-SMA (glomeruli) and collagen IV (glomeruli and tubulointerstitium), as compared to the diabetic wild-type (WT) group. In concordance, *Ace2* deletion in Akita male mice exacerbated albuminuria (E), mesangial matrix expansion (F) and the increase in the glomerular expression of fibronectin (G) and α-SMA (H) associated to T1DM. Panels A-D have been adapted from Shiota *et al.*, *Hypertension Research,* 2010; panels E-H have been adapted from Wong *et al., The American Journal of Pathology,* 2007.

To our knowledge, the effects of *Ace2* genetic ablation in the kidneys of type 2 diabetic animals have not been previously reported.

1.B.IX.3.3 Ace2 overexpression in DN

Cumulative evidence from studies about the specific *Ace2* genetic ablation or pharmacological inhibition has suggested a renoprotective function of this enzyme in the context of DN. This positive role of ACE2 in the diabetic kidney has been further validated in more recent studies testing the effects of genetically or pharmacologically overexpressed ACE2 on the progression and severity of experimental DN.

The administration of human recombinant ACE2 (hrACE2) is one of the strategies that has been tested in experimental studies to slow the progression of DN. In male Akita mice, treatment with daily injections of hrACE2 normalized blood pressure, reduced UAE and decreased glomerular mesangial matrix expansion and glomerular expression of α-SMA and collagen III[323]. These improvements in renal and glomerular function were accompanied by increased ANG(1–7) levels, lowered ANGII levels, and reduced NADPH oxidase activity and renal expression of *p47^{phox}* and *NOX2*[323].

In agreement with the beneficial effects of hRACE2 administration, overexpression of ACE2 through recombinant adenoviruses (Ad) carrying the murine *Ace2* RNA (obtained from previously cloned *Ace2* cDNA) also proved to ameliorate renal and glomerular injury in a rat model of STZ-induced DN[324]. Specifically, a reduction in renal hypertrophy, blood pressure, UAE, glomerular sclerosis and fibrosis, glomerular ACE staining, as well as the prevention of the nephrin decrease, were observed in the diabetic Ad-ACE2 as compared to the non-treated group[324]. The authors concluded that the beneficial effects of intravenous Ad-ACE2 administration were comparable to the observed in other treatment arm receiving the ACE inhibitor benazepril, suggesting that downregulating ANGII levels is crucial to attenuate DN, either by preventing the formation of the octapeptide through ACE downregulation or by facilitating its degradation through ACE2 up-regulation.

The involvement of ACE2-dependent mechanisms of ANGII degradation on the renoprotective effects associated to exogenous ACE2 administration has been further validated *in vitro*, as incubation/transfection of rat mesangial cells with hrACE2 or Ad-ACE2 attenuated both, high glucose and ANG II–induced oxidative stress and NADPH oxidase activity, as well as augmented the metabolism of ANGII to ANG(1-7)[323,324].

Similar effects in terms of attenuated DN in the STZ model were observed when human *Ace2* was overexpressed specifically in podocytes, where the expression of the gene was driven by the nephrin promoter using transgenic methods. In this study, transgenic diabetic mice presented a milder increase in mesangial area, decreased glomerular area, prevention of podocyte loss, and a blunted decrease in nephrin expression, as compared to the WT diabetic group[325].

1.C SEX: A CRITICAL FACTOR IN BIOMEDICAL RESEARCH

During the last years, the necessity and significance of including sex as a biological variable, not only in experimental but also in clinical studies, have gradually become a relevant and timely topic of discussion among the scientific community[326]. In the medical field, several factors such as the susceptibility to develop a certain disease, the severity of disease progression, required drug doses to achieve a certain effect, substance abuse, and responses to stress strongly depend on sex[327]. Despite this knowledge, the effect of sex is still highly ignored by many groups, as reflected in most of the recently published experimental studies. The confounding effects of the estrous cycle in females, together with the lack of understanding about the mechanisms involved in the effect of sex, has led to the convention of relying only in male animal

models, aiming to reduce the complexity when interpreting and discussing the results[326].

To avoid this growing accumulation of sex-biased scientific evidence, the NIH directors have argued that sex should be considered as a biological variable in basic research, by including both males and females, and examining sex differences in every single study. They also suggested to consider both sexes for cell lines when designing *in vitro* experiments, as female and male cells respond differently to chemical and microbial stressors[326]. While these policies are still developing, several scientists have expressed their opinion, discussing the importance and the pros and cons of considering sex differences at different levels[328]. Some authors have shown some skepticism to these new guidelines. As recently reviewed by McCarthy *et al*., there are many concerns regarding the use of both sexes in experiments *in vivo*, such as increasing the cost of the study, quadrupling animal numbers to cover every phase of the estrous cycle, or protocol variations for certain treatments (i.e. dose adjustment to avoid mortality in one of the sexes)[329]. In addition, the NIH policy of considering "the sex of the cells" has also been disputed. Many transformed cell lines are used in cell cultured research, and grow adapted to the laboratory conditions. Thus, equivalent male or female cells are virtually impossible to reproduce. In addition, these cells are derived from a single donor. Considering all these reasons, the concept of "sex" cannot be easily understood at a cellular level[330].

At the clinical level, the sex bias has also been a recurrent issue for decades. Some authors consider that the androcentric nature of science has led to the poor application of the scientific method[331]. Under the false premise that men and women are the same, men have always been predominantly included in clinical trials, with subsequent erroneous extrapolation of the results to women[332]. The arguments for the major exclusion of women from clinical trials have been based on fetal risk during pregnancy, variable results due to the hormonal oscillations during the menstrual cycle, concomitant use of exogenous hormonal contraceptives, difficult recruitment, and higher dropout rates[333]. According to the new perspective driven by NIH, these reasons are precisely why women's participation in clinical studies is necessary.

Sexual dimorphism on the progression of many renal diseases has become an area of active investigation[334,335]. In a systematic review including 130 publications reporting the prevalence of CKD in the general population, the authors found that values of CKD prevalence were stratified by sex in only the 54% of the studies, and recommended sex stratification as a premise for a better method standardization and comparability of reported data among different studies[336].

Among all cardiovascular and renal diseases, the mechanisms responsible for sexual dimorphism in diabetes and its complications have become the focus of attention of several researchers[337]. In diabetic people, men are at higher risk than premenopausal women for microvascular complications, such as nephropathy[338]. Interestingly, sex differences in the renal response to RAS blockade have also been demonstrated [133,339]. Such observations encouraged many investigators to analyze the relationship between sex, RAS, and the progression of diabetic renal disease. In this regard, clinical and experimental studies have shown sex differences in RAS components in several tissues and in the circulation[150,211,340]. In addition, chemical and surgical castration modulate the expression of different RAS components such as AGT, renin, ACE, and ACE2[195,341,342]. However, the specific mechanisms by which sex hormones such as testosterone, dihydrotestosterone (DHT) and 17β-estradiol (EST) modulate RAS expression in DN remain unclear. In front of this background, one may surmise that sex and sex hormones will exert a significant influence on diabetes, DN, RAS, and RAS blockade.

In the following sections, we aim to introduce the more relevant clinical and experimental studies focused on evaluating these sex differences in T1DM and T2DM.

1.D SEX DIFFERENCES IN DIABETES

It is generally accepted that sex and levels of androgens and estrogens determine the incidence, progression and severity of the disease. At clinical level, low testosterone levels due to hypogonadism[343], Klinefelter's Syndrome[344] or androgen deprivation therapy[345] have been associated with an increased risk of T1DM and T2DM. Moreover, correlation between estradiol levels and risk of T2DM in men after controlling for body mass index and waist circumference has been demonstrated[346]. On the other hand, estrogen replacement therapy decreases the incidence of diabetes mellitus in postmenopausal women[347], which are known to be more susceptible to develop diabetes than premenopausal women[348].

1.E SEX DIFFERENCES IN DIABETIC NEPHROPATHY

1.E.I Clinical Studies

1.E.I.1 Sex differences in diabetic nephropathy progression in type 1 diabetic patients.

Several clinical trials suggest that males with T1DM have significantly higher rates of GFR decline, and an increased risk of developing microalbuminuria and progressing to macroalbuminuria than women[349]. In another study, childhood diabetes onset was found to be protective against the development of micro- or macroalbuminuria, while the majority of the patients showing macroalbuminuria or ESRD at the last visit were adults (mean age 37.2 years)[350]. These observations suggest that elevated male sex hormone levels in the onset of diabetes predispose the patients to a worsened outcome in terms of renal disease. Accordingly, male sex has been found to be a predictor of development of microalbuminuria[351], as well as progression to macroalbuminuria[352], in type 1 diabetic patients.

In a population of subjects with insulin-requiring diabetes, some of whom had T1DM, men had significantly more microalbuminuria than women. This study found that hypertension and obesity were associated with an increase in UAE[353]. In addition, the incidence of ESRD in people with diabetes in the US was studied[354]. Among Caucasians younger than 45 years-old, the progression to ESRD was significantly increased in men compared with women (7.3/100,000 vs. 2.8/100,000, average annual increments in risk of ESRD). However, the protective effect of the female sex in the progression to ESRD was lost after menopause[354]. One may surmise that, when women lose female hormones, the positive effect disappears, and the progression of diabetic kidney disease is not favorable (Figure 16).

1.E.I.2 Sex differences in diabetic nephropathy progression in type 2 diabetic patients.

Male sex has also been associated with higher rates of albuminuria compared with females in the context of T2DM[355–357]. A prospective and cross-sectional study of the prevalence and causes of persistent albuminuria (>300 mg/24 h) conducted in 224 males and 139 females with T2DM, younger than 66 years old, revealed a higher prevalence of albuminuria in males (19%) than in females (5%)[355]. To further examine the risk factors associated with UAE in T2DM, Savage *et al*. recruited 933 patients with T2DM from the appropriate blood pressure control in diabetes trial and classified them according to UAE status. Using univariate analyses, male sex significantly correlated

with microalbuminuria and macroalbuminuria, together with Hispanic ethnicity, African-American race, poor glycemic control, insulin use, long duration of diabetes, dyslipidemia, diastolic and systolic hypertension, smoking, and obesity. However, sex differences were lost in the multivariate analysis. It is worth noting that in this study the mean age was 59 years[357]. Another prospective long-term follow-up study conducted on 574 patients (aged 40–60 years) with recent onset of T2DM showed that male sex was associated with DN according to the final value of UAE, together with low levels of high-density lipoprotein, body mass index, cigarette smoking, and low socioeconomic status[356].

In a study of national US and United Kingdom heart disease mortality for three birth cohorts (1916-25, 1926-35, and 1936-45), all birth cohort's linear heart disease mortality rates peaked in men around age 45, with slower age-related increases thereafter. Conversely, in women there was no accelerated increase in heart disease mortality rate at age 50 (menopause). In both sexes, proportional increases fit the data better than absolute increases, presumably reflecting competing risks with aging. The authors concluded that deceleration of the age-related increase in male heart disease mortality in midlife explained sex differences in CV mortality better than postmenopausal estrogen deficiency in women. Thus, at a younger age, diabetic men have an increased risk in cardiovascular diseases and DN compared with women, but once the disease is present and progresses over the years, it seems that renal and CV-related mortality tend to equilibrate[358].

The most relevant clinical studies evaluating sex differences on DN progression in type 1 and type 2 diabetic patients are summarized in Table 5.

Table 5. Sex differences in diabetic nephropathy in clinical studies. DN, diabetic nephropathy; T1DM, type 1 diabetes mellitus; T2DM, type 2 diabetes mellitus; WHR, waist-hip ratio; UAE, urinary albumin excretion; sCrea, serum creatinine concentration; GFR, glomerular filtration rate; ACEi, ACE inhibitor.

Authors and Year	Type of diabetes	Type of study	Study population	N	Focus of the study	Observations related to sex
Orchard et al., 1990	T1DM	Prospective observational study	Patients with 8 to 48 years of age and mean duration of T1DM of 20 years	657	Prevalence and interrelationships among T1DM major complications and their risk factors	Prevalence of DN is higher in females than in males at short durations
Breyer et al., 1996		Prospective, randomized double-blinded, and multicenter clinical trial	Patients 18 to 49 years of age with T1DM for at least seven years, with an onset before the age of 30 years, UAE ≤ 500mg/24 hours, and sCrea < 2.5 mg/dL	409	Predictors of loss of renal function in patients with T1DM and established DN	No differences between sexes in the progression of DN
Jacobsen at al., 1999		Prospective, longitudinal long-term up study	Normotensive T1DM patients	59	Description of the natural history of DN in normotensive T1DM	Male sex is a risk factor for enhanced decline in GFR at baseline, but not during the follow-up
Schultz et al., 1999		Prospective observational study	Children who developed T1DM before the age of 16 years	514	Predictive value of microalbuminuria in children with T1DM	The probability to develop microalbuminuria was greater in females after the onset of puberty
Holl et.al, 1999		Prospective observational study	Children, adolescents and young adults with T1DM	447	Relationship of diabetes onset and duration with UAE in pediatric patients	Female subjects with a long duration diabetes and insufficient metabolic control are especially at risk for microalbuminuria
Laron-Kenet et al., 2001		Prospective observational study	Children and adolescents (0-17 years) with T1DM	1,861	Mortality rate of subjects with childhood onset of T1DM	Among the subjects who died, the prevalence of nephropathy was higher in women
Rossing et al., 2002		Prospective observational study	T1DM patients older than 18 years followed for ≤ 10 years	537	Risk factors for development of microalbuminuria and macroalbuminuria in T1DM	No differences between sexes in the progression of DN
Cherney et al., 2005		Longitudinal cohort study	Normotensive and normoalbuminruic (UAE<20mg/min) adolescents with T1DM for more than 5 years.	22	Renal responses to hyperglycemia and ACEi treatment in diabetes	Females but not males exhibited renal hemodynamic changes during clamped euglycemia. ACEi reduced GFR only in females
Sibley et al., 2006		Observational follow-up study	Patients with T1DM from the Diabetes Control and Complications Trial/Epidemiology of Diabetes Interventions and Complications (DCCT/EDIC) database	1,185	Effect of WHR in the relation sex-microalbuminuria	Male sex presented greater UAE associated to increased WHR. However, DN in women progressed at a faster rate.
Raile et al., 2007		Prospective and multicenter study	Patients with T1DM and largely pediatric and adolescent onset of disease	27,81	Risk factors for micro-and macroalbuminuria	Male sex associated with the development of macroalbuminuria
Parving et al., 1992	T2DM	Prospective study	T2DM patients with less than 66 years of age	370	Prevalence and causes of persistent albuminuria (>300 mg/24 hr)	The prevalence of albuminuria was significantly higher in males (19%) than in females (5%)
Savage et al., 1995		Prospective, randomized, blinded clinical trial	Normotensive and hypertensive patients with T2DM and ages between 40 and 74 years. Participants in the Appropriate Blood pressure Control in Diabetes (ABCD) trial	933	Factors associated to UAE in T2DM	Using univariate analyses, male sex significantly correlated with micro- and macroalbuminuria
Ravid et al., 1998		Prospective, long-term follow-up study	Patientis aged 40 to 60 years with recent onset of T2DM. Normotesive and normal renal function and UAE at baseline	574	Role of hyperglycemia in DN and atherosclerosis in relation to other risk factors	Male sex is a risk factor for DN and arteriosclerosis

Altogether these results suggest that the deleterious effects of the male sex in the development and progression of DN, as well as the attenuation of the sex effect at a more advanced stages of life, are related to the patient age and subsequently the hormonal changes that are observed with aging in both sexes (Figure 16).

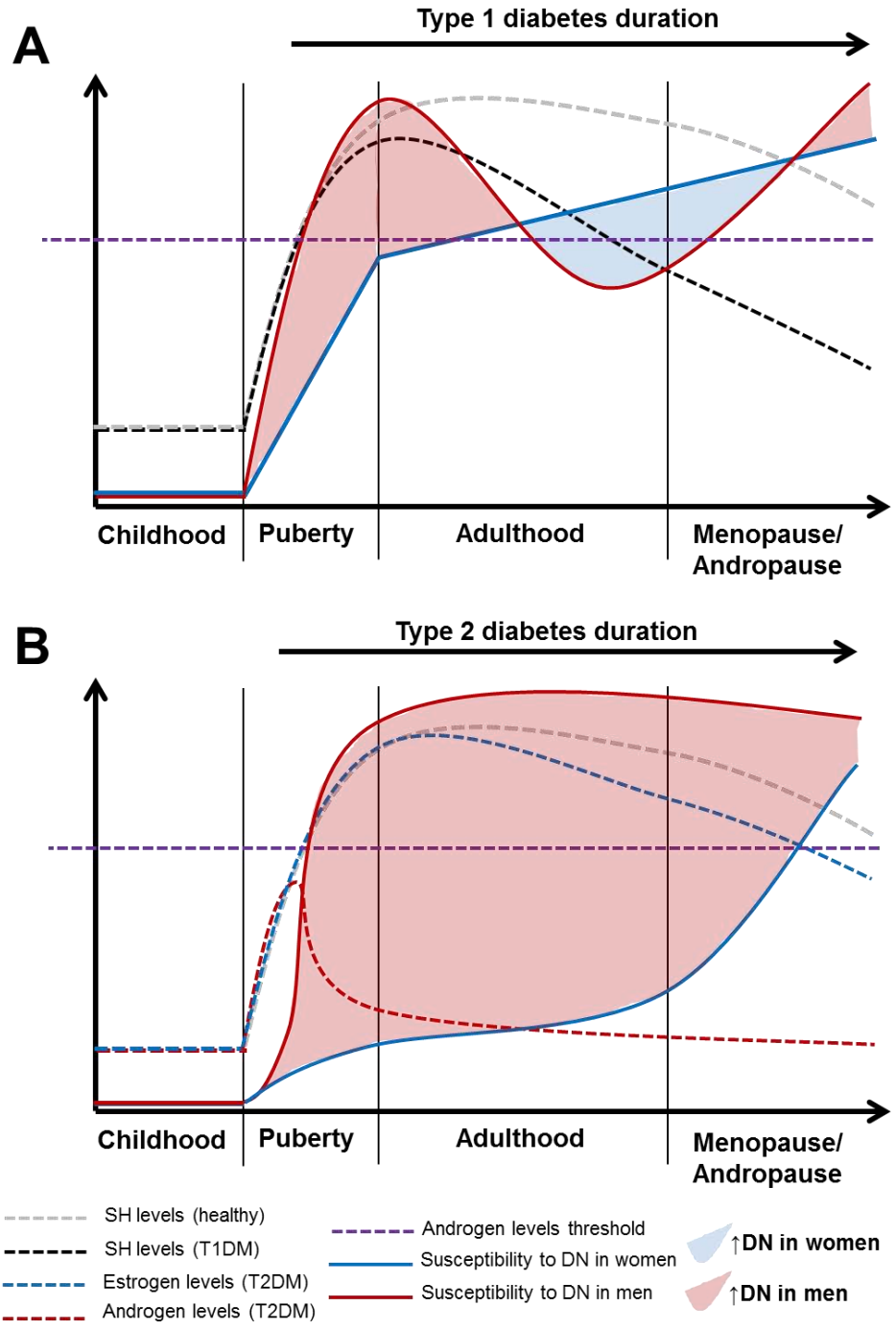

Figure 16. Schematic representation depicting the evolution of sex hormone (SH) levels throughout a lifespan under type 1 (A) or type 2 (B) diabetic conditions, and its corresponding effect on sex-specific susceptibility to develop diabetic nephropathy (DN). Under physiological conditions, male and female sex hormones dramatically increase at puberty, remain elevated during adulthood, and slightly decrease until the onset of andropause or menopause, when such decrease is clearly accentuated. During puberty, high levels of estrogens in female adolescents are protective against DN while high androgen levels predispose male adolescents to albuminuria (area depicted in red). A: after the onset of type 1 diabetes mellitus (T1DM), sex hormone levels are reduced, increasing the susceptibility of women to develop DN compared with men (area depicted in blue). When androgen levels are diminished below a certain threshold due to age and diabetes progression, susceptibility to DN in men increases again. B: type 2 diabetes mellitus (T2DM) is characterized by very low levels of androgens and higher levels of estrogens compared with T1DM. As a consequence, the incidence and severity of DN is clearly augmented in men throughout life. After menopause, the decrease of estrogen levels in type 2 diabetic women is accompanied by a rise in the progression of DN, attenuating the difference between the sexes at later stages in life.

As later explained in section 1.E.V, the influence of male and female sex hormones in the setting of T1DM and T2DM has also been investigated at the experimental level. Before, we will briefly introduce the most abundant and strong effector male and female sex hormones (1.E.II), their main signaling pathways (1.E.III), and their role in the kidney (1.E.IV).

1.E.II Principal male and female sex hormones

Testosterone, the predominant androgen in men, is synthesized from cholesterol precursor in the Leydig cells in the testes and secreted into the circulation, where tends to bind to plasma proteins[359]. Serum total testosterone is composed of 0.5–3.0% free testosterone unbound to plasma proteins, 30–44% sex hormone binding globulin (SHBG)-bound testosterone and 54–68% albumin-bound testosterone[360,361]. The sum of free and albumin-bound testosterone is named bioavailable testosterone, and represents the availability of the hormone at the cellular level[362].

Estradiol, or more precisely, 17β-estradiol, is the primary female sex hormone and is produced especially within the follicles of female ovaries[363]. 17β-estradiol can be synthetized either by testosterone oxidation catalyzed by aromatase cytochrome P-450[364], or by aromatization of androstenedione to estrone, another estrogen, which is further reduced to 17β-estradiol through 17β-Hydroxysteroid Dehydrogenase activity[365].

The metabolic synthesis pathways of androgens and estrogens from cholesterol precursor are represented in more detail in Figure 17.

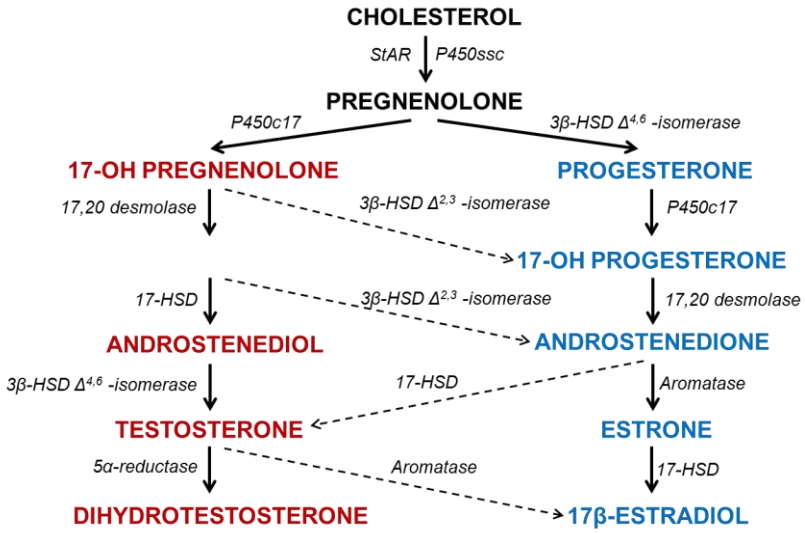

Figure 17. De novo synthesis of androgens (red) and estrogens (blue) from cholesterol. StAR, steroidogenic acute regulatory protein; P450scc, cytochrome P450 cholesterol side-chain cleavage enzyme; P450c17¸cytochrome P450 17α-hydroxylase/17,20-lyase; 17-HSD, 17-beta hydroxysteroid dehydrogenase; 3β-HSD, steroid 3β-hydroxysteroid dehydrogenase.

1.E.III Principal mechanisms of sex hormone signaling

Genomic actions of sex hormones are mediated by primary interactions with their specific nuclear receptors, formation of nuclear co-activator or co-repressor complexes, and subsequent transcriptional activation or suppression of specific target genes. In turn, non-genomic actions of sex hormones are initiated at binding sites on the plasma membrane, in cytoplasm or organelles and do not primarily require formation of intranuclear receptor protein-hormone complexes[366].

1.E.III.1 Androgen signaling pathways

In the body tissues, genomic effects of testosterone are facilitated by its conversion to DHT through 5α-reductase activity and binding to the androgen receptor (AR), which translocates to the nucleus and acts as a transcription factor. Furthermore, androgens can stimulate rapid ERK phosphorylation and activation after interacting with the G-coupled receptor GPRC6A[367,368] on the cell membrane. In addition, androgen activation of membrane localized AR leads to rapid transactivation of EGFR and, as a consequence, activation of MAPK/ERK[369] and AKT pathways[370].

1.E.III.2 Estrogen signaling pathways

Genomic actions of estrogens are mediated by their binding to nuclear estrogen receptors (ERs) α and β in target cells, which are activated and act as transcription factors to regulate the expression of target genes, ultimately controlling cell growth, differentiation, and homeostasis[371].

Subpopulations of ERα and ERβ are located in the plasma membrane, where their activation induces a variety of intracellular signaling cascades, thereby mediating the non-genomic “rapid effects” of estrogens[372,373]. More recently it has been shown that estrogens also promote rapid extranuclear signaling upon binding to the transmembrane G protein-coupled estrogen receptor 1 (GPER)[374], also designated as GPR30 and predominantly located in the endoplasmic reticulum[375] but also in plasma membrane[347]. It is known that non-genomic actions of estrogens involve rapid changes in cAMP[372,376], activation of epidermal and insulin-like growth factor receptors (EGFR and IGFR), recruitment and activation of MAPK/ERK signaling cascade[377], and induction of PI3K/AKT signaling to activate eNOS[378].

1.E.IV Androgen and estrogen signaling in the kidney

Growing experimental evidence suggests that male sex hormones play a deleterious role in kidney disease. Indeed, both androgens and estrogens have shown to trigger genomic and non-genomic events within the renal cortex[379] and in renal tubular cells in culture[380,381]. Testosterone promoted apoptosis in immortalized and primary human proximal tubule cells[380,382]. In addition, pre-incubation with the antiandrogen flutamide prevented the apoptotic effects of testosterone, indicating that deleterious effects of androgens are mediated by testosterone conversion to DHT and binding to AR. In turn, EST significantly attenuated the fibrotic effect of TGFβ-1 in mesangial cells[383]. The counter-regulatory effects of androgens and estrogens have also been observed in podocytes, where EST prevented the testosterone-induced increase in the percentage of TUNEL-positive cells. In this sense, both ERα deficiency and testosterone administration were associated with podocyte loss and augmented apoptosis *in vivo*[384]. In type 1 diabetic castrated male rats, low dose of DHT attenuated, whereas high dose accentuated, the severity of several hallmarks of kidney disease such as glomerulosclerosis and tubulointerstitial fibrosis[385].

1.E.V Experimental studies

1.E.V.1 Sex differences in experimental type 1 diabetes

Different studies in experimental models of diabetes have been performed to analyze the role of sex hormones on DN[385–387]. Sex differences in several hallmarks of diabetic kidney disease have been assessed in the STZ model. In STZ-induced 6-wk-old Sprague-Dawley rats, 12 weeks of T1DM led to significantly higher albuminuria and systolic blood pressure in diabetic males compared with females. In addition, diabetic males, but not females, showed increased renal collagen I and fibronectin gene expression compared with controls[341]. In contrast, when STZ was administrated to 11-wk-old mRen2.Lewis hypertensive rats, diabetic females exhibited a marked increase in the inflammatory marker C-reactive protein that was not evident in the diabetic males. This alteration observed in females was associated with an increase in proteinuria and albuminuria after 4 weeks of follow-up. Diabetic and hypertensive females also exhibited greater glomerular vascular endothelial growth factor staining and higher levels of inflammation in terms of tubulointerstitial $CD68^+$ cells within the kidney[150]. Of note, the onset and duration of diabetes in these studies were clearly

different[150,341], which probably determined a different hormonal status at the end of each follow-up. These data suggest that sex-specific susceptibility to develop certain features of DN can vary according to different factors, such as age, diabetes duration, and the presence of hypertension.

1.E.V.2 Sex differences in experimental type 2 diabetes

Few studies have been focused on the study of sex differences in experimental T2DM. Slyvka *et al*. demonstrated that female obese Zucker rats (*fa*/*fa*) showed better renal function than males at 13 wk of age. In addition, males exerted higher levels of endothelial and neuronal nitric oxide synthases (eNOS and nNOS) mRNA (cortex) and higher protein levels of eNOS (cortex and medulla), nNOS (medulla), and inducible NOS (cortex) than females. These differences observed may indicate up-regulation of NOS isoforms in males compared with females in an attempt to increase NO levels and vasodilation[388]. In another murine model of T2DM, the high-fat diet model, males showed increased blood glucose, UAE, and kidney weight (KW) compared with females. However, GFR was unchanged[131]. To our knowledge, no other studies on DN and sex differences have been performed in models of T2DM.

The most relevant experimental studies evaluating sex differences on DN progression in type 1 and type 2 diabetic animals are summarized in Table 6.

Table 6. Sex differences in diabetic nephropathy in experimental studies. DN, diabetic nephropathy; T1DM, type 1 Diabetes Mellitus; T2DM, type 2 Diabetes Mellitus; GDX, gonadectomy; OVX, ovariectomy; T, testosterone; DHT, dihydrotestosterone; EST, estradiol; UAE, urinary albumin excretion; GS, glomerulosclerosis; GBM, glomerular basement membrane; TGF-β, transforming growth factor beta; CTGF, connective tissue growth factor; α-SMA, alpha smooth muscle actin; ECM, extracellular matrix; TIF, tubulointerstitial fibrosis; SBP, systolic blood pressure; CRP, C-reactive protein; VEGF, vascular endothelial growth factor; TNF-α, tumor necrosis factor alpha; IL-6, interleukin 6; MMP, matrix metallopeptidase.

Authors and Year	Type of diabetes	Animal model	Follow-up	Focus of the study / Interventions	Relevant readouts	Observations related to sex
Sun et al., 2007	T1DM	STZ-induced Sprague-Dawley rats	6 weeks	Effect of rising androgen levels at puberty in DN. GDX and T treatment to adult and juvenile male rats, respectively	Profibrotic markers: TGF-β1, TGF-β2, TGF-β3, CTGF, α-SMA	Testosterone treatment permits profibrotic events in the tubules of juvenile rats with T1DM, although GDX is not completely protective for animals with adult-onset T1DM
Mankhey et al., 2007		STZ-induced Sprague-Dawley rats	12 weeks	Mechanisms by which EST regulates ECM metabolism related to GS and TIF. EST supplementation to diabetic females	GS, TIF, renal fibronectin and collagen I and IV, MMP-2 and MMP-9 protein expression	EST supplementation is renoprotective by attenuating GS and TIF by reducing ECM synthesis and increasing ECM degradation
Dixon et al., 2007		STZ-induced Sprague-Dawley rats	17 weeks	Effects of EST in established DN. EST supplementation to female rats after 9 weeks of diabetes	UAE, GS, TIF, renal collagen I and IV, MMP-2, MMP-9 and TGF-β protein expression	EST attenuates the progression of DN once it has developed by regulating ECM
Xu et al., 2008		STZ-induced Sprague-Dawley rats	14 weeks	Effects of longer-term diabetes on the relative balance of sex hormone levels and their contribution to the pathophysiology of DN. GDX to diabetic male rats	GS, TIF, renal collagen I and IV and TGF-β protein expression, $CD68^+$cells	Castration exacerbated DN
Xu et al., 2009		STZ-induced Sprague-Dawley rats	14 weeks	Influence of DHT supplementation on attenuating castration effects in type 1 DN. Administration of low and high dose of DHT to castrated STZ males	UAE, GS, TIF, renal collagen I and TGF-β protein expression, $CD68^+$cells	Detrimental effects of GDX in the diabetic kidney can be attenuated with low doses of DHT
Yamaleyeva et al., 2012		STZ-induced mRen2.Lewis rats	4 weeks	Impact of early diabetes on the circulating and kidney RAS in male and female hypertensive rats	Proteinuria, albuminuria, glomerular VEGF expression, CRP, $CD68^+$cells	Female mRen2.Lewis rats are more susceptible to vascular damage, renal inflammation, and kidney injury in T1DM
Manigrasso et al., 2012		STZ-induced Sprague-Dawley rats	12 weeks	Effect of combined therapy of DHT supplementation and inhibition of estradiol synthesis in DN in males	UAE, GS, TIF, $CD68^+$cells, renal TGF-β, collagen IV, TNF-α and IL-6 protein expression	Combined therapy of DHT and aromatase inhibitor resulted in attenuation of albuminuria by 84%, glomerulosclerosis by 55%, and tubulointerstitial fibrosis by 62% in T1DM males
De Alencar et al., 2015		STZ-induced Sprague-Dawley rats	12 weeks	Role of androgens in DN. Subcutaneous anti-androgen treatment with Flutamide	UAE, SBP, renal collagen I and fibronectin gene expression	Higher albuminuria, SBP and renal fibrosis markers expression in diabetic males as compared to females. Anti-androgen treatment decreased albuminuria only in diabetic males
Tomiyoshi et al., 2002	T2DM	OLETF rats	58 weeks	Effects of sex hormones on DN. GDX and EST supplementation to male OLETF rats	UAE, GS, glucose tolerance, mesangial expansion, GBM thickening	GDX ameliorated DN. EST failed to attenuate proteinuria and GS
Chin et al., 2005		db/db mice	18 weeks	Therapeutic effectiveness of EST and raloxifene for preventing functional and histological alterations in T2DM female kidneys. EST or raloxifene supplementation to OVX diabetic females	UAE, mesangial expansion, fibronectin protein expression	EST treatment significantly ameliorated albuminuria, attenuated weight gain, and reduced hyperglycemia in OVX female db/db mice.

1.E.V.3 Experimental studies with androgen supplementation or deprivation.

Testosterone administration promotes tubular damage in STZ-induced rats. Sun *et al*. demonstrated that testosterone worsens tubular damage in diabetic rats in terms of increased fibrotic markers, such as α-SMA and fibroblast-specific protein, two markers of cell damage and potential epithelial mesenchymal transition[385]. In concordance, Xu and colleagues demonstrated that the administration of a high dose of DHT also exacerbated the development of albuminuria, index of glomerulosclerosis, and tubulointerstitial fibrosis associated with diabetes. However, a lower dose of DHT attenuated renal injury in castrated diabetic rats. DHT may play an important role in the pathophysiology of diabetic renal disease, and these effects are dose-dependent[387].

Thus, a dual and dose-specific effect of DHT in the diabetic kidney has been observed; while the administration of low doses of DHT is renoprotective, higher doses induce damage. There are several potential explanations for this apparent paradox, including dose-dependent expression and activation of AR interacting with transcriptional coactivator proteins; however, the most likely explanation is that of the indirect effect of EST rather than the direct effects of DHT.

Interestingly, while diabetic male rats previously presented a reduction in the ratio of AR to ER protein expression in the renal cortex compared with non-diabetic animals[389,390], the dual treatment with DHT and anastrozole (an aromatase inhibitor) restored this ratio[391]. Considering that changes in sex hormone receptor expression in the diabetic kidney may reflect altered levels of circulating androgens and estrogens, it is conceivable that the diminished renal alterations observed after this dual treatment were achieved by restoring relative balance between sex hormones.

The effect of surgical androgen depletion by castration is controversial. While Xu *et al*. showed that castration worsens albuminuria as a marker of renal function in type 1 diabetic rats[387], in the Otsuka-Long Evans-Tokushima fatty (OLETF) rat, a model of T2DM[392], and the Cohen diabetic rat, a genetically selected sucrose-fed rat, castration attenuated proteinuria[393]. In addition, in the STZ model of T1DM, castration was shown to have neither a detrimental nor a protective effect on the progression of diabetic renal disease[385]. These apparent discrepancies in the effects of castration on diabetic renal disease may be ascribed to the duration and model of diabetes.

1.E.V.4 Experimental studies with estrogen supplementation or deprivation

Supplementation with EST exerts a protective effect on the development of functional and structural kidney damage by reducing albuminuria, glomeruloesclerosis, and tubulointerstitial fibrosis after several weeks of untreated diabetes[394–396]. These effects have been attributed to different cellular mechanisms, including reduction of TGF-β collagen type IV, laminin, and fibronectin, and increased production of matrix metalloproteinases (MMP)[397–399].

The protective effects of estrogens have also been described in podocytes. EST treatment protected non-diabetic podocytes from apoptosis induced *in vitro* by TGF-β and TNF-α[384]. Such effect may be mediated by activation of the phosphatidylinositol-4,5-bisphosphate 3-kinase (PI3K)- protein kinase B (AKT) signaling cascade, since podocytes isolated from EST-treated *db*/*db* mice presented increased levels of AKT phosphorylation. Activation of extracellular signal-regulated kinases (ERKs), another

downstream pathway of TGF-β signaling, was decreased in these EST-treated podocytes. Lower activation of ERK may lead to increased expression of MMP2 and MMP9, which could explain the amelioration of ECM accumulation and glomerular basement membrane thickening observed in these mice. In addition, estrogens are thought to potentially decrease reactive oxygen species (ROS)-induced events by regulating podocyte antioxidant markers, such as Mn-superoxide dismutase and glutathione[400].

In contrast, EST administration exacerbated renal disease in Cohen sucrose-fed[401] and OLETF rats[392]. It has been demonstrated that, after experimental induction of menopause, renal damage develops more rapidly and severely in diabetic postovarian failure female mice compared with cycling females[402], in association with decreased cortical MMP9 expression. Levels of MMP9 were also downregulated by ovariectomy in diabetic[396] and Dahl salt-sensitive[403] rats. Thus, loss of estrogens after menopause may explain the observed decrease in MMP9 expression, which can possibly lead to pathological accumulation of ECM.

1.E.VI Alterations in circulating and renal sex hormone signaling in diabetes

1.E.VI.1 Alterations in circulating and renal sex hormone levels in T1DM

The relationship between T1DM and serum androgen levels is controversial. In some studies, men with T1DM do not show a high prevalence of androgen deficiency[404,405]. However, Maric *et al*. demonstrated that diabetes without renal disease was associated with decreased testosterone and estrogen levels compared with healthy non-diabetic adult men. In this study, progression of renal disease from micro- to macroalbuminuria accentuated the decrease in serum total testosterone[406]. Renal complications derived from T1DM are rarely observed before puberty[407]. When studying women, Amin *et al*. found that testosterone levels were increased in T1DM patients with microalbuminuria compared with the normoalbuminuric ones[408]. These results suggest that high androgen levels predispose T1DM females to the development of microvascular disease such as DN.

In experimental models of T1DM, assessment of the effect of hyperglycemia on male fertility in rats revealed that animals injected with STZ also showed significant decrease in serum testosterone levels, which were accompanied by diminished testicular and epididymal weight[409]. Interestingly, elevation of circulating testosterone by arecoline in rats with established T1DM was associated with increased levels of

serum insulin and up-regulation of critical genes related to β-cell regeneration, such as glucose transporter 2[410].

Castration in male rats with T1DM worsened renal injury accompanied by a reduction of serum testosterone and kidney AR expression. Interestingly, circulating EST levels and kidney aromatase activity remained increased after removal of male sex hormones, providing stronger evidence for extratesticular sources of EST, while the expression of kidney ERα was not altered[387,390]. These results may suggest that testosterone-EST-ERα, rather than the testosterone-DHT-AR axis, plays a role in the development of nephropathy in T1DM males. Of note, proinflammatory cytokines are known to upregulate the activity of aromatase, to effectively reduce testosterone levels, and increase the intracellular concentration of EST[411]. Thus, the particular inflammatory status in type 1 diabetic males might explain the divergences in EST patterns observed in different studies.

Whether the estrogen signaling pathway is also detrimental for diabetic females is controversial. Several authors have reported that T1DM is associated with decreased EST levels in human[412–414] and animal female subjects[415,416]. In this context, decreased EST levels have been associated with an imbalance in the expression of renal ERs. Specifically, female diabetic kidney exhibited increased protein expression of ERα, but not ERβ[390,416]. While ovariectomy increased renal ERα and reduced ERβ expression in these diabetic females, EST administration caused the opposite effect[390]. In this sense, it has been reported that the deletion of *ERα* in STZ-induced females attenuated the development of albuminuria and glomerular hypertrophy, suggesting a role of ERα on promoting harmful events in the kidney[417]. Interestingly, the absence of ERα in non-diabetic mice was not protective and led to the development of glomerulosclerosis, probably due to accumulation of endogenous testosterone[418]. Thus, despite that ERα-mediated actions may be beneficial under physiological conditions, it is presumable that decreased estrogen levels in females with T1DM promote pathological overexpression and hyperactivation of renal ERα that, together with a downregulation of the protective effects of ERβ, may contribute to a more severe progression of DN.

1.E.VI.2 Alterations in circulating and renal sex hormone levels in T2DM

Grossmann *et al*. demonstrated in a cross-sectional survey that testosterone deficiency is common in men with diabetes, regardless of the type[419]. However, clinical evidence supports that low testosterone levels are more strongly associated with T2DM rather than T1DM. This tendency has been observed when studying either young or old patients with diabetes[420,421]. Poor glycemic control in Korean men with T2DM resulted in increased levels of fasting plasma glucose and HbA1c values, the major markers of diabetes, which appeared to be associated with testosterone deficiency[422]. In addition, diabetic men had also lower levels of sex hormone binding globulin (SHBG) compared with non-diabetic men[405,423]. In fact, several prospective studies have shown that diabetes and metabolic syndrome are more strongly predicted by low SHBG than by low testosterone[424–426].

T2DM is associated with augmented EST levels in men[427,428]. These increased EST levels are associated with complications, such as atherosclerosis, in men with T2DM and metabolic syndrome[429,430]. The activation of GPER30 in isolated rat Leydig cells and adult human testis downregulates testosterone production[431]. It is conceivable that these EST-mediated mechanisms exacerbate the reduction on circulating testosterone levels in T2DM, conferring a reasonable explanation to the fact that type 2 diabetic men show a clearly increased susceptibility to develop DN than women (Figure 16). These findings suggest that in T2DM males there is an imbalance between sex hormones that exacerbates DN. When studying ERs, Doublier *et al*. found that the beneficial effects of EST treatment on attenuating DN in type 2 diabetic female mice were accompanied by increased ERβ but not Erα protein expression within the podocyte[384]. While interaction between EST and ERα seems to be detrimental in T2DM, activation of ERβ can be considered renoprotective. Interestingly, it has been found that aldosterone activates GPER30 inducing its rapid vascular effects. Under physiological conditions, these GPER-mediated non-genomic effects are considered beneficial in the vasculature[432].

However, T2DM in female *db*/*db* mice increased expression of GPER30 in mesenteric resistance arteries and impaired the vascular effects of aldosterone[233]. Thus, hyperactivation of GPER30 also plays a role in the pathophysiology of DN, at least at the vascular level. These vascular alterations can be attributed to the hyperactivation of circulating RAS in diabetes, which may lead to higher ANGII levels and, in consequence, increased stimulation of aldosterone secretion by adrenal glands and further GPER30 activation.

1.F SEX DIFFERENCES ON RAS IN DIABETIC NEPHROPATHY

Renal and peripheral hemodynamic responses to RAS activation and blockade may vary according to sex[433,434]. However, few studies assessing sex differences at different levels of renal and circulating RAS in the context of diabetes have been performed.

1.F.I Sex differences on RAS activation: angiotensinogen and renin

Renal AGT expression was increased in males (but not in females), showing strong association with albuminuria and renal fibrosis, in STZ-diabetic Sprague-Dawley rats. On the contrary, the plasma activity and renal mRNA levels of renin were decreased in both diabetic males and females. AR blockade by flutamide administration decreased UAE only in diabetic males without affecting the endocrine or renal RAS[341]. In concordance to cortical data, diabetes increased the medullary AGT content in male STZ Wistar rats. A diabetes-induced increase of urinary AGT was also found[435](Figure 18). Thus, the increase of renal AGT in the setting of diabetes is mainly observed in males, whereas the AGT decrease in plasma from diabetic animals is observed in both males and females. These results suggest that there is a difference in the regulation of intrarenal and circulating RAS depending on the sex, which add complexity to the system (Figure 18).

In rodent models[436,437] and in patients with diabetes[169], ROS are important for intrarenal AGT augmentation in the progression of DN, highlighting the importance of the activated oxidative stress-AGT-RAS axis in the pathogenesis of DN. In addition, the redox-responsive transition of AGT to a form that preferentially interacts with receptor-bound renin has been demonstrated by crystallography and kinetic analysis[438].

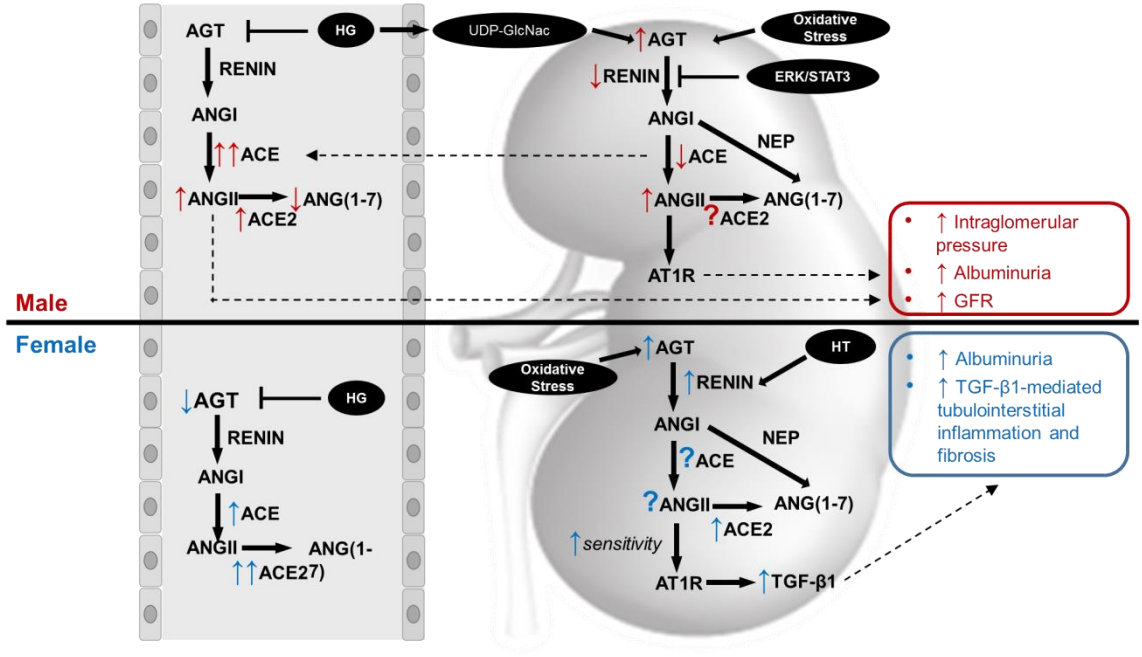

Figure 18. Sex differences in circulating and renal RAS in DN. Red arrows indicate effects associated with androgens or male sex, whereas blue arrows correspond to estrogens/female sex. In diabetic males, hyperglycemia [via the uridine diphosphate N-acetylglucosamine (UDP-GlcNac) pathway] and oxidative stress provoke augmentation of renal angiotensinogen (AGT). Inhibition of renin synthesis via extracellular signal-regulated kinase (ERK)/signal transducer and activator of transcription 3 (STAT3) and reduced renal angiotensin-converting enzyme (ACE) may partially prevent ANGII accumulation. However, despite that the dramatic increases in circulating ACE and consequently ANGII are not always accompanied by elevated blood pressure, they seem to lead to hemodynamic alterations reflected in glomerular hyperfiltration and albuminuria. In diabetic females, the more pronounced increase in circulating ACE2 may result in protection against hypertension. At the kidney level, however, diabetes-associated decrease in estrogen levels results in RAS hyperactivation and stimulation of the most relevant ANGII-mediated effector mechanisms such as TGF-β1. HG, hyperglycemia; HT; hypertension; GFR, glomerular filtration rate.

Clinical and experimental studies have provided evidence that oxidative damage parameters in renal tissue may vary according to sex[439,440]. It is conceivable that sex differences on renal RAS hyperactivation are due not only to genomic actions of sex hormones directly on *Agt* and *Ren* genes, but also to sex-specific modulation of the oxidative stress status within the diabetic kidney (Figure 18). In this regard, mice overexpressing kidney androgen-regulated protein (a proximal tubule specific, androgen-regulated gene), show hypertension and renal alterations mediated by oxidative stress[441].

In the context of diabetes and hypertension, circulating AGT is also decreased in both males and females. Interestingly, diabetic males showed higher plasma AGT compared with females (Figure 18). Surprisingly, hyperglycemia was associated with increased renal AGT and renin expression only in females, whereas the urinary excretion of AGT was similarly increased in both sexes[150]. In this study, T1DM was accompanied with renal inflammation. Inflammatory cytokines, such as IL-1 and IL-6, can inhibit renin promoter activity via ERKs and signal transducer and activator of

transcription 3 (STAT3)[442,443]. Both ERK and STAT3 are involved in DHT-independent AR activation and translocation to the nucleus[444,445]. Activation of the PI3K/Akt pathway results in phosphorylation of AR[446], which can from a heterologous complex with STAT3[447]. This interaction takes place whenever both STAT3 and AR are activated, for example, as a response to epidermal growth factor or IL-6[448] (Figure 19). Diabetes is associated with lower levels of androgens[406,422]; this fact may favor the ERK/STAT3-mediated inhibition of renin expression within the male diabetic kidney. In summary, sex-dependent effect of diabetes and hypertension on renal AGT and renin expression may vary according to sex hormone levels and the activation of inflammatory events such as the IL-6-related pathways.

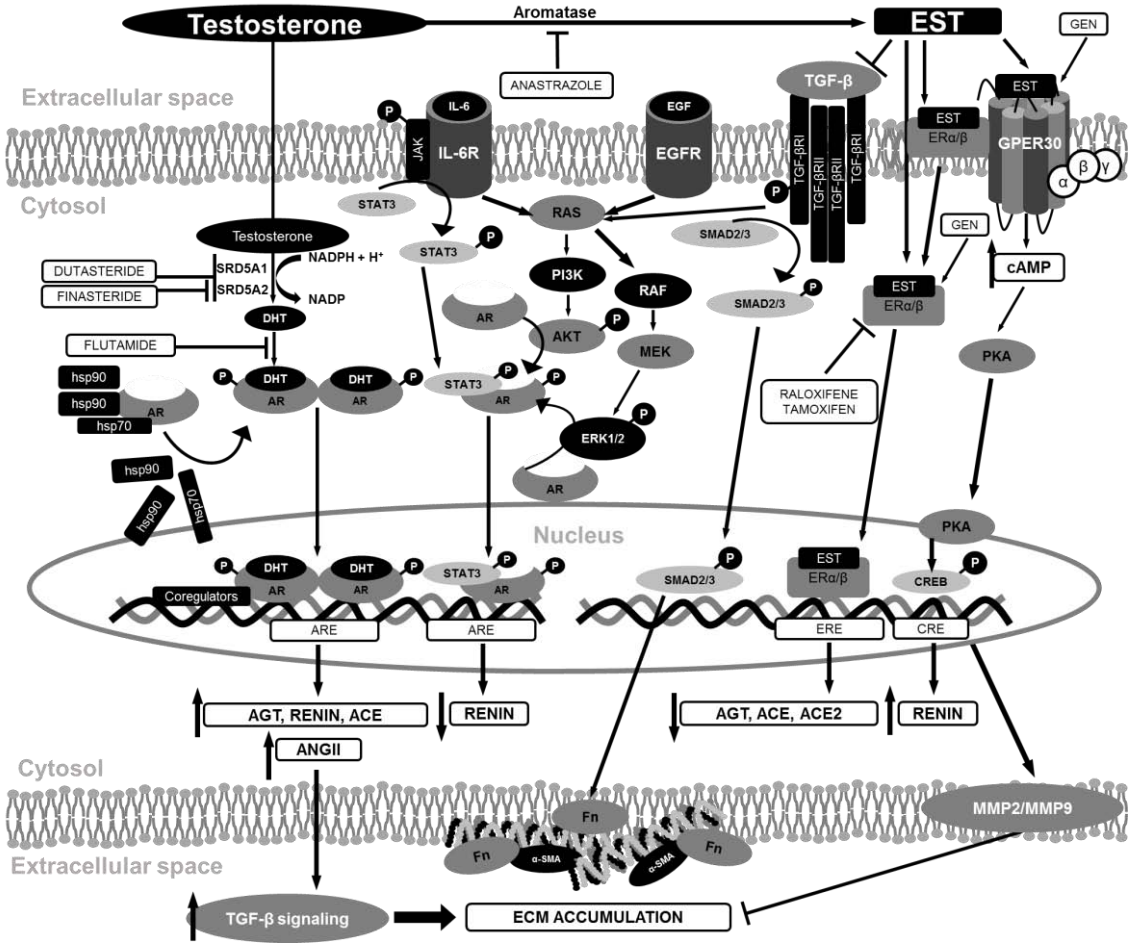

Figure 19. Molecular mechanisms of androgens and estrogens and their putative relationship to RAS and other relevant pathways within the kidney. Classical genomic androgen actions involve conversion of testosterone to dihydrotestosterone (DHT) by 5-reductase, binding of DHT to androgen receptor (AR), and dimerization and phosphorylation of the receptor, resulting in a higher activation of RAS and increased production of extracellular matrix (ECM). However, AR can also exert genomic effects and downregulate renin expression through a DHT-independent mechanism that involves AR phosphorylation by phospho(p)-AKT or pERK1/2 and the formation of a complex with pSTAT3. Testosterone can also be metabolized to estradiol (EST) by aromatase. Genomic actions of estrogens involve their binding to ERα or ERβ in the cell membrane or in the cytosol, followed by translocation to the nucleus, and have been attributed to downregulation of several RAS components, such as AGT, ACE, and ACE2. Estrogens can also exert nongenomic actions by binding to G protein-coupled estrogen receptor (GPER) 30 receptor in the cell membrane, leading to renin up-regulation and increased matrix metalloproteinase (MMP) 2 and MMP9, which are associated with ECM degradation. Thus, changes in sex hormone levels under diabetic

conditions may lead to impaired ECM metabolism and RAS alterations that ultimately contribute to the development of nephropathy. GEN, genistein; ER, estrogen receptor; SRD5A1, 5-reductase type 1; SRD5A2, 5-reductase type 2; hsp, heat shock protein; IL-6, interleukin 6; JAK, janus kinase; AKT, protein kinase B; MEK, mitogen-activated protein kinase; ERK, extracellular signal-regulated kinase; PI3K, phosphatidylinositol-4,5-bisphosphate 3-kinase; EGF, epidermal growth factor; TGF, transforming growth factor; PKA, protein kinase A; ARE, androgen response element; ERE, estrogen response element; CRE, cAMP-response element; CREB, cAMP-response element-binding protein.

1.F.II Sex differences on RAS regulatory arms: ACE and ACE2

Circulating ACE activity was found to be increased in diabetic mRen2.Lewis rats. Interestingly, this increase was more pronounced in males compared with females[150] (Figure 18). In contrast, a decrease in renal ACE expression has been described in both male and female mice[187,314,323]. However, studies focused on the assessment of renal ACE expression in both sexes in the context of diabetes are lacking.

Different groups have studied sex differences regarding ACE2 activity. Soro-Paavonen *et al*. found that males had significantly higher ACE2 activity than females in both, patients with T1DM and healthy individuals[305]. In concordance, in CKD patients without previous history of CV disease, our group recently reported that ACE2 activity from human EDTA-plasma samples is significantly increased in males as compared to females[449]. Increased activity of circulating ACE2 has also been detected in males compared with females after kidney transplant[450] and in hemodialysis patients[451]. Mizuiri *et al*. did not find sexual dimorphism in urinary ACE2 activity or protein levels in patients with CKD[307]. Surprisingly, when analyzing urine, *Ace2* mRNA levels were significantly increased in females compared with males in renal transplant patients with diabetes[452]. The increase of circulating ACE2 activity in males may be an early marker of increased risk of cardiovascular disease in CKD patients.

Oudit *et al*. studied the effect of *Ace2* deletion in non-diabetic kidneys from male and female mice. Their data showed that loss of ACE2 in male (but not female) C57BL/6 mice is associated with the development of age- and ANGII-dependent glomerular damage[319]. Gupte *et al*. also used ACE2-deficient mice to investigate the mechanistic role of ACE2 on the development of obesity-associated hypertension in males vs. females. They observed that male high fat-fed ACE2$^{-/y}$ mice had significantly greater systolic blood pressure compared with high-fat-fed ACE2$^{-/-}$females[212]. These data suggest that males have a higher dependence on ACE2-mediated renoprotection.

In experimental studies with hypertensive and diabetic animals, kidney ACE2 activity did not change in females but showed a 30% reduction in the diabetic males compared with their controls[150]. In addition, circulating ACE2 activity was significantly increased in both male (3-fold) and female (9-fold) diabetic mice. Despite the marked increase in

circulating ACE2 and the maintenance of renal ACE2 activity, female mRen2.Lewis diabetic rats were not protected from vascular damage, renal inflammation, and kidney injury in this model of early STZ-induced diabetes.

1.F.III Sex differences on RAS effector mechanisms: angiotensin peptides and their receptors

Experimental studies demonstrated that males have greater expression of “classic” components of the RAS, including ANGII and AT1R, whereas females have greater expression of “non-classic” components of the RAS, such as AT2R and ANG(1–7)[453,454]. To our knowledge, only one experimental study has assessed sex differences on renal and circulating ANGII levels in DN. In this work, diabetic and hypertensive males showed increased circulating and renal ANGII, as well as decreased plasma ANG(1–7), compared with females[150] (Figure 18). It is well accepted that ANGII mediates progressive diabetic kidney injury by enhancing renal fibrosis and inflammation[218,455] via stimulation of growth factor TGF-β[456,457]. In turn, EST is capable of inhibiting TGF-β actions[458]. Therefore, decreased estrogen levels due to aging or diabetes progression probably increase the susceptibility to ANGII-induced renal alterations in postmenopausal or diabetic women.

2. HYPOTHESES

2. HYPOTHESES

Diabetes is the leading cause of ESRD and has become one of the principal causes of CV mortality. In turn, male sex and androgens are associated to a higher incidence, progression and severity of DN.

Sexual dimorphism in DN seems to be associated to sex-specific modulation of RAS, and can be altered by the presence of hypertension. Within RAS, ACE2 plays a protective role in the kidney. While loss of ACE2 accentuates DN, its amplification ameliorates the progression and severity of the disease. Furthermore, recent studies have demonstrated that circulating and renal ACE2 are altered in DN.

Sex hormones have been shown to be altered in DN. Interestingly, surgical and chemical castration changes the curse of the disease. In this regard, hormonal therapy seems to modulate some of the crucial pathophysiological pathways involved in DN development and progression such as oxidative stress.

Given the importance of sex, RAS, and ACE2, in the progression of DN, we hypothesized that:

1. In the context of experimental T1DM, males will develop a more severe renal disease than females, which will be prevented by androgen reduction through gonadectomy (GDX).

2. Sex differences in DN progression in T1DM will be associated to sex-specific changes on circulating and renal RAS, especially on ACE and ACE2 expression.

3. *Ace2* deletion will accentuate the severity of DN in a sex-dependent manner, and renal alterations in type 1 diabetic and ACE2KO males will be attenuated by GDX.

4. The effect of sex and loss of ACE2 in the diabetic kidney will vary in the context of ANGII-induced hypertension. In addition, loss of ACE2 and infusion of exogenous ANGII will alter the expression of ACE and the other components of RAS in a sex-dependent fashion.

5. Androgens will induce changes in the proteome of renal tubular cells in a more detrimental manner than estrogens.

3. AIMS

3. AIMS

In the ***in vivo*** studies, we aimed to:

1. Evaluate the effect of sex on glomerular and tubular injury markers in **streptozotocin(STZ)-induced type 1 diabetic mice**, and its relationship with sex-specific changes of RAS in the serum and the renal cortex.

2. Study the influence of sex and GDX on the effects of ***Ace2* deletion** on glomerular and tubular injury markers in STZ-diabetic mice, and its relationship with the modulation of ACE and the other components of RAS.

3. Evaluate the sex-specific effects of *Ace2* deletion on renal disease progression in the context of STZ-induced T1DM and **ANGII-induced hypertension**, and its relationship with the modulation of ACE and the other components of RAS.

In the ***in vitro*** studies, we aimed to:

4. Perform an in-depth quantitative analysis of the **sex hormone-regulated proteome** in human proximal tubular epithelial cells (PTEC) after stimulation with DHT or EST.

4. MATERIALS AND METHODS

4. MATERIALS AND METHODS

4.A *IN VIVO* STUDIES

4.A.I Housing

Mice were housed in ventilated cages (Tecniplast) with 15-20 air renewals per hour, as well as full access to chow and water. Temperature was constantly maintained at 20-24^{o}C, and humidity at 40-60%. The light cycle was from 8AM to 8PM. The Ethical Committee of Animal Experimentation of the Barcelona Biomedical Research Park approved this study.

4.A.II *Ace2* deletion

The generation of ACE2KO mice has been previously described by Gurley *et al*.[459] A bacterial artificial chromosome (BAC145d21) containing a portion of the murine *Ace2* gene was identified. A 5.2-kb fragment of BAC145d21 that included the exon containing sequences encoding the active site of the ACE2 enzyme was then subcloned into the yeast shuttle vector YCpLac22 (pMD44). In turn, a 3.4-kb fragment containing the NEO/URA3 cassette from pRAY-1 and flanked by *Ace2* genomic sequence was generated by PCR and cotransformed with pMD44 into yeast strain YPH501 for homologous recombination. The final linearized targeting construct (Figure 20), was electroporated into MPI1-12D ES cells that had been derived from 129/SvEvfBRTac mice. G418-resistant ES cells were screened for homologous recombinants by Southern blot hybridization, and targeted ES clones were injected into C57BL/6H blastocysts to generate chimeras. Male chimeras were crossed with C57BL/6J females, and offspring that received the ES genome were identified by their agouti coat color. Because the ES cell line is XY and the *ace2* gene is located on the X chromosome, all agouti females were heterozygous for the mutation. These heterozygous females were bred with C57BL/6J male mice and the offspring genotyped by Southern blot hybridization.

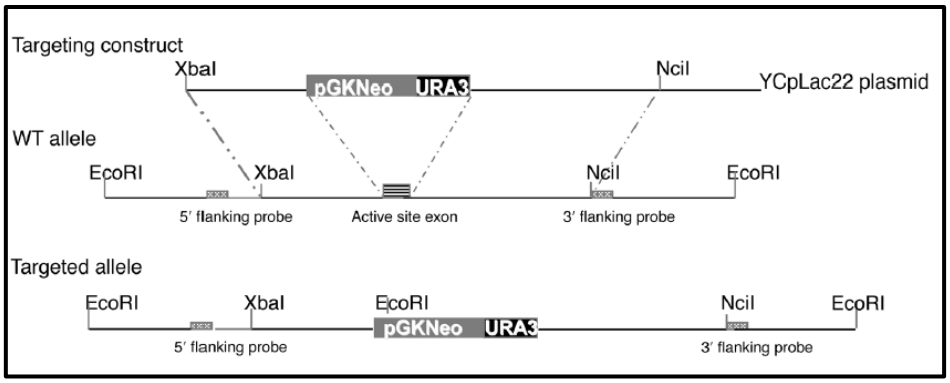

Figure 20. Strategy for producing targeted disruption of the *Ace2* gene. In the targeting vector, the exon containing nucleotides +1069 to +1299 encoding the active site of the ACE2 enzyme (including the Zn-binding signature motif, HEMGH) was replaced with a NEO/URA3 cassette. Figure adapted from Gurley *et al*., *The Journal of Clinical Investigation*, 2006.

4.A.III Breeding

To guarantee the maintenance of wild-type and ACE2KO mice strains and their availability for experiments, polygamous trio was employed as breeding strategy. Specifically, one adult male and two adult females (with at least 6 weeks of age) of the same genotype were housed in the same cage. Pups were weaned at 21 days by the animal facility staff. To minimize the adverse effects of consanguinity in the upcoming generations and birth defects in the pups, male and female mice from the same litter were never paired together as breeders.

4.A.IV Genotyping

4.A.IV.1. Primer design

The nucleotide sequence codifying the active site of ACE2 (HEMGH zinc binding motif) was first localized by Tipnis *et al*. within the exon 9 of the human *Ace2* gene[460]. As shown in Figure 21, CACGAGATGGGACAC sequence corresponding to the active site (highlighted in yellow) is part of the 230bp sequence deleted in our ACE2KO mice. To distinguish ACE2KO mice from WT, this region was included in the sequence flanked by the forward and reverse primers. Both primers (green sequences) were chosen using Primer3 software. Primer sequences presented 890bp of length between them (sequence in bold).

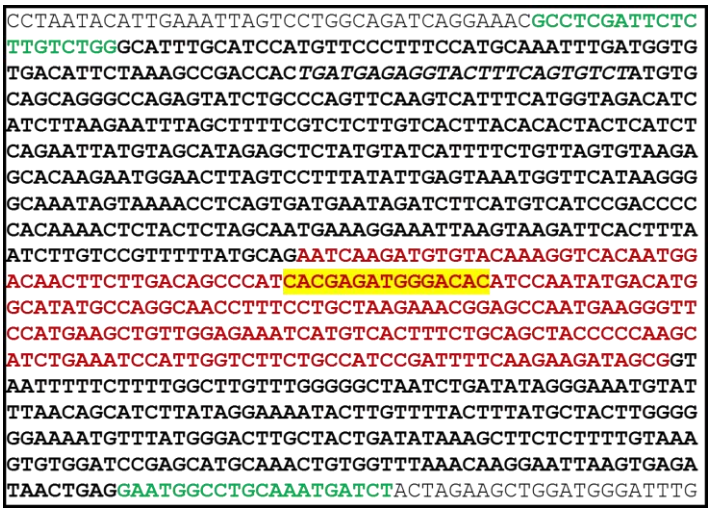

Figure 21. ACE2 DNA genomic sequence in the mouse X chromosome: PCR primers selection. Black regions correspond to introns and red region to the exon. Yellow highlighted sequence corresponds to active site coding sequence. The primer sequences flanking the region of interest for the identification of *Ace2* deletion are marked in green.

4.A.IV.2. DNA extraction

DNA for genotyping was extracted from a little tail portion (2-4mm) obtained by thermocautery in 21- to 24- day-old mice mechanically immobilized in a plastic flat bottom restrainer. We employed this procedure because 1) it has been shown to be not particularly painful in mice[461]; and 2) higher DNA yield has been reported from tail snips at this young age, due to the low percentage of ossified sample. Briefly, mice younger than 24 days were mechanically immobilized in a plastic flat bottom restrainer and tail was snipped with a sanitized disposable blade. Tail tips were placed into microcentrifuge tubes. Biologic material (e.g. blood or fur) was cleaned off from the blade and all the materials were sanitized after each snipping.

DNA extraction and isolation was performed using Wizard® Genomic DNA Purification Kit (Promega), following manufacturer instructions. Briefly, tissue was lysated by o/n enzymatic digestion at 55ºC with 500µL of nuclei lysis solution, adding 120µL of 0.5M, pH 8.5 ethylenediamine-tetraacetic acid (EDTA) and 17.5µL of proteinase K (20mg/mL). Samples were incubated with 200µL of protein precipitation solution for 5 minutes while chilled in ice. After 5 minutes of centrifugation at 14000g, nucleic acids in the supernatant were transferred in a new tube. 600µL of isopropanol were added followed by one minute centrifugation at 14000g for DNA precipitation. Precipitation was washed with 600µL of 70% ethanol and centrifuged for 1 minute at 14000g to obtain a DNA pellet. Ethanol excess was removed and the samples were dried at room temperature (RT). Finally, dried pellet was resuspended in 100µL of rehydratation solution and incubated at 65ºC for 60 minutes.

4.A.IV.3. DNA quantification

Extracted DNA was quantified by spectrophotometry (NanoDrop® ND-1000). Before each DNA quantification experiment, the Nanodrop instrument was cleaned with 1μL of ddH_2O water and calibrated with 1μL of rehydratation solution (blank). In addition, Nanodrop was cleaned with tissue between samples. The ratio of absorbance at 260nm and 280nm is used to assess the purity of DNA and RNA. A ratio of ~1.8 is generally accepted as "pure" for DNA. If the ratio is appreciably lower, it may indicate the presence of protein, phenol or other contaminants that absorb strongly at or near 280nm. If the ratio is notably higher, it may suggest that the sample also contains RNA. In our experiments, samples were not considered for further analysis if their DNA concentration was lower than 10μg/μL or if the ratio was out of the range 1.6-2.3.

4.A.IV.4. Polymerase chain reaction

Genotyping of ACE2KO animals was carried out by classic PCR. This technique is used in molecular biology to amplify a fragment of DNA across several orders of magnitude, generating thousands to millions of copies of this particular DNA sequence. The method relies on thermal cycling, consisting of cycles of repeated heating and cooling of the reaction for 1) DNA melting, 2) primer annealing and 3) enzymatic elongation of the newly synthetized DNA strain, usually catalyzed by a heat-stable DNA polymerase, such as Taq polymerase (an enzyme originally isolated from the bacterium *Thermus aquaticus*). As PCR progresses, the DNA generated is itself used as a template for replication, setting in motion a chain reaction in which the DNA template is exponentially amplified. In our studies PCR reaction was performed using 15-60ng of DNA in a final volume of 25μL. The reagents and the conditions employed for the preparation of the PCR mix are described in the following table.

Table 7. Reagents used for the PCR reaction. For each reagent, the volume employed per sample, as well as its final concentration, are specified.

REAGENT	VOLUME (μl/sample)	FINAL CONCENTRATION
10x PCR Buffer (Sigma)	2.5	1x
10mM dNTPs (Sigma)	0.5	0.2mM
Forward primer 100μM	0.05	0.2mM
Reverse primer 100μM	0.05	0.2mM
ddH_2O	Up to 25.0	-
DNA polymerase (Taq pol, Sigma)	0.125	0.025units/μL
Sample	1-2	-

PCR was performed for our target gene (*Ace2*) and a housekeeping gene (G*apdh*) as an intrasample positive control. Thus, two different PCR mixes were prepared in each genotyping assay. For each of the genes, one extra reaction was included where

ddH_2O water was added instead of sample as negative control. Primers sequences used for the amplification of *Ace2* and *Gapdh* sequences are depicted below.

Table 8. Primers used for *Ace2* and *Gapdh* genes amplification.

GENE	FORWARD primer sequence (5' → 3')	REVERSE primer sequence (5' → 3')
Ace2	GCCTCGATTCTCTTGTCTGG	AGATCATTTGCAGGCCATTC
Gapdh	AACTTTGGCATTGTGGAAGG	TGTGAGGGAGATGCTCAGTG

PCR was programmed in a thermocycler (Biometra) with the following settings:

Table 9. PCR program used for *Ace2* and *Gapdh* genes amplification. Denaturing, annealing and elongation of the sequences were performed during 25 cycles. *Ace2* and *gapdh* sequences were amplified in the same PCR reaction but in different tubes.

STEP	TEMPERATURE	TIME
Denaturing	94°C	1:00
Annealing	55°C	0:45
Elongation	72°C	1:20
Number of cycles	25	
Cooling	10°C	

After the PCR finished, samples were loaded into a 1% agarose gel (Promega) in TBE1x buffer (220mM Tris; 180mM Borate; 5mM EDTA; pH8.3). Gelred (Biotium) was employed as intercalating nucleic acid stain; this substance supposes a less toxic and more sensitive alternative to ethidium bromide. Amplicons were separated depending on its MW and visualized under the ultraviolet light in a ChemiDocTM transiluminator (Biorad). 1kb DNA Ladder (Sigma) was used as a MW marker.

As shown in Figure 22, PCR amplification of *Ace2* by classic PCR allowed us to differ between the presence and the absence of the gene in the DNA of WT and ACE2KO mice, respectively.

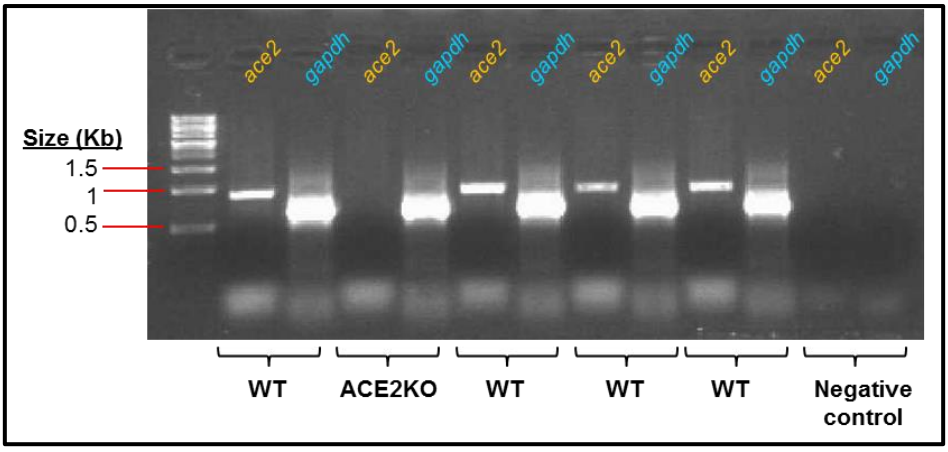

Figure 22. Representative photograph of PCR amplification products from the DNA of WT and ACE2KO mice. As depicted in the figure, the 890bp fragment was observed in WT and not in ACE2KO mice. As negative control, ddH_2O water instead of DNA sample was incubated with the PCR mix.

4.A.V Diabetes induction

Among all murine models of T1DM, we decided to employ the STZ-induced mice because of the following reasons:

- In the majority of our *in vivo* studies, we aimed to simultaneously evaluate the effect of several factors (e.g. sex, loss of ACE2, and ANGII infusion). To achieve this aim, we chose the STZ mice as it is a well stablished model, and it would allow us to follow reproducible timing across all different experiments, as well as include a high number of mice in each set. This experimental design cannot be applied in other models such as the NOD or the Akita mice, where the follow-up of each single mouse needs to start when diabetes spontaneously appears and hyperglycemia is first detected.

- This project was design to study the effect of sex in experimental DN. Therefore, the NOD and the Akita mice models were discarded due to the sexual dimorphism in the incidence of diabetes across sexes.

- The possibility of dose adjustment, as well as the choice of the age of induction, notably increase the versatility of this model and allow a better method optimization, which is a clear advantage when working with a high number of experimental groups.

High Dose STZ Induction Protocol

Diabetes was induced to 10-week-old mice following the High Dose STZ Induction Protocol from the Diabetic Complications Consortium (https://www.diacomp.org) with slight modifications.

Before STZ administration, mice were weighted and chow was retired from their cages at 9AM approximately. Mice were fasted for 4 hours with full access to water.

Sodium citrate buffer was prepared by dissolving 1.47g of Na Citrate in 50mL of ddH_2O. pH was tested with the pH meter (Crison) and adjusted to pH4.5 with monohydrate Na Citrate solution. 18.75mg of STZ (Sigma) were weighted in microcentrifuge tubes and diluted prior to use with 840μL of sodium citrate buffer (final concetration: 22.3mg/mL).

Freshly prepared STZ solution was loaded into a 1mL syringe capped with a 26G needle. For a dose of 150mg/Kg, the volume to inject was adjusted to the body weight (BW) of each animal using the formula:

$$V(\mu L) = \frac{150\,\frac{mg}{Kg} \cdot BW(g)\,\frac{1Kg}{1000g}}{22.3\,\frac{mg}{mL} \cdot \frac{1mL}{1000\mu L}}$$

Each mouse was injected intraperitoneally. The entire protocol for diabetes induction was repeated after one week for the administration of the second dose of STZ.

4.A.VI Experimental design

To evaluate the impact of sex, diabetes, loss of ACE2, sex hormone reduction and ANGII-induced hypertension in our animal model, we performed 3 different studies. The experimental design for each study is detailed below.

4.A.VI.1. Study 1: Effect of sex on diabetes, kidney disease and RAS alterations in type 1 diabetic mice.

As mentioned above, T1DM was induced through intraperitoneal injection of STZ to 10-week-old male and female C57BL/6 mice (Figure 23). Citrate buffer was used as vehicle and given to controls. At 12 weeks of age, a subgroup of both, control and diabetic mice, was gonadectomized. SHAM surgery was practiced to the remaining males. Mice were then followed by 19 weeks. During this period, blood glucose and BW were monitored every 2 weeks under fasting conditions (3h).

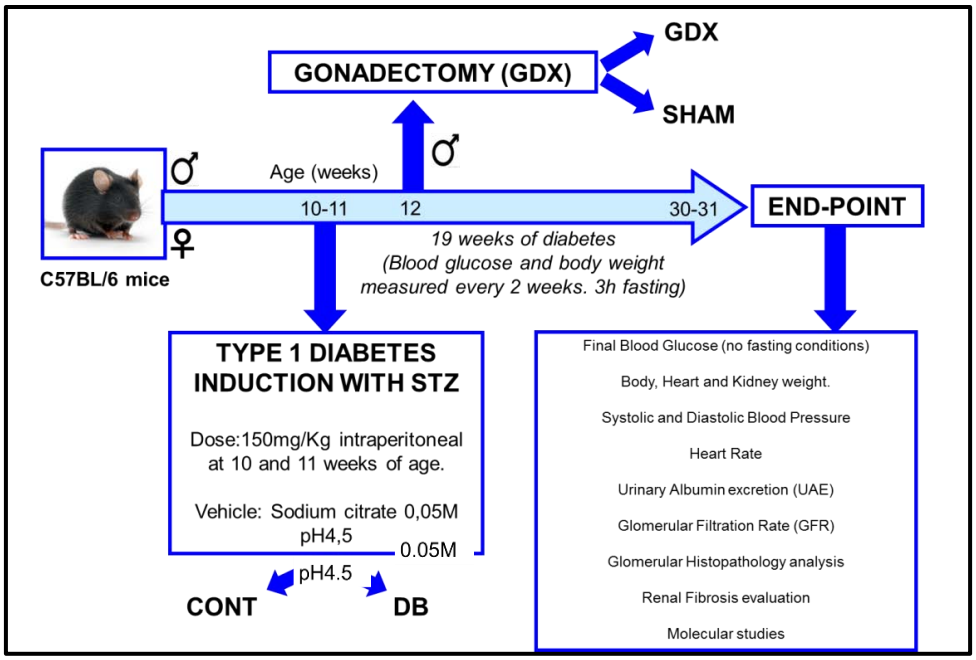

Figure 23. Experimental design for study 1. The most relevant methodological aspects regarding diabetes induction, surgical castration, diabetes duration, and main readouts at the end of the study are represented in the timeline. CONT, control; DB, diabetic.

It is worthy to mention that, in a first pilot experiment (n=6-8), we administered 50mg/Kg of STZ in five consecutive doses, as specified in the Low Dose STZ Induction Protocol from the Diabetic Complications Consortium (https://www.diacomp.org). After STZ administration to our mice, no diabetic females were obtained. This lack of STZ effect in females was not observed when employing the high dose protocol for diabetes induction. However, the incidence of diabetes after high dose of STZ administration was relatively low in females (about 50%), especially when compared to the >90% incidence observed in males (data not shown).

4.A.VI.1.1. Gonadectomy

Gonadectomized or the corresponding sham operated mice were previously anesthetized through intraperitoneal injection of ketamine (75mg/kg) and medetomidine (1mg/kg).The scrotal sac of non-conscious mice under anesthesia was shaved and sanitized with povidone-iodine before the surgery. A vertical incision was then performed in the middle of the scrotal sac, exposing the inner sacs, testes and epididymis. After ligation of the epididymis with 4-0 stitches, the tunica vaginalis and albuginea were perforated and testes were removed. Ligated epididymis was returned to the scrotal sacs, which was sutured with 4-0 stitches. To obtain the corresponding sham-operated groups, mice were anesthetized and the scrotal sac was exposed but not perforated. Testes were then returned to the original position in the perineal region.

At the end of each surgical intervention, mice were recovered from anesthesia by subcutaneous atipamezol injection (1mg/kg). Intraperitoneal buprenorphine (0.5mg/kg) was administered as anti-inflammatory treatment.

4.A.VI.2. Study 2: Sex-specific effects of *Ace2* deletion on kidney disease after 19 weeks of T1DM. Role of GDX.

4.A.VI.2.1. Study 2A: Effects of Ace2 deletion in type 1 diabetic female mice.

In this study, female mice genotype was confirmed by PCR at 3-4 weeks of age and animals were divided between WT and ACE2KO (Figure 24). T1DM was induced as previously mentioned. Again, diabetes duration was 19 weeks. During this period, blood glucose and BW were monitored every 2 weeks under fasting conditions.

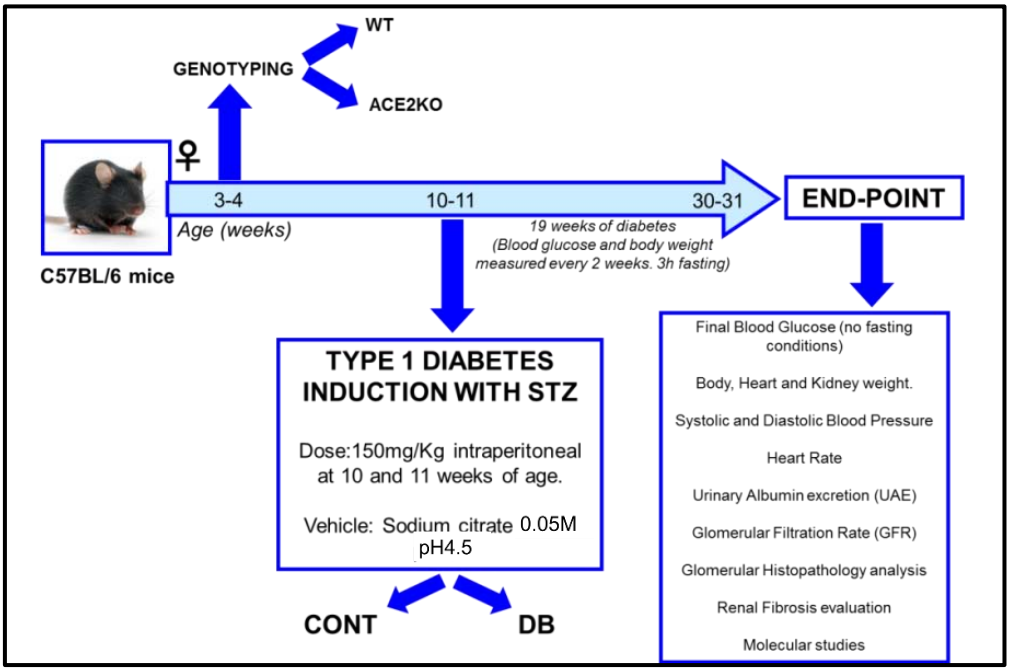

Figure 24. Experimental design for study 2A. The most relevant methodological aspects regarding genotyping, diabetes induction and duration, and main readouts at the end of the study are represented in the timeline. WT, wildtype; ACE2KO, ACE2 knockout; CONT, control; DB, diabetic.

4.A.VI.2.2. Study 2B Effects of ACE2 deletion in type 1 diabetic male mice.. Role of gonadectomy.

In this study, male mice genotype was confirmed by PCR at 3-4 weeks of age and animals were divided between WT and ACE2KO. At 9 weeks of age, a subgroup of both, WT and ACE2KO mice, was gonadectomized. Of mention that, in this study, removal of male gonads was performed one week previous to STZ administration (Figure 25). T1DM was induced as previously mentioned and animals were followed for 19 weeks. During this period, blood glucose and BW were monitored every 2 weeks under fasting conditions.

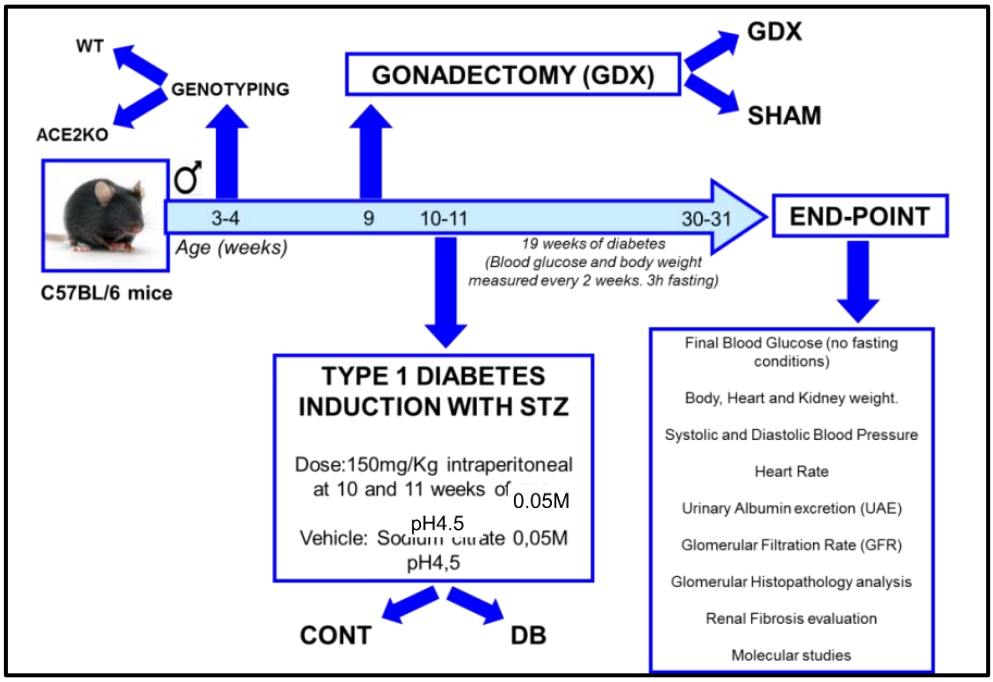

Figure 25. Experimental design for study 2B. The most relevant methodological aspects regarding genotyping, surgical castration, diabetes induction and duration, and main readouts at the end of the study are represented in the timeline. WT, wildtype; ACE2KO, ACE2 knockout; CONT, control; DB, diabetic.

4.A.VI.3. Study 3: Sex-specific effects of *Ace2* deletion on kidney disease in hypertensive ANGII-infused mice with type 1 diabetes.

Male and female mice genotype was confirmed by PCR at 3-4 weeks of age and animals were divided between WT and ACE2KO (Figure 26). T1DM was induced as mentioned before. In this study diabetic mice and their controls were followed for 12 weeks. After 8 weeks of diabetes, mice underwent sham surgery or implantation of an osmotic pump loaded with ANGII. ANGII was infused for 4 weeks until the end of the study.

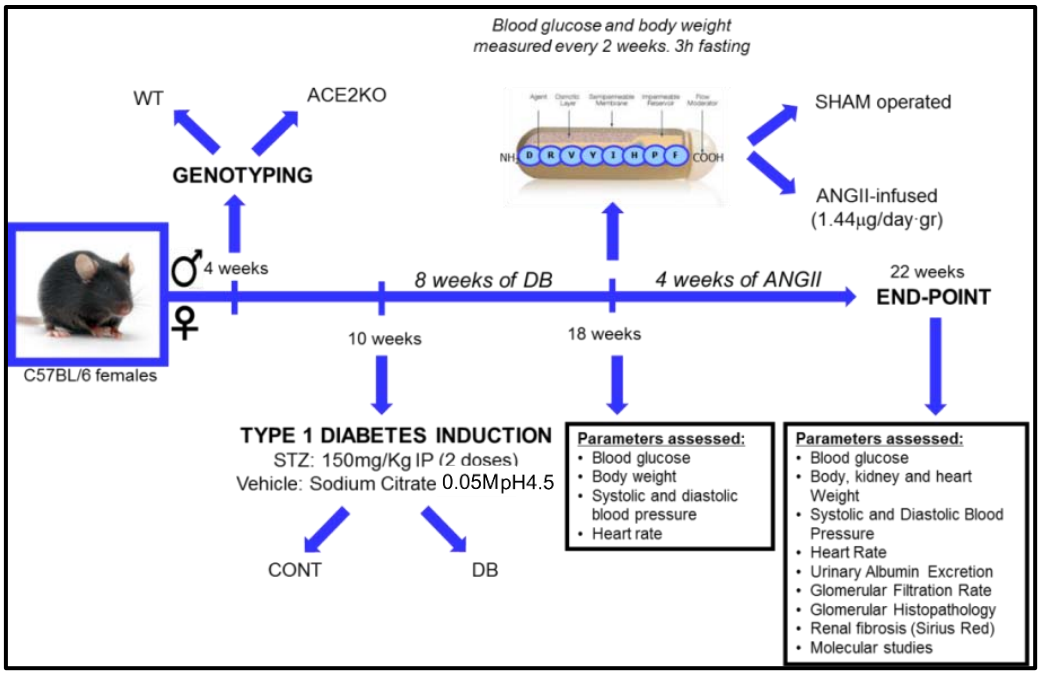

Figure 26. Experimental design for study 3. The most relevant methodological aspects regarding genotyping, diabetes induction, ANGII administration, and main readouts before and after ANGII infusion are represented in the timeline. WT, wildtype; ACE2KO, ACE2 knockout; CONT, control; DB, diabetic.

Mice receiving osmotic minipump implantation or the corresponding sham operations were previously anesthetized through intraperitoneal injection of ketamine (75mg/kg) and medetomidine (1mg/kg).

4.A.VI.3.1. Preparation of ANGII solution

The stock solution was prepared by dissolving 50mg of human ANGII in 2mL of ddH_2O water. Then was passed through a syringe filter (0.2µm pore size) and divided into 146µL aliquots, each of those contained 3.654mg of ANGII at a concentration of 25mg/mL. Aliquots were then frozen and lyophilized overnight under vacuum and stored at -20ºC until use. The day previous to the start of ANGII treatment, BW was assessed in all studied 8-week diabetic and control mice. In parallel, lyophilized ANGII was resuspended in 100 µL of 0.9% NaCl. This solution contained 0.03654mg/µL of ANGII and was named “ANGII working solution (ANGII_WS)”. Considering that

a) the aimed ANGII infusion rate of our study was 1.44µg ANGII / (day·gBW),
b) the delivery rate of the osmotic pumps (ALZET) was 0.14µL/hr, and
c) the duration of ANGII treatment was set to 28 days,

an specific volume of ANGII working solution was individually calculated for each animal following the formula:

$$V_{ANGII\_WS}(\mu L) = 1.44 \frac{\mu g\ ANGII}{day \cdot gBW} \cdot 28\ days \cdot BW(g) \cdot \frac{1\ mg\ ANGII}{10^3 \mu g\ ANGII} \cdot \frac{1 \mu L\ ANGII\_WS}{0.03654\ mg\ ANGII}$$

This volume was pipetted into a 1.5mL microcentrifuge tube and flushed up to 100µL with 0.9% NaCl. The entire volume was then loaded to the osmotic pump employing a 1mL syringe with a 27G detachable needle. Of mention that the entire protocol of ANGII preparation and loading of the pumps was performed under sterile conditions in a vertical laminar flow hood.

Pumps were activated for 24h at 37ºC in 1.5mL microcentrifuge tubes containing 300µL of 0.9% NaCl.

4.A.VI.3.2. Subcutaneous implantation procedure

Once the animals were anesthetized, their skin was shaved and washed with povidone-iodine over the back, especially in the area slightly posterior to the scapulae. A horizontal mid-scapular incision was then performed and the dermis was perforated in this area. The subcutaneous tissue was spread by opening and closing the incision with sterile tweezers to create a pocket for the pump. Activated osmotic pumps loaded with ANGII or saline solution were placed into the subcutaneous space. Finally the wound was closed with 4-0 stitches.

Through this method, the contents of the pump were delivered into the local subcutaneous space at a rate of 0.14µL/hr, ensuring the absorption of ANGII by local capillaries and its systemic administration.

4.A.VI.3.3. Recovery

At the end of each surgical intervention, mice were recovered from anesthesia by subcutaneous atipamezol injection (1mg/kg). Intraperitoneal buprenorphine (0.5mg/kg) was administered as anti-inflammatory treatment.

The most relevant characteristics relative to the experimental design of the *in vivo* studies mentioned above are summarized in Table 10.

Table 10. Characteristics of the *in vivo* studies. Experimental groups, number of animals for each group, factors analyzed, time of diabetes and age at the end of the study. CONT, control; DB, diabetic; WT, wildtype; ACE2KO, ACE2 knockout; GDX, gonadectomy.

Study		Experimental groups	n	Factors analyzed	Diabetes duration	Age
1		Female CONT	15	**Diabetes** (DB vs. CONT)	19 weeks	30 weeks
		Male CONT	15			
		Male CONT + GDX	9	**Sex** (Male vs. Female)		
		Female DB	15			
		Male DB	12	**Androgen reduction** (GDX vs. non-GDX)		
		Male DB + GDX	11			
2	2A	Female CONT-WT	15	**Diabetes** (DB vs. CONT)	19 weeks	30 weeks
		Female CONT-ACE2KO	14			
		Female DB-WT	15	**Loss of ACE2** (ACE2KO vs. WT)		
		Female DB-ACE2KO	10			
	2B	Male CONT-WT	15	**Diabetes** (DB vs. CONT)		
		Male CONT-ACE2KO	15			
		Male CONT-ACE2KO + GDX	9	**Loss of ACE2** (ACE2KO vs. WT)		
		Male DB-WT	12			
		Male DB-WT + GDX	11	**Androgen reduction** (GDX vs. non-GDX)		
		Male DB-ACE2KO	14			
		Male DB-ACE2KO + GDX	14			
3		Female CONT-WT + SHAM	10	**ANGII-induced hypertension** (ANGII vs. SHAM)	12 weeks	22 weeks
		Female CONT-WT + ANGII	12			
		Female DB-WT + SHAM	11			
		Female DB-WT + ANGII	11			
		Female CONT-ACE2KO + SHAM	10			
		Female CONT-ACE2KO + ANGII	10	**Diabetes** (DB vs. CONT)		
		Female DB-ACE2KO + SHAM	11			
		Female DB-ACE2KO + ANGII	9			
		Male CONT-WT + SHAM	9			
		Male CONT-WT + ANGII	9			
		Male DB-WT + SHAM	8	**Loss of ACE2** (ACE2KO vs. WT)		
		Male DB-WT + ANGII	12			
		Male CONT-ACE2KO + SHAM	8			
		Male CONT-ACE2KO + ANGII	8			
		Male DB-ACE2KO + SHAM	9	**Sex** (Male vs. Female)		
		Male DB-ACE2KO + ANGII	8			

4.A.VII Blood glucose and body weight monitoring

After diabetes induction, blood glucose and BW were measured weekly or every two weeks, depending on the study. Mice were weighted and fasted for 3 hours with full access to water. For glucose level determination, fasting blood samples from the saphenous vein were obtained for measurements with the ACCU-CHEK Compact® meter system (Roche). Mice were considered diabetic if blood glucose levels higher than 250mg/dl were detected during the 4 first weeks after STZ administration. At the end of the follow-up, blood glucose and BW were assessed under non-fasting conditions prior to sacrifice.

4.A.VIII Systolic and diastolic blood pressure and heart rate measurement

Systolic and diastolic blood pressure (SBP, DBP) and heart rate were measured during the last week of follow-up using the CODA™ non-invasive tail-cuff system (Kent

Scientific Corporation, figure 10). In mice receiving ANGII-infusion or SHAM surgery, these parameters were also assessed at baseline (starting at 7 weeks after STZ/citrate administration). Values were obtained from conscious-trained mice on five consecutive morning sessions.

Mice were immobilized in acrylic cylindrical holders and placed for 10 minutes on a heating platform at 37ºC to induce the vasodilation of the tail blood vessels. As shown in Figure 27, occlusion cuffs and volume pressure recording sensors were disposed around the mouse tail. This CODA™ device incorporates a specially designed differential pressure transducer that measures SBP, DBP and heart rate by determining the blood volume in the tail.

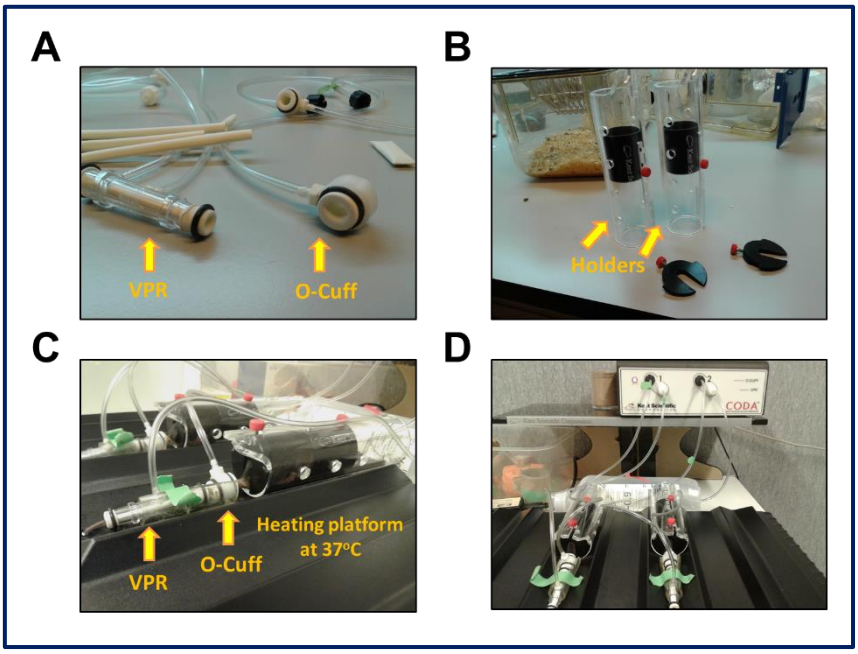

Figure 27. Equipment for blood pressure and heart rate measurement. Panel A illustrates the volume pressure recording (VPR) and occlusion cuff (O-Cuff) sensors. Panel B shows the acrylic cylindrical holders for mice immobilization. Panel C shows the disposition of the sensors around the tail of two mice which, in turn, are immobilized in the holders and placed on the heating platform at 37°C. As shown in panel D, VPR and O-Cuff sensors were connected to the CODA device prior to each recording session.

SBP and DBP are expressed in mmHg, and heart rate is expressed in beats per minute (bpm). Mean values obtained from less than 10 valid measurements were not considered for analysis.

4.A.IX Glomerular filtration rate

GFR was estimated using clearance kinetics of plasma FITC-inulin after a single bolus injection as previously described [462].

4.A.IX.1. FITC-Inulin preparation

FITC-inulin solution was prepared following the protocol from the Diabetic Complications Consortium (https://www.diacomp.org) with slight modifications. 60mg of FITC-inulin (Sigma) were dissolved in 1.2mL of 0.9% NaCl by heating the solution in boiling water. To remove residual FITC not bound to inulin, the solution was filled into a 1000Da cut-off dialysis membrane. The dialysis membrane filled with FITC-inulin was put into 1000mL of 0.9% NaCl for 24 hours at RT. Prior to use, this dialyzed solution was sterilized through a 0.2µm filter (Millipore).

4.A.IX.2. Inulin injection and blood collection

Mice were anesthetized at the end of the study through a single intraperitoneal injection of sodium pentobarbital (45mg/Kg). BW was assessed and dialyzed 5% FITC-inulin was injected into the tail vein (Volume injected = 3.74µL/gBW). Approximately 30µL of caudal vein blood were collected at 3, 7, 10, 15, 35, 55, and 75 min after the injection into heparinized capillary blood collection Microvette® system (Sarstedt).

4.A.IX.3. Sample processing

Blood samples were centrifuged at 8000g for 10min and plasma was transferred to new 1.5mL microcentrifuge tubes. For each animal, 5µL of sample from each time point were loaded into a black 96-well plate. After adding 45µL of 0.5mM HEPES, pH7.4 to each well, plasma fluorescence was read at each time point using a Tecan Infinite 200 reader (TECAN Instruments) at an excitation wavelength of 485nm and an emission wavelength of 538nm. To determine the total fluorescence emitted by the inulin employed in each experiment, 0.5µL of the inulin used that same day was loaded into an additional well with 4.5µL of non-fluorescent mice plasma and 45µL of 0.5mM HEPES, pH 7.4.

4.A.IX.4. GFR calculation

For each animal, we first plotted the evolution of plasma fluorescence over time (Figure 28).

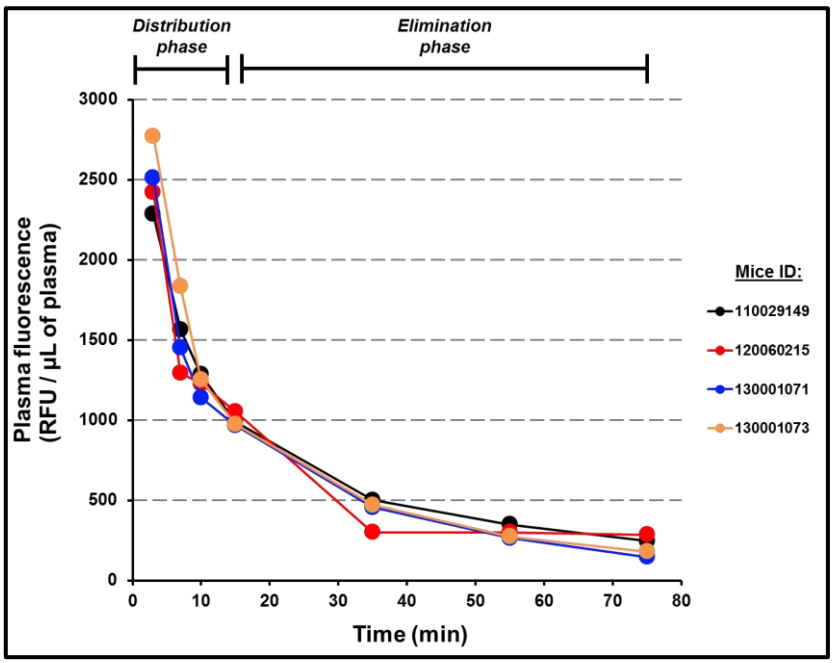

Figure 28. Representative plots depicting the evolution of plasma fluorescence in four different animals over time. The two-phase decay curves indicate that FITC-inulin is rapidly distributed and gradually eliminated from the plasma and filtrated into urine in the kidney glomeruli. RFU, relative fluorescence units.

Mice with curves that did not show a clear two-phase decay fashion were not considered for further analysis. The decay in plasma fluorescence levels was fit to a two-phase decay curve using nonlinear regression (GraphPad Prism, GraphPad Software, San Diego, CA). GFR was calculated as previously described [48] using the equation:

$$GFR = \frac{I}{\frac{A}{\alpha} + \frac{B}{\beta}}$$

Where I = amount of FITC-inulin delivered by the bolus injection, A (Span 1) = y-intercept value of the distribution phase decay, B (Span 2) = y-intercept value of the elimination phase decay, α = decay constant for the distribution phase, and β = decay constant for the elimination phase. These parameters could be calculated using a non-linear regression curve-fitting with Graphpad and values were expressed as µL of cleared FITC-inulin / (min * g of BW).

GFR values were then transformed to µL/min/gr of BW as previously published[325].

4.A.X Urinary albumin excretion

We determined UAE on morning spot urine collections in which ACR was calculated and expressed as µgAlb/mgCrea.

4.A.X.1. Urine collection

Urine morning spot was obtained through abdominal massage and collected into a 1.5mL microcentrifuge tube. For each mouse, this procedure was performed during three consecutive days. The three corresponding urine samples were clarified by centrifugation and the supernatants were transferred to the same tube, labeled as “total urine”.

4.A.X.2. Measurement of albumin levels

Urinary albumin concentration was measured in total urine samples by ELISA (Albuwell M, Exocell). This assay was performed in 96-well plated coated with mouse albumin (stationary phase). In the fluid phase added to the albumin-coated wells, the antigen in urine samples (albumin) is recognized by a specific rabbit anti-murine albumin antibody. This primary antibody interacts and binds with the albumin immobilized to the stationary phase or with that in the fluid phase. After washing, only the antibody-conjugate that bound to the albumin of the stationary phase remains in the well. Primary antibody molecules are then labeled by anti-rabbit IgG-HRP secondary antibody and detected using a chromogenic reaction. In this indirect competitive assay, albumin molecules in urine samples compete with the fixed albumin for binding to the primary antibody. Thus, albumin concentration in urine samples is inversely correlated with the detected color intensity.

For albumin determination in our urine samples, a standard curve was first prepared by serial dilutions of murine serum albumin (MSA) standard in NHE-BSA, the diluent provided by Exocell. Final concentrations for the standard curve were: 0.156, 0.313, 0.625, 1.25, 2.5, 5, and 10 µg/mL. A 1/13 dilution was performed for each sample by diluting 10µL of total urine in 120µL of NHE-BSA diluent. 50µL of standard curve point or diluted sample were loaded in duplicate into albumin-coated wells. 50µL of primary antibody were added to every well and plates were covered and incubated for 30 minutes at RT. In each assay, the first and second wells were employed as blank (100µL of NHEBSA) and primary antibody positive control (50µL NHEBSA + 50µL primary antibody), respectively. Fluids were removed from the wells and plates were

washed 10 times with wash buffer (0.15M NaCl, 0.05% Tween). 100μL of anti-rabbit HRP conjugate were added to every well and plates were covered and incubated for 30 minutes at RT. Plates were washed 10 times with wash buffer and 100μL of TMB color developer were added. After 5 minutes of developing, 100μL of acid color stopper were added to each well. Absorbance was measured by spectrophotometry at 450nm in a Tecan Infinite 200 reader (TECAN instruments).

The mean absorbance value for replicate wells was calculated and extrapolated in a semi-logarithmic plot of the standard curve dilutions, with the standard curve: log[MSA] on the x-axis and mean absorbance on the y-axis. The obtained value was corrected by the dilution factor and was expressed as μgAlb/mL urine.

4.A.X.3. Measurement of creatinine levels

Creatinine is a breakdown product of creatine phosphate in the muscle, and is usually produced at a fairly constant rate by the body (depending on muscle mass) [463]. Since creatinine is excreted unchanged by the kidneys, urine creatinine levels are commonly used to normalize albumin concentration [464]. In our studies, urinary creatinine levels were determined in same urinary spots using a colorimetric assay (Creatinine Companion, Exocell), based on the classic technique that estimates the interaction of creatinine with alkaline picrate (Jaffe reaction) [465]. Briefly, creatinine in the sample interacts with the picric acid under alkaline conditions and forms the complex picric acid-creatinine. This interaction is accompanied by a colorimetric reaction (orange color) proportionally to the amount of creatinine.

20μL of diluted urine in ddH_2O (1/20) and 20μL of the standard curve were mixed with alkaline picrate in a 96-well plate. After 10 minutes of incubation at RT, absorbance was measured by spectrophotometry at a wavelength of 500nm in a Tecan Infinite 200 reader (TECAN instruments). Acid solution was then added and, after 5 minutes of incubation, the plate was read again in the conditions mentioned above. Samples were measured in duplicate and results were expressed as mg of creatinine/dL.

4.A.XI Necropsy

At the end of the study mice were sacrificed by terminal surgery. Mice were anaesthetized by intraperitoneal injection of pentobarbital at a lethal dose of 45mg/Kg.

After weighting and measuring blood glucose levels in non-conscious mice, blood was extracted by cardiac puncture and serum was obtained by centrifugation at 8000g for 10min. Mice were perfused with cold phosphate buffer solution (PBS) prior to kidneys removal and weighting. Left kidney and half of the right kidney were snap frozen with liquid nitrogen and kept at -80^{o}C for further analysis. Half of the right kidney was maintained in 10% formalin solution and paraffin embedded for histological studies.

4.A.XII Kidney histopathology studies

4.A.XII.1. Sectioning of paraffin embedded kidney tissue

Paraffin blocks were cut into 3µm sections with a rotary microtome (Leica Biosystem). Sections were stretched in a water bath at 40ºC and collected onto SuperfrostTM microscope slides (Fischer Scientific). The excess of water from the obtained sections was removed by contact with a heat platform (1h) and posterior air drying overnight at RT. Samples were then stored at 4ºC until use.

4.A.XII.2. Deparafinning

Excess of paraffin was melted by incubating the sections for 30 min in a stove at 60ºC for 30 min. Sections were then deparaffined in xylene (2x15min) and rehydrated through graded alcohols at 100% (2 x 10min), 96%(1 min), 70% (1 min) and 50% (1 min).

4.A.XII.3. Evaluation of renal morphology in PAS-stained samples

To evaluate the presence of structural alterations in the tubular and glomerular compartments, deparaffined kidney sections were stained with periodic acid–Schiff (PAS) as previously described [466].

4.A.XII.3.1. Qualitative blinded evaluation of tubular and glomerular injury

The pathologist systematically evaluated structural alterations in the different renal compartments. All the studied experimental groups were evaluated in a blinded fashion.

4.A.XII.3.2. Measurement of glomerular and mesangial area

Determination of glomerular and mesangial area was based on glomerular morphometry studies by Image J software on PAS stained samples. For each mouse, 20 microphotographs were taken at 40x magnification with an Olympus BX61 motorized microscope. On these images, glomerular area, glomerular tuft area, and mesangial area were measured. With the values obtained in each glomerulus, bowman space area (BSA) and mesangial index (MI) were calculated (Figure 29).

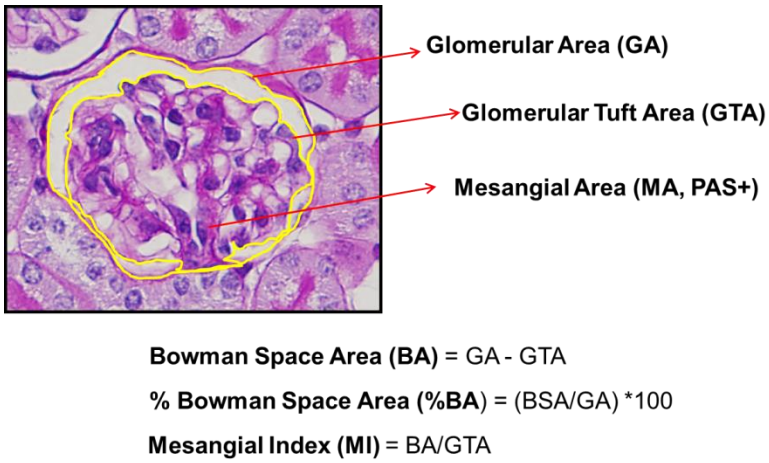

Figure 29. Glomerular morphometry. Glomerular area, glomerular tuft area and mesangial area were measured in renal PAS stained sections by using Image J software. These parameters allowed us to calculate the percentage of Bowman' space area and the mesangial index in our groups of study.

For each animal, the mean value for glomerular area, glomerular tuft area, mesangial area, and bowman space area was calculated from the values obtained from each blinded observer. Of mention that only glomeruli showing the vascular pole were considered for analysis of all these parameters.

4.A.XII.3.3. Assessment of podocyte number and glomerular cellularity

Assessment of podocyte number and glomerular cellularity was performed on renal sections stained for Wilms Tumor 1 (WT-1). WT-1 is a zinc-finger transcription factor involved in tumor suppression, embryonic development and maintenance of organ function. In the adult kidney, WT-1 expression is limited to the glomerular podocytes

and plays a crucial role on preserving their function[467]. For these reasons, this protein is considered a marker for measurement of podocyte number[468].

20 microphotographs per animal were taken at 40x magnification with an Olympus BX61 motorized microscope. On these images, positive and negative nuclei were counted in a double blinded fashion. The protocol for WT-1 immunostaining is described in section 4.A.XIII.5. For each animal, the mean value for podocyte number and glomerular cellularity was calculated from the values obtained from each blinded observer.

4.A.XII.4. Evaluation of tubulointerstitial fibrosis

Tubulointerstital fibrosis (TIF) was evaluated by two different approaches:

- Determination of cortical alpha-smooth muscle actin (α-SMA) protein expression as a marker of fibrosis.
- Evaluation of collagen deposition by picrosirius red staining.

4.A.XII.4.1. Determination of cortical α-SMA expression

For each kidney section stained for α-SMA, 10 microphotographs of the renal cortex were taken per animal at 10x magnification. On these images, positive α-SMA staining was quantified by ImageJ Software. Specific brown signal was digitally isolated and expressed as mean grey value. This analysis was performed in a blinded fashion. Details about α-SMA immunostaining are specified in section 4.A.XIII.5.

4.A.XII.4.2. Evaluation of collagen deposition by picrosirius red staining

Picrosirius red staining was performed on 4.5μm kidney sections. Briefly, deparaffined samples were incubated for 5min in acidified water and then transferred to a container with picrosirius red reagent (Direct Red 81 Dye, Sigma). Stained samples were rinsed twice with acidified water (2x5min) and dipped in ddH_2O water. Finally, sections were dehydrated through graded alcohols prior to the drying with DPX mountant media (Sigma) for conservation. Cortical collagen accumulation was semiquantitatively evaluated (0-4 score) under circularly polarized light as previously described[469]. Tubulointerstitial, periglomerular and intraglomerular collagen deposition were evaluated independently. All analyses were performed in a double blinded fashion.

4.A.XIII Molecular studies

4.A.XIII.1. Workflow for the *in vivo* molecular studies

The most relevant techniques employed to carry out the molecular studies of this project, as well as the most representative readouts, are summarized in Figure 30.

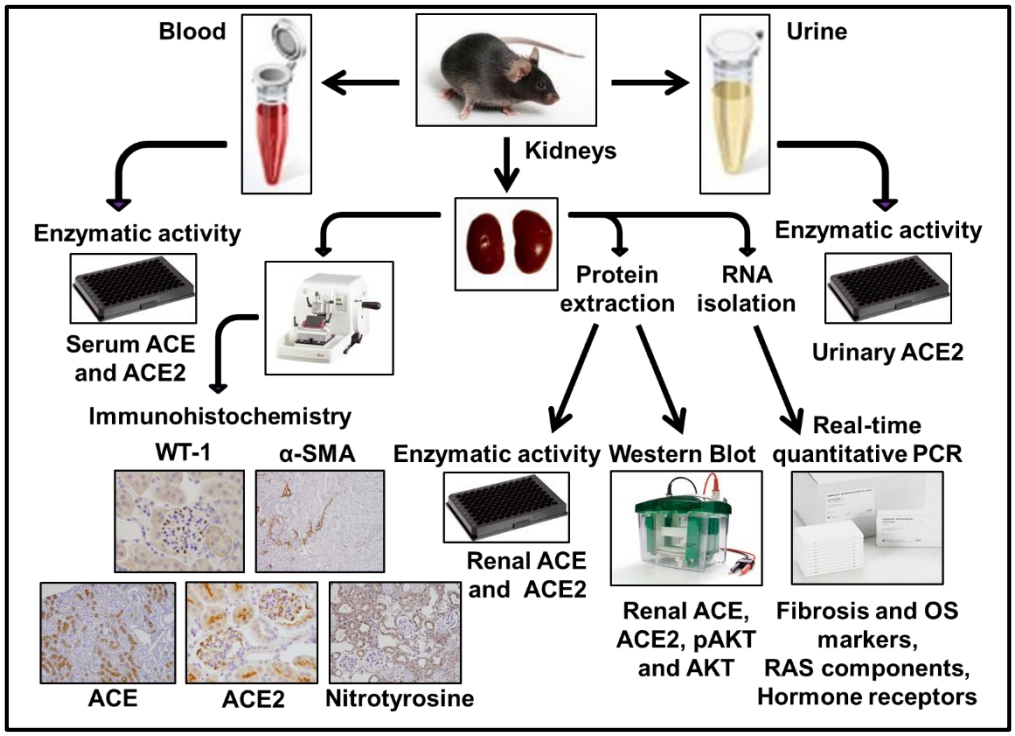

Figure 30. Molecular *in vivo* studies. At the end follow-up, urine was collected and blood and kidneys were extracted from all the studied animals. Classic molecular biology techniques, including enzymatic activity assays, Western Blot, immunohistochemistry, and real-time quantitative PCR were conducted to evaluate the degree of renal injury and the modulation of RAS at different levels of expression in the study groups.

The protocols for all of these methods are detailed in the following sections.

4.A.XIII.2. Protein extraction

Kidney cortex samples (25-50mg) were homogenized through a syringe in a buffer consisting on 50mM HEPES (pH 7.4), 150mM NaCl, 0.5% Triton X-100, 0.025mM ZnCl2, 0.1mM Pefabloc SC Plus (Roche), and EDTA-free protease inhibitor cocktail tablet (Roche).

For detection of phosphorylated proteins, additional total protein extracts were performed in a buffer with the following composition: 25mM HEPES (stock at pH 7.5), 150mM NaCl, 1% Triton X-100, 10mM $MgCl_2$, 1mM EDTA (stock at pH 8.5), 10% glycerol, 0.1mM Pefabloc SC Plus (Roche), and EDTA-free protease inhibitor cocktail

tablet (Roche). To minimize the loss of phosphate groups in the extracted proteins, phosphatase inhibitor cocktail (Sigma) was added to the extraction buffer at 1% final concentration according to manufacturer instructions. Protein extracts were clarified by centrifugation at 14,000xg for 10min at 4°C.

4.A.XIII.3. Protein quantification

Protein concentration was determined using the bicinchoninic acid (BCA) Protein Assay Kit (Thermo Scientific Pierce®). This technique is based on Biuret reaction, which consists on the reduction of the copper ions ($Cu^{2+} \rightarrow Cu^{1+}$) in an alkaline environment in the presence of protein in the samples[470]. The colorimetric reaction that takes place after addition of BCA allows the detection of the Cu^{1+} cation.

150µL of diluted protein extracts (1/750 in ddH_2O water) and BSA standard curve were loaded into 96-well plates. 150µL of a working solution containing BCA and Cu^{2+} were then added to each well, and plates were incubated for 2h at 37°C. Absorbance was measured by spectrophotometry at a wavelength of 562nm in a Tecan Infinite 200 reader (TECAN instruments). Absorbance values were extrapolated in the standard curve, and protein concentration in the sample was expressed as µg of protein/ µL of sample.

4.A.XIII.4. Protein expression analysis by Western Blot

Western blot analyses of renal protein extracts were performed by separation of proteins through polyacrylamide gel electrophoresis (PAGE) followed by transfer onto polyvinylidene fluoride (PVDF) membranes (Hybond-P, GE Healthcare).

One-dimensional SDS-PAGE gels are composed by a mixture of acrylamide/bisacrylamide (29:1), 1.5M Tris-HCl (at pH 6.8 for the stacking gel and pH 8.8 for the separating gel) and 2.5% sodium dodecyl sulphate (SDS). Acrylamide/bisacrylamide polymerization generates a solid matrix. In turn, SDS is a protein denaturing detergent that destabilizes the tertiary structure of proteins and, in addition, gives them a global negative charge that allows protein migration under an electric field. Migration of denatured and negatively charged proteins through the poliacrylamide matrix promotes their separation in function of their MW. To ensure proper protein separation, two concentrations of acrylamide/bisacrylamide are used: first, a low concentration (4%) for protein stacking, and second, a high concentration (7-15%) for protein separation. Once proteins have been separated along the SDS-PAGE gel, they are transferred onto a PVDF membrane, which shows high affinity for

aminoacids and makes proteins accessible to antibody binding. Transfer is performed under the presence of an electric field and a buffer that allows the migration of the proteins from the SDS-PAGE gel to the PDVF membrane. After that, the membrane is incubated with a blocking solution (BS) to minimize unspecific binding. Finally, proteins are detected using specific antibodies.

Samples were diluted in 6x loading buffer containing 0.21M TrisHCl (pH 6.8), 6% SDS, 34% glycerol, 19% beta-mercaptoethanol and bromophenol blue and boiled for 10 minutes at 100ºC for protein denaturation. Samples were then loaded into SDS-PAGE gels, and proteins were separated by employing the Mini-format Electrophoresis System (Bio-Rad) in the presence of running buffer containing 25mM Tris, 192mM Glycine and 0.1% SDS. Electrophoresis was performed at 70V for protein stacking and 110V for separation. As a reference for MW, 2µL of Precision Plus Protein™ Dual Color Standard (Bio-Rad) were loaded in the first lane. Once proteins were separated based on their MW, they were transferred onto PDVF membranes previously activated with 100% methanol. Transfer was performed using a semi-dry system (Trans-Blot® Turbo™, Bio-Rad) and a buffer containing 25mM Tris, 192mM de Glycine pH 8.3 and 10% methanol. Membranes were then incubated for 45 minutes at RT with blocking solution (BS), which consisted on skimmed milk or BSA diluted in TBS containing 0.1% Tween-20 (TBST 0.1%). Membranes where then probed with the corresponding primary and secondary antibodies. After each incubation, membranes were washed three times with TBST 0.1% for 5-10min. Detection of proteins was performed by a chemiluminescent reaction (Clarity™ ECL Western Blotting Substrate, Bio-Rad) followed by exposure to photographic films (X-Ray Film, AGFA). Control for protein loading was performed by reblotting the membranes with antibodies for β-actin. Following detection, films were scanned and bands were quantified by densitometry with ImageJ software. The specific conditions for optimized detection of our proteins of interest, including the percentage of acrylamide in the separating gel, protein amount loaded, BS composition, and antibody dilution and incubation time, are detailed in Table 11.

Table 11. Proteins detected by Western Blot. Molecular weight (MW) and conditions for optimal protein detection by Western Blot are provided.

Protein	MW (Kda)	% Acryl. (Separating)	µg of protein	Blocking solution	Primary antibody				Secondary antibody			
					Origin	Reference	Dilution	Incubation	Origin	Reference	Dilution	Incubation
ACE	180	7%	20	5% skimmed mik	Rabbit polyclonal	F940 (Bioworld)	1/500	ON, 4ºC	Goat	A0545 (Sigma)	1/2000	1h, RT
ACE2	96	7%	20	5% skimmed mik	Rat monoclonal	MAB3437 (R&D Systems)	1/6000	ON, 4ºC	Rabbit	A-5795 (Sigma)	1/10000	1h, RT
β-actin	46	7% or 11%	20	5% skimmed mik	Mouse monoclonal	A1978 (Sigma)	1/10000	45min RT	Goat	P-0447 (Dako)	1/20000	45min RT
pAKT (Ser473)	63	7%	30	5% skimmed mik	Rabbit polyclonal	9271 (Cell Signaling)	1/1000	ON, 4ºC	Goat	A0545 (Sigma)	1/2000	1h, RT
Total AKT	63	7%	30	5% skimmed mik	Rabbit polyclonal	9272 (Cell Signaling)	1/2000	1h, RT	Goat	A0545 (Sigma)	1/4000	1h, RT
GNPNAT1	21	11%	15	7% skimmed mik	Rabbit polyclonal	HPA044647 (Atlas)	1/6000	ON, 4ºC	Goat	A0545 (Sigma)	1/12000	1h, RT
GPI	63	11%	15	7% skimmed mik	Rabbit polyclonal	PA5-26787 (Thermo)	1/10000	1h, RT	Goat	K4002 (Dako)	1/12000	1h, RT
HADHA	83	11%	15	7% skimmed mik	Rabbit polyclonal	ab54447 (Abcam)	1/12000	1h, RT	Goat	K4002 (Dako)	1/12000	1h, RT
HEXB	63	11%	20	7% skimmed mik	Rabbit polyclonal	PA5-36146 (Thermo)	1/500	ON, 4ºC	Goat	K4002 (Dako)	1/12000	1h, RT

4.A.XIII.5. Immunohistochemistry

Following deparaffining and rehydration of kidney sections, antigen retrieval was performed under one of these three different conditions:

- Incubation with 0.01M sodium citrate buffer (pH 6.0) for 5 min, in a microwave oven (160W).
- Incubation with 0.01M sodium citrate buffer (pH 6.0) for 5 min, in a pressure cooker (100^{o}C).
- Incubation with 0.01M Tris, 2mM EDTA, 0.1% Tween buffer (pH 9.0) for 5 min, in a pressure cooker (100^{o}C).

After antigen retrieval, samples were cooled for at least 30 min and transferred to a container with ddH_2O water. Endogenous peroxidase activity was blocked for 20 min by incubating the renal sections with 3% H_2O_2 in PBS. Samples were washed twice with PBS or TBST (5 min for each wash). Unspecific binding was blocked with a solution containing BSA and goat serum (if necessary) in washing buffer for 45 min at RT. For protein immunolocalization, samples were incubated with rabbit, mouse, goat, or rat primary antibodies diluted in BS. HRP-conjugated anti-rabbit (EnVisionTM, Dako), anti-rabbit/mouse (EnVisionTM, Dako), anti-rat IgG (Sigma) or anti-goat IgG (Santa Cruz) were used as secondary antibodies. Binding of all antibodies was detected by oxidation of 3,3'-Diaminobenzidine (DAB) using the Liquid DAB+Substrate Chromogen System (Dako). After each antibody incubation samples were washed again as before. Samples were counterstained with hematoxylin (45 seconds) and dehydrated through graded alcohols. Finally, stained sections were dried and preserved with DPX mounting

media (Sigma). The specific conditions for optimized detection of our proteins of interest, including the antigen retrieval conditions, BS composition, and antibodies dilution and incubation time, are detailed in Table 12.

Table 12. Proteins localized by immunohistochemistry. Conditions for optimal staining are provided.

Target protein	Antigen retrieval	Washing buffer	Blocking solution	Primary antibody				Secondary antibody			
				Origin	Reference	Dilution	Incubation	Origin	Reference	Dilution	Incubation
ACE	0.01M citrate (pH 6.0),PC	PBS 1x	1% BSA, 3% GS	Rabbit polyclonal	F940 (Bioworld)	1/250	ON, 4°C	Goat	K4002 (Dako)	Original	45min, RT
ACE2	0.01M citrate (pH 6.0),PC	TBST 0.05%	1% BSA	Rat monoclonal	MAB3437 (R&D Systems)	1/100	ON, 4°C	Rabbit	A-5795 (Sigma)	1/200	45min, RT
AT1R	0.01M Tris (pH 9.0), PC	PBS 1x	1% BSA, 1% GS	Goat polyclonal	31181 (Santa Cruz)	1/150	ON, 4°C	Donkey	2020 (Santa Cruz)	1/200	45min, RT
GNPNAT1	0.01M citrate (pH 6.0),PC	PBS 1x	1% BSA, 3% GS	Rabbit polyclonal	HPA044647 (Atlas)	1/500	1h, RT	Goat	K4002 (Dako)	Original	45min, RT
GPI	0.01M Tris (pH 9.0), PC	PBS 1x	1% BSA, 3% GS	Rabbit polyclonal	PA5-26787 (Thermo)	1/500	ON, 4°C	Goat	K4002 (Dako)	Original	45min, RT
HADHA	0.01M Tris (pH 9.0), PC	PBS 1x	1% BSA, 3% GS	Rabbit polyclonal	ab54447 (Abcam)	1/1000	1h, RT	Goat	K4002 (Dako)	Original	45min, RT
HEXB	0.01M citrate (pH 6.0),PC	PBS 1x	1% BSA, 3% GS	Rabbit polyclonal	PA5-36146 (Thermo)	1/50	ON, 4°C	Goat	K4002 (Dako)	Original	45min, RT
N-Tyr	0.01M citrate (pH 6.0),PC	PBS 1x	3% BSA, 3% GS	Rabbit polyclonal	06-284 (millipore)	1/500	1h, RT	Goat	K4002 (Dako)	Original	45min, RT
α-SMA	0.01M citrate (pH 6.0),MW	TBST 0.1%	1% BSA	Mouse monoclonal	A-2547 (Sigma)	1/800	1h, RT	Goat	K4065(Dako)	Original	45min, RT
WT-1	0.01M citrate (pH 6.0),MW	TBST 0.05%	3% BSA, 3% GS	Rabbit polyclonal	SC-192 (Tebu-Bio)	1/1000	ON, 4°C	Goat	K4002 (Dako)	Original	45min, RT

Of mention that, for α-SMA immunolocalization, samples were incubated for 1h with Fab Goat anti-mouse IgG (Jackson ImmunoResearch) diluted 1/10 in PBS. This step was performed prior to the incubation with BS in order to prevent non-specific binding of the anti-mouse secondary antibody to murine immunoglobulins.

4.A.XIII.6. ACE enzymatic activity assay

4.A.XIII.6.1. Determination of renal ACE activity

For renal tissue ACE activity determination, 2µL of protein extract previously diluted to 0.5µg/µL was incubated with 73µL of working buffer containing 0.4M sodium borate pH 8.3 and 5.5mM of N-Hippuryl- L -histidyl- L –leucine (HHL, Sigma) for 25 minutes at 37ºC. The reaction was stopped by adding 180µL of 0.28M sodium hydroxide. Next, samples were incubated with 15µL o-Phthaldialdehyde (20 mg/mL in methanol) in the dark for 10 minutes at RT. The adduct formation was stopped by adding 30µL of 3N hydrochloric acid (HCl) and samples were centrifuged for 5 minutes at 800g. 200µL of the supernatants were transferred into a black plate (Nunc™ F96 MicroWell™ Black Polystyrene Plate) and intensity was measured by fluorescent spectroscopy. Values were corrected by time of reaction (15min) and protein amount (1µg). For each sample, ACE activity was measured in duplicate by fluorescent spectroscopy at a wavelength of 360nm (excitation) and 485nm (emission) in a Tecan Infinite 200 reader (TECAN

Instruments). Data are expressed as relative fluorescence units (RFU)/min/µg of protein.

4.A.XIII.6.2. Determination of circulating ACE activity

For determination of ACE activity in serum, 2µL of sample previously diluted 1/8 in saline solution were incubated with 73µL of working buffer containing 0.4M sodium borate pH 8.3 and 5.5mM HHL for 15 minutes at 37ºC. From this point, the technique was performed as described above. Values were corrected for the dilution factor (1/4) and data are expressed as RFU/min/µL serum.

4.A.XIII.7. ACE2 enzymatic activity assay

4.A.XIII.7.1. Determination of renal ACE2 activity

Homogenized kidney cortex samples were diluted in an assay buffer at pH 7.5 containing 100mM Tris-HCl, 600mM NaCl, 10µM $ZnCl_2$, and 100µM of the ACE inhibitor captopril, in the presence of protease inhibitors: 5µM amastatin, 5µM bestatin (all from Sigma), and 10µM Z-Pro-prolinal (Enzo Life Sciences). 40µL of diluted tissue sample containing 0.5µg of total protein were transferred to each well. 10µL of buffer (with or without a specific ACE2 inhibitor, MLN-4760, 1/200) were then added. The reaction was initiated by the addition of 50µl of Mca-Ala-Pro-Lys(Dnp)-OH substrate (5µmol/l, final concentration). Kidney cortex ACE2 activity was determined after 4-hour incubation at 37°C. The plates were read at λ_{ex}320 nm and λ_{em}400nm (Tecan Infinite 200 reader, TECAN Instruments). Experiments were carried out in duplicate for each data point. For each sample, the inhibition value was subtracted from the raw value. Data are expressed as RFU/hr/µg of protein.

4.A.XIII.7.2. Determination of circulating ACE2 activity

For serum and urine analysis, 2µl of sample were incubated with the same assay buffer used for tissue samples and 10µM of fluorogenic substrate in a final volume of 100µL at 37°C for 16 h. The plates were read as before. For serum ACE2 activity, data are expressed as RFU/hr/µl. For urinary ACE2 activity, values were normalized to creatinine levels and data are expressed as RFU/hr/mgCrea.

4.A.XIII.8. Gene expression analysis

4.A.XIII.8.1. RNA extraction

RNA was obtained from frozen kidney samples using the Tripure Isolation Reagent (Roche). Briefly, 40-50 mg of cortical renal tissue were homogenized with 800µL of Tripure. Following manufacturer's instructions, 160µL of chloroform were added and the mixture was centrifuged at 12000xg and 6ºC for 15 minutes. Colorless upper phase was separated and RNA precipitation was performed by addition of 400µL of isopropanol and later centrifugation at 12000g and 6ºC for 15 minutes. RNA pellet was washed with 75% ethanol and resuspended with 50µL of ddH_2O water.

4.A.XIII.8.2. Determination of RNA quality and concentration

RNA quantity and purity were analyzed by spectrophotometry (NanoDrop® ND-1000). Nanodrop instrument was employed as explained in section 4.A.IV.3. In our experiments, samples were not technically validated for reverse transcription if their RNA concentration was lower than 100µg/µL or if the ratio 260nm/280nm was out of the range 1.6-2.3.

4.A.XIII.8.3. First-strand cDNA synthesis

First-strand cDNAs were synthesized from 1µg of RNA using the High-Capacity cDNA Reverse Transcription (RT) Kit (Applied Biosystems, Foster City, CA). Briefly, appropriate volumes of RNA and ddH_2O water were mixed with 10µL of RT Master Mix 2x to obtain a final volume of reaction of 20µL (Table 13).

Table 13. Components of RT Master Mix 2x.

REAGENT	VOLUME (µl/sample)
10x RT Buffer	2.0
25x dNTP Mix (100mM)	0.8
10x RT Random Primers	2.0
Multiscribe™ Reverse Transcriptase	1.0
RNase Inhibitor	1.0
Nuclease-free H_2O	3.2

Retrotranscription was performed in a thermocycler (TProfessional Basic, Biometra) by incubating for 10 minutes at 25ºC, 120 minutes at 37ºC and 5 minutes at 85ºC.

4.A.XIII.8.4. Real-time quantitative PCR (RT-qPCR)

qPCR technique was performed using SYBRGreen Master Mix 2x (Roche). The fluorescence was measured at real-time at λ_{ex}465nm and λ_{em}510nm. The reaction was carried out in LightCycler 480 multiwell-384 plates (Roche) in a final volume of 10µL. The reagents employed and the composition of the reaction mix are described in Table 14.

Table 14. Reagents used for the real-time quantitative PCR reaction. For each reagent, the volume employed per sample, as well as its final concentration, are specified.

REAGENT	VOLUME (µl/sample)	FINAL CONCENTRATION
SYBRGreen Master Mix 2x	5.0	1x
Forward primer (100µM)	0.025	0.25nM
Reverse primer (100µM)	0.025	0.25nM
ddH_2O	3.95	-
cDNA simple (diluted)	1.0	-

Gene expression for several genes related to the renin-angiotensin system, fibrosis, inflammation, oxidative stress, and sex hormone signaling was determined. *Gapdh* and *Hprt* were used as housekeeping genes. Primers sequences were designed using Primer3 software and were manufactured by Sigma. Different cDNA dilutions were used according to the technical validation of each pair of primers (Table 15).

Table 15. Analyzed genes, primer sequences and cDNA dilution used for Real-time qPCR analysis.

Gene	Gene name	Forward primer (5' → 3')	Reverse primer (5' → 3')	cDNA dilution
Actin-alpha smooth muscle	***Acta***	ACTGGGACGACATGGAAAAG	AGTGTCGGATGCTCTTCAGG	1/50
Angiotensin Converting Enzyme	***Ace***	CGCCGCTATGGGGACAAATA	ATGTCTCCCAGCAAATGGGC	1/50
Angiotensin Converting Enzyme 2	***Ace2***	CGCAGAGATCAAGCCATTGT	TCCATCAACTTCCTCCTCACA	1/50
Aminopeptidase A	***Apa***	CACTGTGAGTGGAAGGCAGA	TGTGTAACCGAGCTCTGACG	1/50
Aminopeptidase N	***Apn***	ATCTGGACCTGTGGGAACAC	AATCCAGCGGTCCATGATAG	1/50
Androgen receptor	***Ar***	AGCCTCAATGAGCTTGGAGA	ATCTGGTCATCCACATGCAA	1/50
Angiotensin type 1 receptor	***At1r***	CAAAGCTTGCTGGCAATGTA	ACTGGTCCTTTGGTCGTGAG	1/50
Angiotensin type 2 receptor	***At2r***	TTTGGCTACCCTCCCTCTCT	CACAGGTCCAAAAAGCCAAT	1/10
Angiotensinogen	***Agt***	CGTGCCCCTAGGTGAGAGAG	TCCAAGTCAGGAGGTCGTTC	1/50
Cathepsin G	***Ctsg***	AGATGAGGCAGGGAAGATCA	CACTCAGCCCTTCTGGACTC	1/2
Collagen alpha-2(I) chain	***Col1a2***	GCAGGTTCACCTACTCTGTCCT	CTTGCCCCATTCATTTGTCT	1/50
Collagen alpha-1(IV) chain	***Col4a1***	TGTCCATGGCACCCATCTCT	CACAAACCGCACACCTGCTA	1/50
Connective tissue growth factor	***Ctgf***	AAGACACATTTGGCCCAGAC	TAGAACAGGCGCTCCACTCT	1/50
Estrogen receptor alpha	***Esr1***	GCAGATAGGGAGCTGGTTCA	AGGTGGACCTGATCATGGAG	1/50
Fibronectin	***Fn1***	GCCACCGGAGTCTTTACTACC	TCTCTGTCACCTCGGTGTTG	1/50
Glyceraldehyde-3-phosphate dehydrogenase	***Gapdh***	AACTTTGGCATTGTGGAAGG	TGTGAGGGAGATGCTCAGTG	1/50
G-protein coupled estrogen receptor 30	***Gper30***	TCTAGGGAGAAAGCCATCCA	GGCACCCAGAGTGTGTGAGT	1/50
Hypoxanthine-guanine phosphoribosyltransferase	***Hprt***	TGTTGTTGGATATGCCCTTG	AATGACACAAACGTGATTCAAA	1/50
Mas receptor	***Mas1***	CATCTAGGACTGGGCAGAGC	ACCCTGACCCATGGTATGAA	1/2
Monocyte chemoattractant protein 1	***Mcp1***	AGGTCCCTGTCATGCTTCTG	CGTTAACTGCATCTGGCTGA	1/10
NADPH oxidase 2	***Nox2***	TCTCAGGTGTGCATGTAGCC	TTGCTGCATTCAGTTCAAGG	1/100
NADPH oxidase 4	***Nox4***	CTTGGTGAATGCCCTCAACT	TTCTGGGATCCTCATTCTGG	1/100
NADPH oxidase cytosolic protein p47phox	***p47phox***	AGATGGCAAGAATAACGTAGCTG	ACTCTTCTCGTAGTCAGCAATGG	1/10
Neprilysin	***Nep***	AGCCAAAGCAAGCAGCTAAA	TCGGCCTGAGGAATAAAATG	1/50
Renin	***Ren***	ACCTTGCTTGTGGGATTCAC	CCTGATCCGTAGTGGATGGT	1/50
Transforming growth factor beta-1	***Tgfb1***	TGAGTGGCTGTCTTTTGACG	AGCCCTGTATTCCGTCTCCT	1/50

Real-time qPCR was performed in the Light cycler 489 System (Roche) following the settings described in the following table.

Table 16. Real-time PCR settings in the Light cycler 489 System. After the amplification cycles are completed, melting step is performed in order to assess that the PCR has produced single, specific products.

STEP	TEMPERATURE	RAMP RATE	TIME
PRE-INCUBATION	95°C	4.8°C/s	5 minutes
AMPLIFICATION (45 cycles)			
A) DENATURING	95°C	4.8°C/s	10 seconds
B) ANNEALING	58°C	2.5°C/s	20 seconds
C) ELONGATION	72°C	4.8°C/s	20 seconds
MELTING			
A) DENATURING	95°C	4.8°C/s	5 seconds
B) ANNEALING	58°C	2.5°C/s	1 minute
C) DENATURING	95°C	0.11°C/s	-
COOLING	40°C	2.5°C/s	10 seconds

4.A.XIII.8.5. Gene expression data analysis

Data from real-time qPCR were analyzed using Light Cycler® 480 SW1.5 (Roche) software. For each qPCR reaction that took place in each of the microplate wells, the threshold cycle (C_T value) was calculated using the "Abs Quant/2nd Derivative Max" analysis; only samples with a standard deviation lower than 0.20 across replicates were considered for further analysis. The gene expression ratio of each target over the housekeeping gene was calculated using the delta-delta-Cp equation as previously described[471].

4.B *IN VITRO* STUDIES

To complement our *in vivo* observations and have a better understanding of the mechanisms involved in the sex differences in DN and RAS expression in the renal cortex, we aimed to explore in a global fashion how sex hormone signaling can alter the proteome of renal tubular cells. To achieve this aim, we undertook a quantitative proteomic approach as a tool to elucidate which molecular events and biological processes are more directly and significantly regulated by sex hormones at protein level. We employed stable isotope labeling with amino acids in cell culture (SILAC) in an indirect spike-in fashion to accurately quantify the proteome in DHT- and EST-treated human proximal tubular epithelial cells (PTEC).

4.B.I. SILAC

The most relevant feature of SILAC methodology is the *in vivo* incorporation of specific amino acids into all mammalian proteins. Mammalian cell lines are grown in media lacking one or more standard essential amino acids but supplemented with a non-radioactive, isotopically labeled "heavy" form of those amino acids[472]. The heavy amino acid can contain ^{2}H instead of H, ^{13}C instead of ^{12}C, or ^{15}N instead of ^{14}N. Incorporation of the heavy amino acid into a peptide leads to a known mass shift compared with the peptide that contains the light version of the amino acid (for example, 6 Da in the case of $^{13}C_6$-arginine), but to no other chemical changes[473]. In our study, the heavy amino acids present in our SILAC media were +6 arginine (with $^{13}C_6$ in the amino acid backbone) and +8 lysine (with $^{13}C_6{}^{15}N_2$).

Trypsin is a common proteolytic enzyme in proteomics workflows, as it is a very aggressive yet specific protease that cleaves at the carboxi-terminal of lysine and arginine residues[474]. Therefore, SILAC using arginine and lysine as labeling amino acids in combination with trypsin digestion is an ideal combination as all peptides of a protein (except the C-terminal peptide) are, in principle, quantifiable[475].

Growth of cells maintained in heavy media is no different from growth in normal media as evidenced by cell morphology, doubling time, and ability to differentiate. Complete incorporation of amino acids usually occurs after five population doublings in the cell lines and proteins studied[476]. As shown in Figure 31, protein populations from "heavy (H)" and "light (L)" samples are mixed directly after harvesting, prior to tryptic digestion.

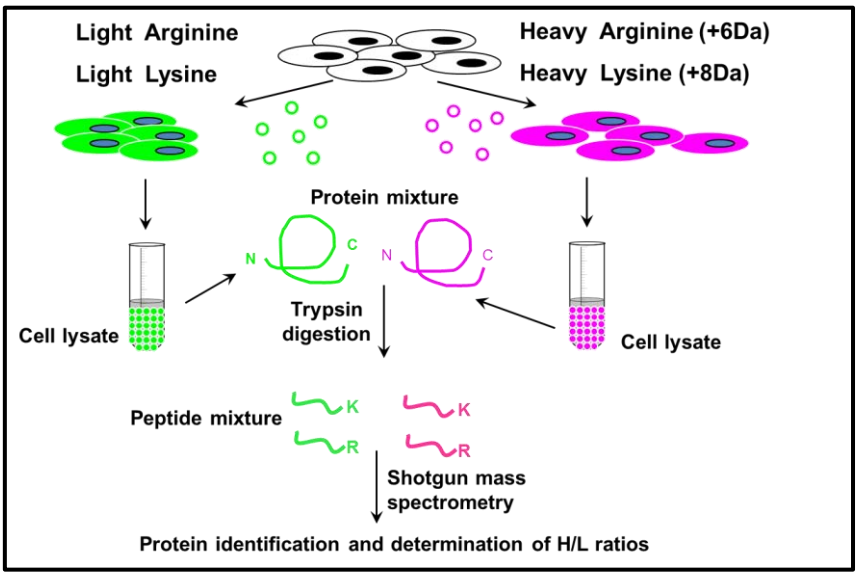

Figure 31. The basis of SILAC methodology. For one experimental condition (green), cells are grown in light (L) media. For the other experimental condition (pink), cells are grown in SILAC heavy (H) media. Proteins from both cell populations are mixed and digested into peptides. For each peptide, the differential mass between the light and the heavy forms (H/L ratios) allows relative quantification.

Mass spectrometric identification is straightforward as every arginine- or lysine-containing peptide incorporates either all normal light or heavy forms of the amino acids.

We performed a quantitative strategy by using SILAC in combination with a high resolution mass analyzer. To quantify the proteome of a single cell line, the SILAC experiment can be performed in a classical or in a spike-in format[477]. One of the advantages of spike-in SILAC is that the experimental cells are maintained in their normal state and are not affected by the special media required for SILAC or by the use of dialyzed serum. Furthermore, the same standard can be used for multiple samples and similar cell lines, and there is therefore no need to label all of them[478]. Single cell line spike-in standard has been previously and efficiently used when multiple samples with high similarity were studied, or in cases where growing the cells in SILAC media was challenging[479].

4.B.II. Our approach: spike-in SILAC in two renal cell lines

Since SILAC-labeling of primary PTEC is not trivial and the several passages needed for the full incorporation of the labeled amino acids may lead to cell culture-induced loss of differentiation, we have employed spike-in SILAC to accurately quantify their proteome after sex hormone treatment. In particular, we SILAC-labeled immortalized human kidney HK-2 cells, and used their “heavy” proteome as internal standard to quantify the treated proteome from PTEC. Both PTEC and HK-2 are epithelial cells and originate from human renal proximal tubule. Thus, we reasoned that HK-2 proteome would allow us to accurately quantify a large proportion of PTEC proteome. In addition, HK-2 cells have been reported to show excellent labelling efficiency[480]. In turn, we selected PTEC for stimulation experiments because they express both DHT and EST receptors[481,482] and were previously shown to respond to sex hormones[381,382]. Furthermore, tubules constitute most of the renal parenchymal mass, and tubular atrophy with interstitial fibrosis carries prognostic significance, and represents the common final pathway of most causes of CKD[483,484]. The spike-in strategy employed for our *in vitro* studies is represented in Figure 32.

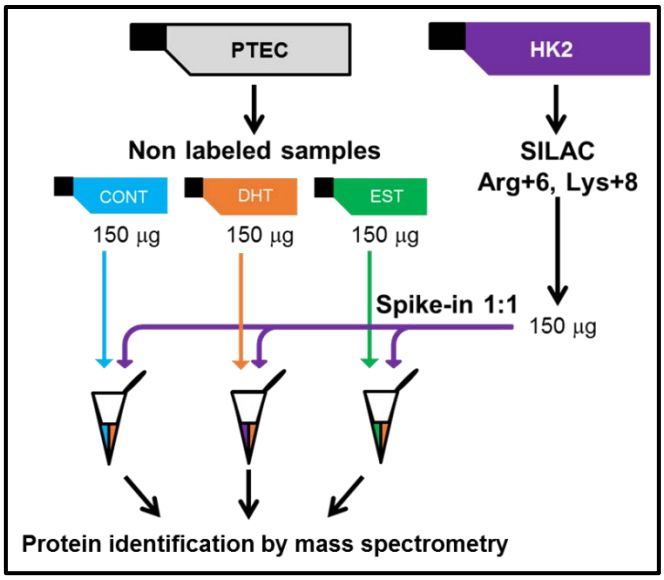

Figure 32. Spike-in SILAC in human kidney cells. 150µg of total protein from control, DHT- or EST-treated PTEC were mixed with 150µg of total protein from SILAC labeled HK-2 cells. The heavy proteome from HK-2 cells was used as an internal standard for relative quantification.

Cell culture conditions and protocols for PTEC and HK-2 cells are detailed in the following sections.

4.B.II.1. Sex hormone treatment to PTEC

PTEC were purchased from Lonza Walkersville Inc. They were cultured in T25 flasks in custom-made Dulbecco's modified Eagle's medium (DMEM), and supplemented with 10% v/v dialyzed fetal bovine serum (FBS), 10ng/mL EGF, 5µg/mL transferrin, 5µg/mL insulin, 0.05µM hydrocortisone, 50units/mL penicillin, and 50µg/mL streptomycin, as previously described[485]. Cells were serum starved for 18h and treated with 100nM DHT (n=4) or EST (n=3) for 8h (aiming to activate sex hormone nongenomic and genomic signaling for proteomic analysis. Ethanol treated cells were used as controls (CONT, n=4).

In each experiment, a subpopulation of cells from the same suspension was seeded in 6-well-plates, serum starved for 18h and treated with 100nM DHT or EST for only 10min, aiming to detect AKT and ERK phosphorylation as a proof of rapid and nongenomic stimulation of the widely known downstream events triggered by sex hormones[369,370,377,378]. This control experiment was performed in order to demonstrate that our PTEC showed a biological response to sex hormone stimulation. Only experiments were PTEC showed increased AKT and ERK phosphorylation after 10min of DHT- and EST-stimulation were selected for proteome analysis after 8h treatment

(Figure 33). After stimulation, cells were washed three times with PBS, harvested with trypsin, and snap-frozen at -80 °C until further analysis.

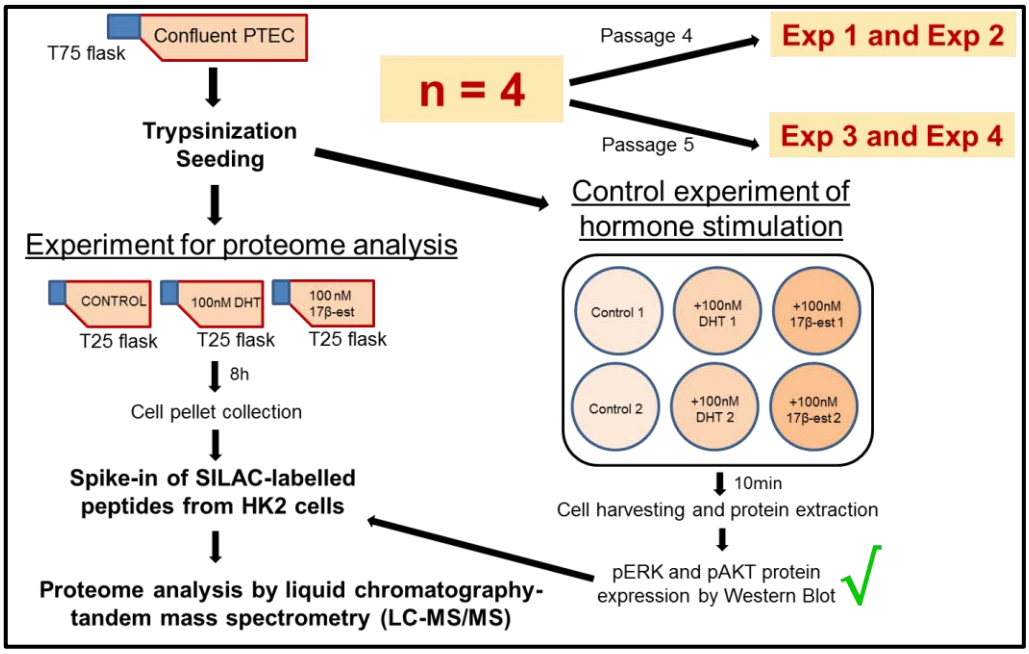

Figure 33. Sex hormone treatment to PTEC. Cells were subcultured and treated with sex hormones for control signaling experiments (10min) or for proteome analysis (8h). 2 experiments were performed in 2 different passages.

4.B.II.1.1. Determination of AKT and ERK phosphorylation

For control experiments, total protein was extracted and levels of pAKT and pERK were assessed by Western Blot. Briefly, proteins from sex hormone-treated cell pellets were solubilized in modified RIPA buffer (150mM sodium chloride, 50mM Tris-HCl (pH 7.4), 1 mM EDTA, 1% v/v Triton X-100, 1% w/v sodium deoxycholic acid, 0.1% v/v SDS) and extracted by sonication. Protein concentration was determined using a Coomassie (Bradford) protein assay reagent (Pierce). 40μg of protein were loaded onto 12% acrylamide gels and separated by SDS-PAGE. Membranes were incubated with antibodies to pSer473 AKT (193H12, Cell Signaling, 1/1000) and p44/42 ERK1/2 (9102, Cell Signaling, 1/1000). The secondary antibody was anti-rabbit antibody developed in goat (sc-2004, Santa Cruz Biotechnology). Control for protein loading was performed by reblotting membranes for β-actin using a mouse monoclonal antibody (A1978, Sigma) and an anti-mouse secondary antibody (sc-3697, Santa Cruz Biotechnology). Following detection, bands were quantified by densitometry with Image J software.

4.B.II.2. SILAC metabolic labeling of immortalized HK-2 cells

HK-2 cells used for SILAC labeling were cultured in DMEM/F12 (1:1) free of arginine, lysine, methionine and leucine (AthenaES), and supplemented with 10% v/v dialyzed FBS, 50 units/ml penicillin, 50 μg/ml streptomycin, 2 mM glutamine, 5 μg/ μL transferrin, 5 μg/ μL insulin, 0.05 μM hydrocortisone, 1 nM T3 hormone, 10 ng/mL EGF, 147.5 mg/L heavy arginine ($^{13}C_6$), 91.25 mg/L heavy lysine ($^{13}C_6{}^{15}N_2$), 17.24 mg/L light methionine, and 59.05 mg/L light leucine. After 5, 6, 8 and 10 cell population doublings of SILAC labeling, HK-2 cells were serum starved for 18h and cell pellets were collected as mentioned above for further spike-in experiments. At each point, $1 \cdot 10^5$-$2 \cdot 10^5$ cells were separated and collected as a different pellet for determination of labeling efficiency (Figure 34). All media were freshly made and filtered using a 0.22μm syringe filter.

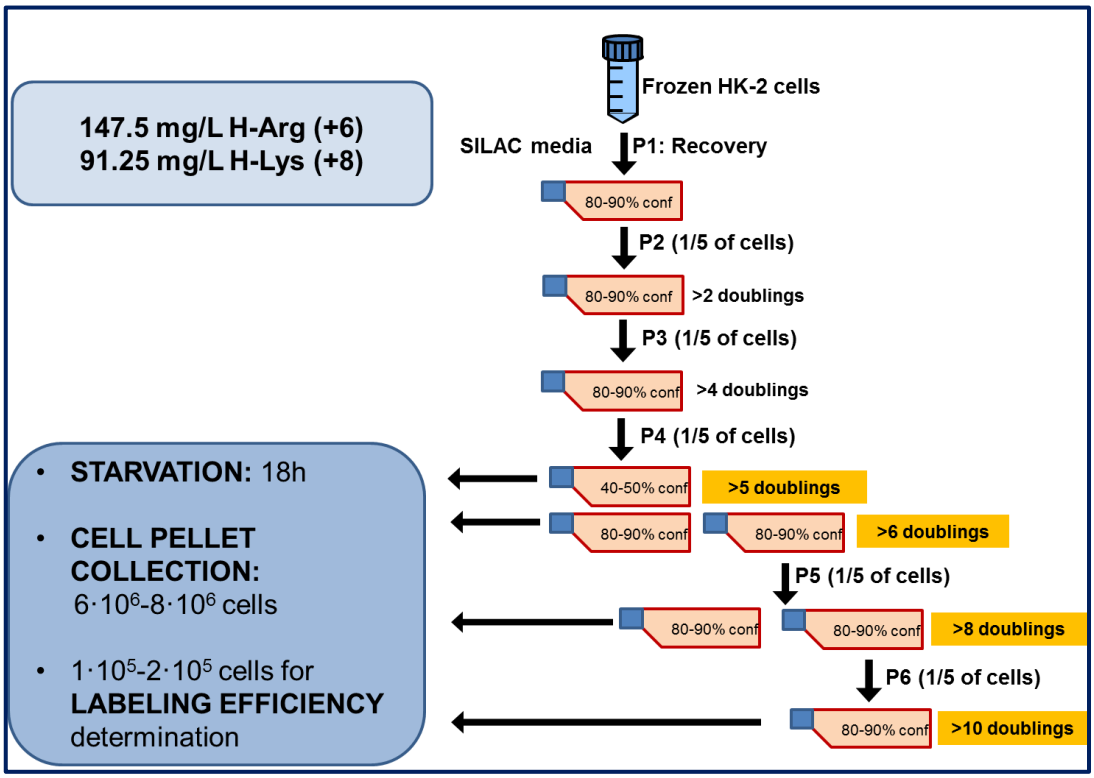

Figure 34. Experimental scheme of HK-2 culture in SILAC media containing heavy arginine and lysine. To guarantee that at least 2 cell population doubling would take place in each passage, 1/5 of the total number of cells were seeded and grown until they reached a confluence of 80-90%. Orange boxes indicate that cell pellets were collected and labeling efficiency was calculated after 5, 6, 8 and 10 population doublings in SILAC media.

Percent label incorporation for individual peptides was calculated manually using the equation (Intensity H / Total Intensity) * 100. 100% labeling efficiency was considered for peptides with intensity equal to 0 in the light form.

4.B.III.Coupling cell culture to mass spectrometry: General workflow

As shown in Figure 35, mixed proteomes from treated PTEC and SILAC labeled HK-2 were subjected to protein reduction, alkylation and tryptic digestion to obtain the corresponding peptides for protein identification. We followed the most widely adopted strategy for shotgun proteomics, which uses strong cation exchange (SCX) to fractionate peptide digests, followed by reverse phase by liquid chromatography coupled to tandem mass spectrometry (LC-MS/MS) to acquire peptide MS/MS spectra[486,487]. Hence, the SCX peptide fractionation step is critical for the optimization of the number of hits identified by the mass spectrometer. This approach will allow the achievement of excellent proteome coverage.

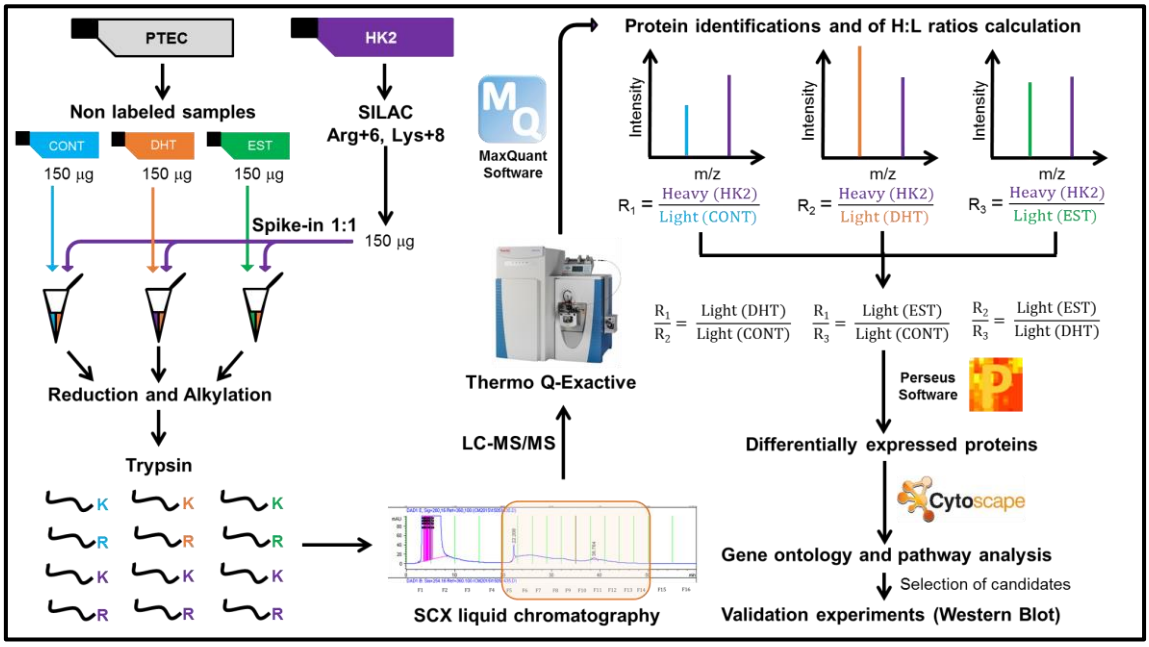

Figure 35. Experimental scheme. The figure shows a simplified workflow, including sex hormone treatment to PTEC, SILAC labeling of HK-2 cells, 1:1 mixing of labeled and non-labeled proteins, protein digestion, SCX fractionation followed by LC-MS/MS, data analysis by MaxQuant, assignment of heavy/light protein ratios, calculation of DHT/CONT, EST/CONT and EST/DHT ratios, selection of differentially regulated proteins, validation studies and bioinformatic analysis.

All the steps depicted in the figure are further described in the following sections.

4.B.IV. Sample processing for proteome analysis

Cell pellets from treated PTEC (light) and labeled HK-2 cells (heavy) were thawed on ice, resuspended in 200µl of 0.1% w/v acid-labile detergent RapiGest SF (Waters, Milford, MA) in 25mM ammonium bicarbonate, vortexed, and sonicated three times for 30s. All lysates were centrifuged for 20min at 15,000rpm at 4°C. Total protein concentration was measured using a Coomassie (Bradford) protein assay reagent

(Pierce). 150μg of protein from heavy HK-2 cells were spiked to 150μg of each sample from light treated PTEC (1:1 mixing ratio). Proteins in detergent solution were denatured at 60°C, and the disulfide bonds were reduced with 10mM dithiothreitol. Following reduction, the samples were alkylated with 20mM iodoacetamide. Proteins were then digested overnight at 37°C with sequencing grade modified trypsin (Promega, Madison WI). A trypsin/total protein ratio of 1:50 (w/w) was used. After digestion, RapiGest SF detergent was cleaved with trifluoroacetic acid, 1% (v/v) final concentration, and samples were centrifuged for 15 minutes at 15,000rpm at 4°C.

4.B.V. Proteome analysis of DHT- and EST-stimulated PTEC using two-dimensional LC-MS/MS

4.B.V.1. SCX peptide fractionation

The dynamic concentration range and the large number of proteins in a proteome require the development of multidimensional separation strategies to allow for the identification of the largest number of proteins. In this sense, SCX chromatography has been used extensively for the fractionation of proteins and peptides in cell and tissue proteomics[125]. The SCX stationary phase usually contains aliphatic sulfonic acid groups that are negatively charged in aqueous solution, therefore tightly binding any strongly basic analytes. The analytes of interest are eluted with a solvent neutralizing this ionic interaction (Figure 36). Most tryptic peptides in acidic pH are characterized by a net charge of +2 and above, and they can be therefore separated by SCX from peptides possessing a net charge of +1, such as trypsin-generated phosphopeptides, C-terminal peptides, or peptides with blocked N-terminal (i.e., by N-acetylation), as well as from peptides containing higher charges, including ones containing missed cleavages and therefore more arginine and lysine residues.

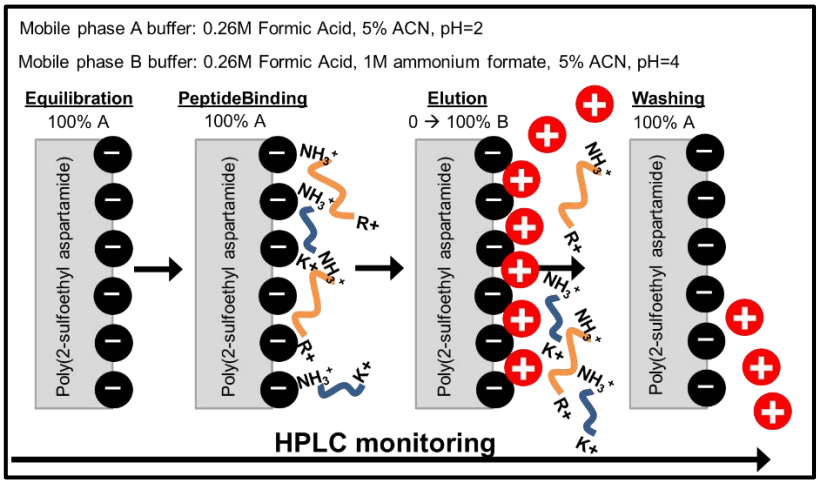

Figure 36. SCX chromatography. After equilibration with mobile phase A buffer at pH 2.0, positively charged tryptic peptides are loaded to the column and bind to the resin by electrostatic interaction. Ammonium formate in mobile phase B provides the NH_4^+ cations that strongly bind to the column and induce the elution of the peptides, which are gradually recovered in different fractions. To remove residual and unspecific binding from the resin, several washings with mobile phase A are required between samples.

Upon removal of Rapigest, our tryptic peptides were diluted to 500µl SCX mobile phase A (0.26 M formic acid in 5% v/v acetonitrile; pH2) and loaded directly onto a 500µl loop connected to a PolySULFOETHYL ATM column (2.1-mm inner diameter x 200 mm, 5 µm, 200 Å, The Nest Group Inc.). The SCX chromatography and fractionation were performed on an HPLC system (Agilent 1100) using a 60 min two-step gradient. An elution buffer that contained all components of mobile phase A with the addition of 1 M ammonium formate was introduced at 10 min and increased to 20% at 30 min and then to 100% at 45 min. Fractions were collected every 3 min from the 20 min time point onward. The resulting 10 fractions (600µl each) corresponding to chromatographic peaks of eluting peptides were collected (Figure 37).

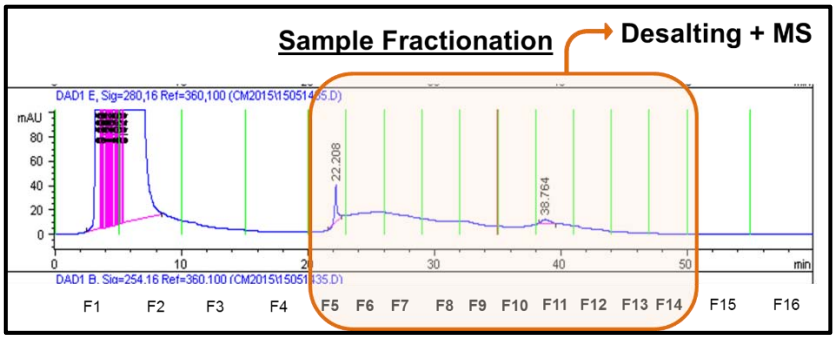

Figure 37. Representative HPLC chromatogram showing the elution profile from the SCX column. F1, F2…F16 nomenclature designates each of the fractions. Green lines indicate the times at which fractions were collected. Unspecific binding was always eluted first (F1 and F2) and discarded from analysis. In this particular sample, peptides were eluted between F5 and F14. These fractions were selected for further desalting and MS processing.

4.B.V.2. Peptide identification by LC-MS/MS

Peptides in each fraction were identified by LC-MS/MS as described previously[488]. Briefly, peptides were extracted with 10μl of OMIX C18 MB tips (Varian, Lake Forest,CA), eluted in 3μl of 65% v/v acetonitrile, diluted to 41μl with 0.1% v/v formic acid in pure water, and loaded onto a 3 cm C18 trap column (with an inner diameter of 150 μm; New Objective), packed in-house with a 5μm Pursuit C18 (Varian). Eluted peptides from the trap column were subsequently loaded onto a resolving analytical PicoTip Emitter column, 5cm in length (with an inner diameter of 75μm and 8μm tip, New Objective) and packed in-house with 3μm Pursuit C18 (Varian, Lake Forest, CA). The trap and analytical columns were operated on the EASY-nLC system (Thermo Fisher Scientific, San Jose, CA), and this liquid chromatography setup was coupled on line to a Q Exactive hybrid quadrupole-Orbitrap mass spectrometer (Thermo Fisher Scientific, San Jose, CA) using a nano-ESI source (Proxeon Biosystems, Odense, Denmark). Each fraction was run using a 60 min gradient, and analyzed in a data-dependent mode in which a full MS1 scan acquisition from 450 to 1450*m*/*z* in the Orbitrap mass analyzer (resolution 60,000) was followed by MS2 scan acquisition of the top six parent ions in the linear ion trap mass analyzer. The following parameters were enabled: monoisotopic precursor selection, charge state screening, and dynamic exclusion. In addition, charge states of +1, >4, and unassigned charge states were not subjected to MS2 fragmentation. For protein identification and data analysis, Xcalibur software (version 2.0.5; Thermo Fisher) was utilized to generate RAW files of each MS run.

4.B.V.3. MS data Analysis

The MS files were processed with the MaxQuant software version 1.2.6.20[489] and searched with Andromeda search engine[490] against the human UniProt database[491] (release 01_07_2015, 148,986 entries). The raw files from all biological replicates were analyzed simultaneously with MaxQuant. To assess the false-positive rate, a reverse hit database was created by MaxQuant. The false discovery rates at the protein and peptide level were set to 1%. To search parent mass and fragment ions, an initial mass deviation of 6 ppm and 0.5 Da (CID) or 20 ppm (HCD), respectively, were required. The minimum peptide length was set to 7 amino acids and strict specificity for trypsin cleavage was required, allowing up to two missed cleavage sites. Searches were performed with fixed carbamidomethylation of cysteines, variable oxidation of methionine and proline residues, and N-terminal acetylation. Multiplicity of 2 was used,

selecting Arg (+6 Da) and Lys (+8 Da) as heavy labels. A fragment tolerance of 0.5 Da and a parent tolerance of 20 Da were used. Re-quantification and matching between runs was selected. Protein was identified with a minimum of one unique peptide. Quantification was performed using unmodified unique and razor peptides and a minimum of one counted ratio.

4.B.V.4. SILAC ratio analysis

The reverse and common contaminant hits were removed from MaxQuant output. Only proteins identified with at least one peptide uniquely assigned to the respective sequence were considered for the analysis. Since the distributions of all Log2 transformed H/L and H/L normalized ratios were shown to be normal (Figure 38), the H/L normalized ratios of biological replicates were used to calculate DHT/CONT, EST/CONT and EST/DHT ratios. These ratios express the fold change between 2 different conditions and were calculated in all four experiments.

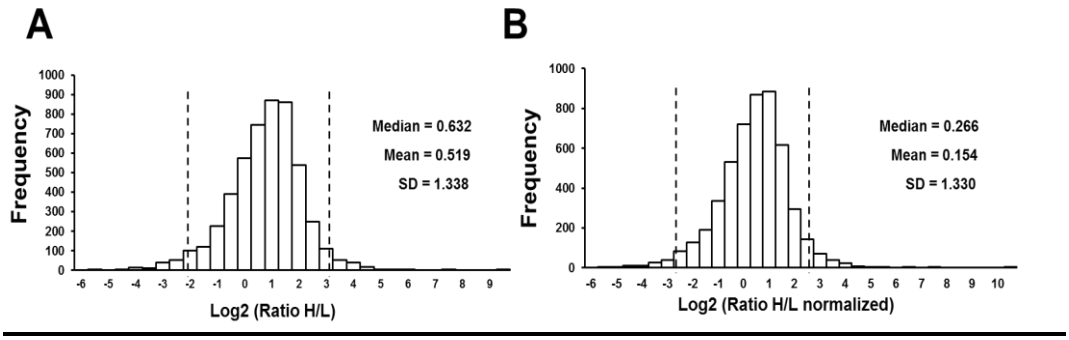

Figure 38. Distributions of heavy (H) to light (L) ratios. Histograms depicting the distributions of Log2 transformed H/L (A), and normalized H/L (B) ratios of all 5043 quantified proteins. Vertical lines represent 1.96•SD.

Significance A of DHT/CONT, EST/CONT and EST/DHT ratios was calculated for all the quantified proteins. A protein was considered to be significantly differentially regulated if its ratio was significant by significance A with $p<0.01$ in at least 2 experiments. Proteins were eliminated if their ratios in the other 2 experiments showed changes in the opposite direction. Only proteins with at least one unique peptide with two or more ratio counts were further pursued. In addition, if ratios of proteotypic (unique) peptides of the same protein were changing in opposite directions, these proteins were also discarded for the validation studies. A total of 104 proteins were found to be differentially regulated in at least one of the three comparisons.

4.B.VI. Verification and validation studies

SILAC ratios of top candidate proteins were verified *in vitro* and validated *in vivo* following the methodology explained below.

4.B.VI.1. *In vitro* verification of SILAC ratios

SILAC ratios of top candidate proteins were confirmed by Western Blot in the same protein extracts used for the proteomic study. 15μg of protein were loaded onto 12% acrylamide gels and separated by SDS-PAGE. Membranes were incubated with antibodies to glucose-6-phosphate isomerase (GPI, PA5-26787, Thermo Scientific), glucosamine-6-phosphate-N-acetyltransferase 1 (GNPNAT1, HPA044647, Atlas Antibodies) and mitochondrial trifunctional protein subunit alpha (HADHA, ab54447, Abcam). The secondary antibody was anti-rabbit antibody developed in goat (sc-2004, Santa Cruz Biotechnology). Control for protein loading was performed by reblotting membranes for β-actin. Following detection, bands were quantified by densitometry with Image J software.

4.B.VI.2. *In vivo* validation of SILAC ratios

4.B.VI.2.1. Study animals

The *in vivo* validation of the selected differentially expressed proteins found in SILAC experiments was performed using 16-week-old C57BL/6 healthy female and male mice. To assess the effect of sex in the context of diabetes, we employed female and male STZ-induced mice after 12 weeks of diabetes. We also studied 16-week-old female and male diabetic Akita (*Ins2*$^{WT/C96Y}$) mice. Five to eight animals were included in each experimental group. Mice were anesthetized with isoflurane and sacrificed by terminal surgery. Kidneys were removed, weighted, snap frozen and kept at -80^{o}C until further analysis. Half of the right kidney was maintained in 10% formalin solution and paraffin embedded for histological studies. Mice were housed in ventilated cages with full access to chow and water at the Division of Comparative Medicine at University of Toronto (control and Akita mice), or at the Animal Facility of Barcelona Biomedical Research Park (STZ-induced mice). All experiments were conducted under the guidelines of the University of Toronto Animal Care Committee and the Ethical Committee of Animal Experimentation of Barcelona Biomedical Research Park (CEEA-PRBB).

4.B.VI.2.2. Western Blot of top candidate proteins

Western Blot for GPI, GNPNAT1 and HADHA were performed in the renal cortex of female and male control, STZ-induced and Akita mice. Total protein was extracted with RIPA modified buffer as described in section 4.B.II.1.1. For Western blot analysis, the same conditions used for the *in vitro* verification studies were applied.

4.B.VI.2.3. Renal immunolocalization of top candidate proteins

To localize top candidate proteins from our proteomic data set in the murine kidney, immunohistochemistry staining was also performed for HADHA, GPI and GNPNAT1. Samples were boiled in 10mM sodium citrate solution (pH 6.0) for GNPNAT1 staining, whereas antigen retrieval for HADHA and GPI was performed in 10mM Trizma® base, 0.5M EDTA, 0.05% Tween buffer (pH 9.0). Sections were incubated with rabbit primary antibodies for HADHA (1:1000; ab54447, Abcam), GPI (1:1000; PA5-26787, Thermo Scientific) or GNPNAT1 (1:500; HPA044647, Atlas Antibodies). HRP-conjugated anti-rabbit (EnVisionTM, Dako) was used as secondary antibody. Slides were counterstained with hematoxylin.

4.B.VII. Bioinformatics analyses

4.B.VII.1. Gene ontology and functional enrichment analysis

The corresponding gene IDs of the differentially expressed proteins from our *in vitro* and *in vivo* proteomics experiments were used to perform gene ontology enrichment analyses using BiNGO plugin[492] in Cytoscape software[493] (version 3.2.1). In addition, Enrichment Map plugin[494] was used to assess the significantly enriched functional categories among our sex-regulated proteins and other published data sets at transcriptomic and proteomic level. For the statistical analysis, hypergeometric test with Benjamini-Hochberg correction were applied and 0.05 was assigned as significance level.

4.B.VII.2. Validation of the bioinformatics findings

4.B.VII.2.1. Oxidative stress

Oxidative stress, which emerged as a significant functional group in our bioinformatics analyses, is generally identified by indirect markers such as peroxynitrite production[495]. For this reason, nitrotyrosine staining was used to evaluate superoxide and peroxynitrite levels in renal tissues as previously described[496]. Deparaffined samples were boiled in 10mM sodium citrate solution (pH 6.0) for antigen retrieval. Kidney sections were stained with rabbit antinitrotyrosine antibody (1:500, Millipore, Billerica, MA). Fifteen microphotographs at x40 were taken for each sample, and brown-stained areas were quantified with ImageJ software. Data were expressed as percentage of positive area. All analyses were performed in a blinded fashion.

4.B.VII.2.2. Glycosphingolipid metabolism

To confirm enrichment of glycosphingolipid (GLS) metabolism in our DHT proteomic signature, we analyzed cortical protein expression of hexosaminidase B (HEXB), a top candidate protein representing this functional group, in female and male STZ-diabetic mice and their controls. For HEXB immunostaining, samples were boiled in 10 mM sodium citrate solution (pH 6.0) and incubated with rabbit primary antibody for HEXB (1:50; PA5-36146, Thermo), and HRP-conjugated anti-rabbit (EnVisionTM, Dako) secondary antibody. For Western blot detection, 20μg of protein were loaded onto 12% acrylamide gels and separated by SDS-PAGE. Membranes were incubated with the same anti-HEXB antibody (1:500), washed and incubated with 1:2000 of anti-rabbit antibody developed in goat (sc-2004, Santa Cruz Biotechnology). Control for protein loading was performed by reblotting membranes for β-actin. Following detection, bands were quantified by densitometry with Image J software.

4.C STATISTICAL ANALYSES

4.C.I. Significance tests and correlations

The distribution of all studied variables was analyzed by histogram plots and Shapiro-Wilk normality tests. Significant differences between groups were calculated by using the following non-parametric tests: Kruskal-Wallis for multiple comparisons and Mann-Whitney U-test for two group comparisons (SPSS 18.0 for Windows). Since

the majority of the studied variables followed a non-parametric distribution, Spearman's correlation coefficient was calculated when appropriate. $P < 0.05$ was considered statistically significant. Of mention that, although the majority of the studied variables followed a non-parametric distribution, we decided to present our data as means ± SEM for clarity.

For the *in vitro* proteomics data, Perseus software (version 1.5.1.6) was used for calculation of significance A of protein ratios. Benjamini-Hochberg FDR was used for adjustment for multiple hypotheses testing with a threshold value of 0.05.

4.C.II. Principal component analysis

To evaluate the predominant effects of sex, *Ace2* deletion, diabetes, and angiotensin II infusion in the assessed renal injury markers and renal expression of RAS components, principal component analysis (PCA) was performed using Perseus software (version 1.5.1.6). The mean value for each variable in each experimental group was used for the PCA. Category enrichment was in two principal components, and Benjamini-Hochberg FDR was used as a cutoff method with a threshold value of 0.05.

5. RESULTS